DISS. ETH NO. 27397

Design of spatial and time resolved plasma diagnostics for small gap discharges

A thesis submitted to attain the degree of

DOCTOR OF SCIENCES of ETH ZURICH
(Dr. sc. ETH Zurich)

presented by

Moritz Wiessner
MSc ETH ME

born on
8th November 1988

citizen of
Germany

accepted on the recommendation of

Prof. Dr.-Ing. Dr. h. c. K. Wegener
Dr. rer. nat. C. Hollenstein
Prof. Dr.-Ing. A. Schubert

2021

ACKNOWLEDGEMENTS

The years at the IWF have been among the most instructive in my life so far. This was due to the freedom I had while working at the IWF. Not only did I had the opportunity to explore different research directions besides my PHD, but I also got to know many aspects of science and university work beyond the experiments. This ranged from teaching in front of 500 students to the honour of organizing and co-chairing the largest conference on non-conventional manufacturing, ISEM XX. Therefore, first, I would like to thank Prof. Konrad Wegener, not only for giving me the opportunity to do the PhD at ETH, but also for continuously inspiring me with machine tools, manufacturing technology and production engineering since my first day of studies in the bachelor in 2008.

A key person in the development of this work was Dr Christoph Hollenstein. His technical support and his passion have been a fundamental contribution to this work. Above all, he supported me in not losing my way in the complex topics of plasma physics and for that I am very grateful. I am also pleased that Prof. Andreas Schubert accepted the invitation to be my co-supervisor and I would like to thank him for his contributions to the improvement of this work. I would also like to thank Dr Fredy Kuster. He was always there for me as a group leader until his retirement and beyond. Whether it was to answer organizational questions or to solve difficult situations with the industry, I could always rely on his expertise and am very grateful that I could work with him. I am grateful to Felipe, for the joint research and the many discussions. Even after his departure from the IWF, I could count on his support. I would also like to thank him for the joint supervision of the Brazilian interns and for allowing me to get to know the Brazilian culture. I would like to thank Albert Weber and Sandro Wigger, who were very supportive in preparing the experimental setups, Josef Meile, who assisted me in all IT issues, Knut Krieger for his support in metallography and I am glad that Eva Grob, Miriam Fahsi and Athina Kipouridis managed the institute in the background. I would also like to express my gratitude to our long-time industrial partner Georg Fischer especially Umang Maradia and Marco Boccadoro.

I would like to thank all colleagues at the IWF for the good and interesting work together. During my time at the IWF, many new friendships were formed, many barbecues and beers were enjoyed together. Therefore, I would first like to thank my two office colleagues Henning Büttner and Mikhail Kliuev, Christoph Baumgart for the many lunches together in the Unimensa, Stefan Fabbro for the collaborative ISEM organization and the associated beer tastings. The interest in beer was also shared by Hagen Klippel, Stefan Süssmaier, Andreas Zschippang, Matthias Röthlin and Marcel Gerstgrasser and celebrated in regular meetings. Fabian Kneubühler and Benno Käch introduced me to the taste for good coffee. I also thank the Indira Dey, Lukas Seeholzer, Linus Meier, Martina Spahni, Michal Kuffa, Philip Blaser, Sebastian Böhl, Varun Urundolil and many others for the good time at IWF. And finally, I would also like to thank my family and friends outside IWF for all their support.

CONTENTS

SYMBOLS AND ACRONYMS

Acronyms

CR	-	Collisional-radiative
EAM	-	Electric arc machining
ECDM	-	Electrochemical discharge machining
ECM	-	Electrochemical machining
EDF	-	Energy distribution function
EDM	-	Electrical discharge machining
EPFL	-	École polytechnique fédérale de Lausanne
ETH	-	Eidgenössische Technische Hochschule
FWHM	-	Full width of a half maximum
GFMS	-	Georg Fischer Machining Solutions
HAVA	-	Hot anode vacuum arc
HAZ	-	Heat affected zone
IWF	-	Institute of Machine Tools and Manufacturing
LTE	-	Local thermodynamic equilibrium
MRR	-	Material removal rate
OES	-	Optical emission spectroscopy
WEDM	-	Wire electrical discharge machining

Latin symbols

A	-	Probability of state transition
A_c	s^{-1}	Atomic transmission coefficient or Einstein coefficient
A_{qp}	s^{-1}	Spontaneous emission
Al	-	Aluminium
Al I	-	Optical emission line of neutral aluminium
Al II	-	Optical emission line of singly ionized aluminium atom
Al III	-	Optical emission line of doubly ionized aluminium atom
B_{qp}	s^{-1}	Stimulated absorption
B_{pq}	s^{-1}	Stimulated emission
C_{qp}	$s^{-1} \cdot cm^{-3}$	Collisional excitation
Cu	-	Copper
Cu I	-	Optical emission line of neutral copper
Cu II	-	Optical emission line of singly ionized copper
C_z	$s^{-1} \cdot cm^{-3}$	Sum of rates of possible radiative and collisional transitions
D_{pq}	$s^{-1} \cdot cm^{-3}$	Collisional deexcitation
e	C	Elementary charge
E_L	eV	Electron energy level
g	-	Statistical weight of the excited level
h	$kg \cdot m^2 \cdot s^{-1}$	Planck constant
H_α	-	Optical emission line of neutral hydrogen α
I	A	Electric current
I_L	cd	Light intensity
I_{qp}	s^{-1}	Beam and non-thermal electron collisions
I_R	a.u.	Relative optical emission line intensity
$\bar{J}$	-	Frequency-averaged mean intensity
k_B	$eV \cdot K^{-1}$	Boltzmann's constant
L	$W \cdot sr^{-1} \cdot m^{-2}$	Radiance
L_λ	$W \cdot sr^{-1} \cdot m^{-2} \cdot nm^{-1}$	Spectral radiance
n_z	cm^{-3}	Density of species of charge z
n_e	cm^{-3}	Density of electrons
N_L	-	Number of energy levels
N_z	-	Number of plasma zones with constant emission coefficient
S_λ	$W \cdot sr^{-1} \cdot m^2$	Source function
t_{on}	μs	Electric discharge pulse duration
T_i	K	Temperature of ions
T_e	K	Temperature of electrons
U_{open}	V	Open voltage
W_{pq}	s^{-1}	Sum of upward transitions
W_{qp}	s^{-1}	Sum of downward transitions
z	-	Ion charge

Greek symbols

α_{pq}	$s^{-1} \cdot cm^{-3}$	Radiative recombination of an ion
β_{qp}	s^{-1}	Photoionization plus stimulated recombination
γ_{pq}	$s^{-1} \cdot cm^{-3}$	Collisional ionization
Γ	-	Coupling parameter
ε	$W \cdot sr^{-1}$	Emission coefficient
ε_{λ}	$W \cdot sr^{-1}$	Emission from a plasma slab
δ_{pq}	$s^{-1} \cdot cm^{-6}$	Collisional recombination
κ	m^{-2}	Wavelength-dependent absorption coefficient
κ_{pq}	$s^{-1} \cdot cm^{-3}$	Electron capture
λ	nm	Wavelength
σ_{qp}	s^{-1}	Autoionization
ϕ_a	eV	Work function
ν	s^{-1}	Wave frequency
τ	-	Optical depth

ABSTRACT

Electrical discharge machining is one of the most widely applied non-conventional machining processes. Even though the process is well researched, and industry is continuously developing new technologies to improve the EDM process, the physical process is still not fully understood. In contrast to conventional machining, EDM involves many phenomena and requires interdisciplinary research. To examine the EDM process down to the smallest details, high requirements are imposed on the measuring equipment. The observation equipment must have a high temporal and spatial resolution. Additionally, they must be very small to allow in-situ observations. This either requires an endoscope or a special design of the optical experimental setup.

In this work an experimental setup is developed to observe time-resolved single EDM discharges with high-speed imaging and spatially resolved emission spectroscopy. The measured data was processed to obtain a radially resolved spectral information about the plasma. The plasma and its parameters are investigated by reverse parameter identification with the collisional-radiative code PrismSPECT. Plasma parameter profiles are discussed and compared with common discharge physics. Exemplary discharges between copper and aluminium electrodes in air as a dielectric are analysed.

The Spatial analysis of the plasma parameters and the observation with high-speed imaging confirm the assumptions of having a fraction of fast electrons in the plasma centre, which is also explain the observed high current densities in the plasma centre. Additionally, it is concluded that EDM plasmas are not homogenous but show profiles for all plasma parameters investigated, namely electron temperature, electron density, densities of excited and ionised Al species, fast electrons and fraction of fast electrons.

Furthermore, the EDM discharges have been investigated with respect to their anode and cathode behaviour. Micro discharges are still underrepresented in scientific literature. Nevertheless, parallels between vacuum arc literature and the observed micro discharges have been found. The similarities and differences lead to the assumption that two different types of micro-discharge are studied. The observations have especially an impact on the design of heat sources used in EDM single crater simulations.

Keywords

Electrical discharge machining, micro discharge plasmas, optical emission spectroscopy, high-speed imaging, emission spectra simulations, plasma diagnostics

KURZFASSUNG

Die Funkenerosion ist eines der am weitesten verbreiteten nichtkonventionellen Bearbeitungsverfahren. Obwohl dieses Bearbeitungsverfahren gut erforscht ist und die Industrie ständig neue Technologien entwickelt, um den Erodierprozess zu verbessern, sind die Grundlegenden physikalische Zusammenhänge des Prozesses immer noch unklar. Im Gegensatz zu konventionellen Fertigungsprozessen beinhaltet die Funkenerosion viele physikalische Aspekte und erfordert interdisziplinäre Forschung. Um den Erodierprozess bis ins kleinste Detail zu untersuchen, werden hohe Anforderungen an die Versuchsaufbauten und Messinstrumente gestellt. Diese müssen eine hohe zeitliche und räumliche Auflösung gewährleisten. Zudem müssen sie sehr klein sein, um in-situ-Beobachtungen zu ermöglichen. Dies erfordert entweder ein Endoskop oder einen speziellen Versuchsaufbau.

In dieser Arbeit wird ein experimenteller Aufbau entwickelt, um zeitaufgelöste einzelne EDM-Entladungen mit Hochgeschwindigkeitsabbildung und ortsaufgelöster Emissionsspektroskopie zu beobachten. Die Messdaten wurden verarbeitet, um eine radial aufgelöste spektrale Information über das Plasma zu erhalten. Das Plasma und seine Parameter werden durch inverse Parameteridentifikation mit Hilfe von PrismSPECT, einer Software mit der Emissionspektren simuliert werden können, untersucht. Plasmaparameterprofile werden diskutiert und mit gängiger Plasmaentladungsphysik verglichen. Exemplarisch werden EDM Entladungen zwischen Kupfer- und Aluminiumelektroden in Luft analysiert.

Die räumliche Analyse der Plasmaparameter und die Beobachtung mit Hochgeschwindigkeitsaufnahmen bestätigen die Annahmen, dass sich ein Bruchteil schneller Elektronen im Plasmazentrum befindet, was auch die beobachteten hohen Stromdichten im Plasmazentrum erklärt. Zusätzlich wird gezeigt, dass EDM-Plasmen nicht homogen sind, sondern Profile für alle untersuchten Plasmaparameter zeigen, namentlich Elektronentemperatur, Elektronendichte, Dichten der angeregten und ionisierten Aluminiumatome, schnelle Elektronen und den Teil der schnellen Elektronen.

Weiterhin wurden die EDM-Entladungen hinsichtlich ihres Anoden- und Kathodenverhaltens untersucht. Mikroentladungen sind in der wissenschaftlichen Literatur immer noch unterrepräsentiert. Dennoch wurden Parallelen zwischen der Vakuumlichtbogen-Literatur und den beobachteten Mikroentladungen gefunden. Die Ähnlichkeiten und Unterschiede führen zu der Annahme, dass zwei verschiedene Arten der Mikroentladung beobachtet wurden. Die Beobachtungen haben insbesondere Auswirkungen auf die Auslegung von Wärmequellen, die in EDM-Einzelkratersimulationen verwendet werden.

Schlüsselwörter

Funkenerosion, Mikroentladungsplasmen, optische Emissionsspektroskopie, Hochgeschwindigkeitsaufnahmen, Emissionsspektren-Simulation, Plasma Diagnose

1 INTRODUCTION

Electrical discharge machining (EDM) was developed by the scientists Dr Boris Lazarenko and Dr Natalya Lazarenko in 1943. After failing to prevent erosion on electrical contacts, they developed a machining process using this phenomenon to machine conductive materials with electrical discharges using one electrode as tool and one electrode as workpiece as reported by Schumacher [86].

In the mid-1950s, the first commercial EDM Machines were developed in Switzerland by the companies Agie and Charmilles (now Georg Fischer Machining Solutions, GFMS), shown in Fig. 1.1.

Fig. 1.1: First commercial EDM machines: Left Eleroda (1955, Charmilles); Right Agietron AB (1956, Agie); Photos taken at GFMS research centre, Losone 2019

Nowadays, EDM is one of the most widely applied non-conventional machining processes. Electrical discharge machining is mainly applied in sectors such as tooling, medicine and aerospace, including job-shop and series production.

The EDM process is known for:

- High shape precision
- High aspect ratios possible
- Very low process forces

- Machining any conductive material, independent of its hardness
- Slow material removal rate (MRR) which makes it a costly process
- Formation of heat-affected zones (HAZ) on the surface of the machined pieces and/or chemical modifications e.g. formation of carbides by erosion in oil.
- Good roughness achievable and special surfaces characteristics that can be created to increase the functionality of parts e.g. to improve demoulding of injection moulding

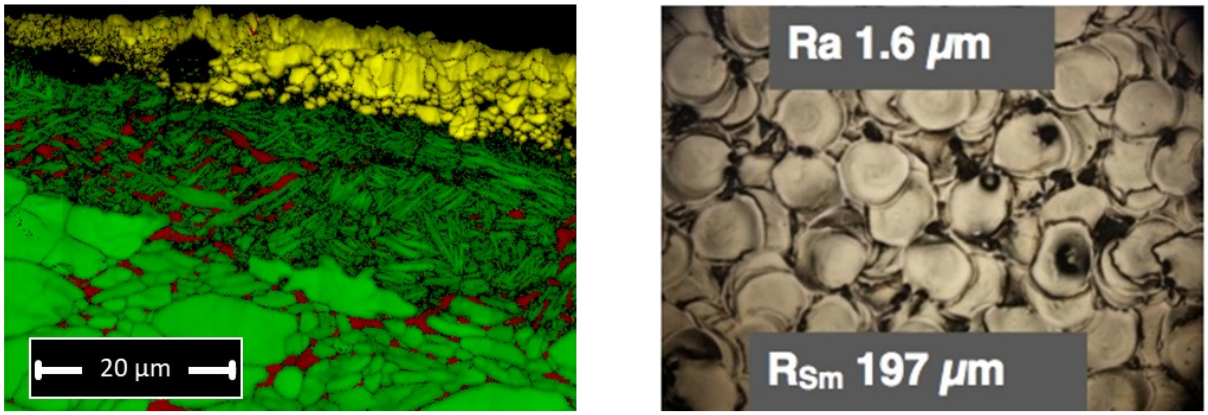

Fig. 1.2: Left: EDM machined Ti-6Al-4V surface with different surface layers caused by heat affection (lamellar grains, green and red) and chemical transformation (Ti-carbides, yellow) reported by Wiessner et al. [95] Right: 3DS surface from GFMS [22] and Maradia et al. [62] suited for reduced demoulding force in injection moulding

Several types of EDM machining processes are currently available on the market. The three main types, schematically seen in Fig. 1.3, are die-sinking, wire cutting (WEDM) and drilling respectively milling.

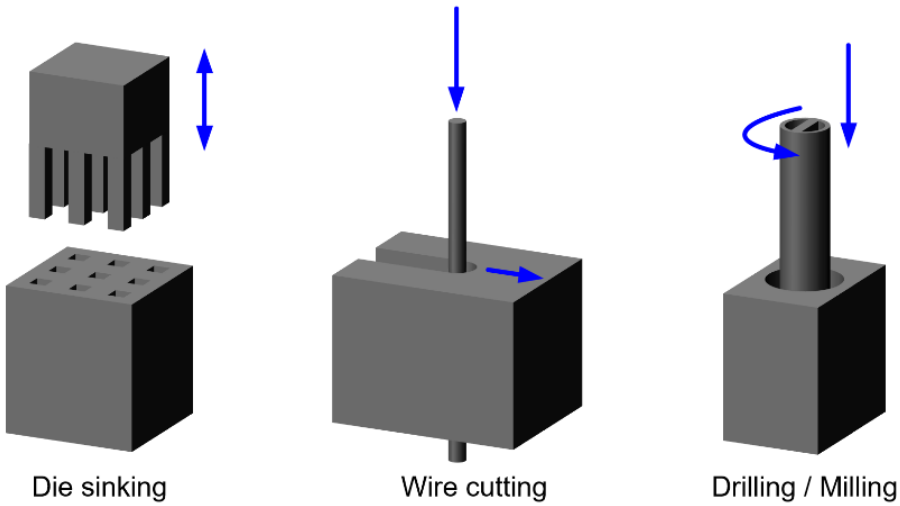

Fig. 1.3: Three main EDM technics: Blue arrows indicate the electrode motion. In drilling, a planar motion can be added to enable milling.

Die sinking is usually performed in oil as a dielectric with a geometrically defined tool electrode, which is imprinted on the workpiece surface. WEDM uses a running wire as

tool electrode, which operates in oil or deionized water as dielectric. EDM processes allow to cut workpieces either with high speed or very high precision. EDM drilling and milling are normally carried out using tubular electrodes with internal deionised water flushing to remove particles from the erosion gap. EDM drilling can be used in simple operations, such as removal of broken drill bits from machined parts but also in sophisticated high-end machining in aerospace applications like cooling holes. Milling adds also sideway movements of the tool which allows 3D shaping e.g. adding diffusers to cooling holes in turbine blades. For micromachining, this process is performed in a gaseous dielectric medium [44,90], which is then called dry EDM.

As previously mentioned, EDM is mainly performed in liquid dielectric media, such as hydrocarbon oil or deionized water. EDM in water can lead to a higher removal rate than in oil [41]; however, the presence of water can also cause chemical corrosion and/or creation of oxides on the workpiece surface. Oil as dielectric however has a lower MRR but comes along with high surface quality. EDM in oil can achieve roughness levels lower 0.1 µm Ra [64] and does not hold the risk of corrosion. Instead, the carbon content can cause wanted or unwanted chemical modification of the workpiece material by creating carbides [95]. With the support of modern technologies, many problems could be solved e.g. special surface modification by changing the discharge polarity and shape as well as tracking of the discharge condition in real-time to prevent surface damage and lower the HAZ.

Since EDM is an expensive process, special research and innovation are being done to make it more efficient and profitable to remain competitive and not be replaced by competitor technologies such as electrochemical machining (ECM), laser machining and micro-milling. Although it has often been assumed that laser machining is replacing EDM, it is still a growing market thanks to some unique selling points like high aspect ratio machining with high precision as well as an increase in performance and cost reduction in the past years [63,86]. Recent approaches in machining complex and nonconductive materials [5,37] allow EDM to remain competitive and be ready for the future.

New related and hybrid processes have been developed from EDM technology, such as electric arc machining (EAM), which uses long arc discharges, or electrochemical discharge machining (ECDM), a hybrid process between ECM and EDM. All these processes have in common that their working principle is based on microplasmas. Research on microplasmas has only recently begun to gain more importance, as this type of plasmas plays an increasingly important role in several applications [20]. Whether for the production and machining of new materials as shown by Mariotti and Sankaran [65], as an analytical tool e.g. for chemical analysis [21,31] or even for biomedical applications [1,28,84].

Development is done through intensive process parameter studies as well as though modelling and simulation of the different types of processes. Normal empirical approaches like regression models are often too limited to describe the complexity of this process. To develop more sophisticated models, the demand for a better understanding of the basic process is increasing. Nowadays researchers try to improve those models even with artificial intelligence and physical approaches. A key

element for the development of such models is the understanding of the interaction of the different fields of physics involved in the process.

The present work aims to provide a more precise and deeper insight into the microplasma physics of the process by introducing new tools and methods of analysis. Electrode material erosion and plasma parameters are investigated with the use of advanced plasma diagnostics developed at the Institute of Machine Tools and Manufacturing (IWF) of ETH Zürich.

2 STATE OF THE ART

Electrical discharge machining (EDM) is a 70-year-old non-conventional machining process, but when compared to other manufacturing processes, such as chipping or forming, EDM is still considered to be a rather young process. Although EDM is already well established in the industry, EDM machine manufacturers continuously make big leaps in innovation and develop the process further mainly due to advances in electrical engineering and computer science. Furthermore, since only few of the underlying physical phenomena are explained well, EDM is currently mostly described by empirical methods and recipes. Hence, there is still great potential for research and development for this manufacturing technology.

In contrast to conventional machining, investigation of the EDM process requires interdisciplinary research. Apart from mechanical engineering, also electrical engineering and computer scientists are needed to advance development of fast-reacting generator technologies, whereas physicists contribute to the analysis and understanding of the complex discharge physics and plasma-material interactions that take place in this process.

Most important is the understanding of the material removal on workpiece and tool, and how it can be influenced. Therefore, scientists developed models to describe the electrical breakdown, the formation of the gas bubble and plasma in between the electrodes. Furthermore, modelling of a single crater shape up to the simulation of a whole eroded surface are crated in order to mimic an investigate the process.

Following chapter aims to give a condensed overview and insight into the state-of-the-art theories and models of EDM, with a special focus on the plasma physics part of the process.

2.1 Electrical discharge erosion

The material removal in EDM machining is based on single electrical discharges which are applied with a high frequency. A state-of-the-art wire EDM machine produces discharges at a frequency from 10 kHz to 1 MHz. To understand the whole process, the physics of a single discharge and crater must be considered. The formation of a single crater in EDM follows several phases, illustrated Fig. 2.1.

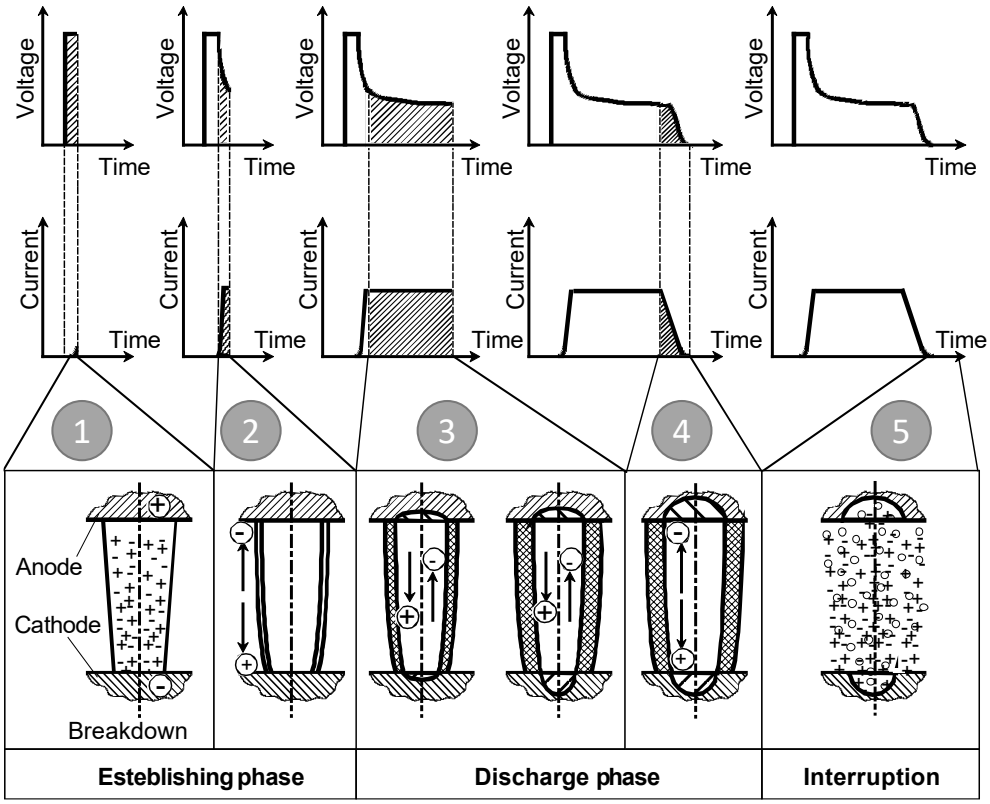

Fig. 2.1: Phases of an EDM Single discharge, adapted from [38]

1. Apply voltage and/or reduce the gap
2. Electrical breakdown
3. Plasma channel is created, an electrical current flow, a bubble is formed (for liquids) and material is partially removed
4. Current stops, the plasma channel collapses, and material is removed
5. The bubble collapses and additional material is removed

All these points are in themselves a research topic. However, in the EDM process the overall focus is usually on the material removal which is additionally influenced by follow-up discharges. Applying conclusions from single discharge analysis to investigate multiple discharge material removal is difficult. With the energy used to melt material might be the same for single and multiple discharges the average removed material can differ since in multiple discharges material is redeposited and eroded repeatedly. Additionally, the chemical transformation modifies the material properties in such a way that the erosion behaviour changes drastically, e.g. formation of carbides can increase the melting point by 1,000 K. The main material removal can occur due to several phenomena:

- Vaporization of the material
- Particle removal
- Dynamic of the melt pool
- Bubble collapse in liquid dielectrics

In all these processes, thermal energy is involved caused by the discharge plasma, cathode or anode processes and electron/ion material interaction. When modelling the EDM process, researchers typically use a thermal-based with a simplified heat source generating craters. The heat source is often derived from plasma or crater observations and is usually linked to the electrical parameters. Even though in publications the simulated craters often fit with sub-micron precision to the experimental ones, the boundary conditions of the heat source are only estimated. The fraction of energy transferred to the electrodes is usually adjusted or assumed based on crater observations. Due to the lack of knowledge about the physics of plasma-material interactions, simulations are often simplified without proper justification.

In the following sub-chapters, a description of the important points of discharge physics, breakdown and discharge plasma is presented. The current state of the art in EDM plasma analysis methods and their findings are given. Finally, the important topic of EDM simulation is briefly addressed to demonstrate the complexity of modelling and the lack of understanding between plasma and the resulting heat source.

2.2 Electrical breakdown

The electrical breakdown can occur in solid, liquid and gas insulators as well as in vacuum. EDM works with liquids and gaseous media, which also have the task to remove particles out of the working gap. In EDM voltages up to 250 V are generally used, and either the electrodes move towards each other until the breakdown occurs or the gap is adjusted to a constant value. Usually this is a gap of around 10 to 100 µm, whereby voltage is applied until the electrical breakdown occurs. Apart from the electrode distance, materials and dielectrics, the electrical breakdown also depends strongly on the applied electrical parameters, mainly voltage. In consecutive discharges the breakdown is additionally influenced by small debris or and ionised regions from a previous discharge.

In EDM it is generally assumed that either way an electron avalanche or positive streamers form the breakdown as described by Klocke [38]. But there are also theories supporting electron field emission or ion enhanced field emission for microscale gas discharges since for micro gaps the well-known Paschen’s law often fails. In recent times, researchers such as Loveless and Garner [53], Go and Pohlman [24] or Radmilović-Radjenović and Radjenović [79] have therefore developed adapted models to close this gap in the theory. They also emphasized the importance of field emission in small gap discharges. These breakdown models are schematically illustrated in Fig. 2.2. The electrode shapes and characteristics like sharp edges and micro protrusions on the electrode surface additionally enhances different breakdown phenomena. Since streamers and avalanches are already well discussed in EDM, the mechanism of field emission is discussed here more in detail.

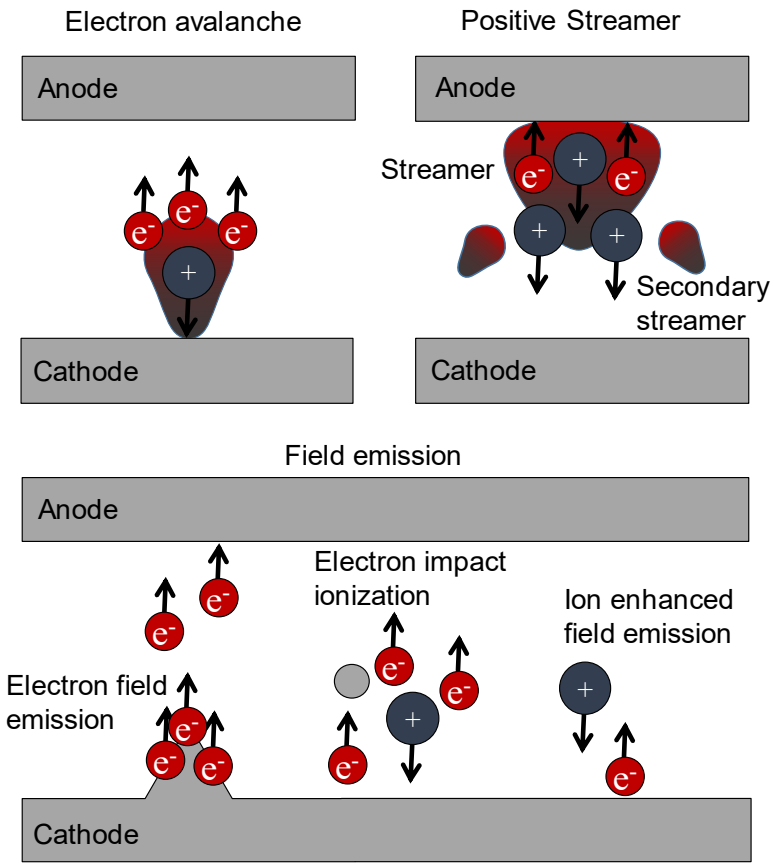

Fig. 2.2: Illustration of different breakdown mechanism

The classic electron field emission is strongly linked to the work function of the electrode material and surface integrity. Spikes and irregularities enhance locally the electric field enhancing the electrons to overcome the barrier. The theory of the ion enhanced field emission states that the presence of ions or positive charged particles increase the potential drop locally, thus increasing the field emission current [49]. Existing electrons ionize particles close to the electrode on impact enhancing this effect strongly. If those electrons collide with more ions on their way to the anode the process is called electron avalanche which is described by the Townsend mechanism.

2.3 Electrical discharge plasma

After the electrical breakdown, a plasma is formed, and current is conducted. Many kinds of plasmas exist, Fig. 2.1 helps to distinguish the different discharge plasma on basis of their electron temperature and density. There is a large number of books about plasma physics and the following basic information was taken from these books unless cited otherwise, [45,50,75,82,88]

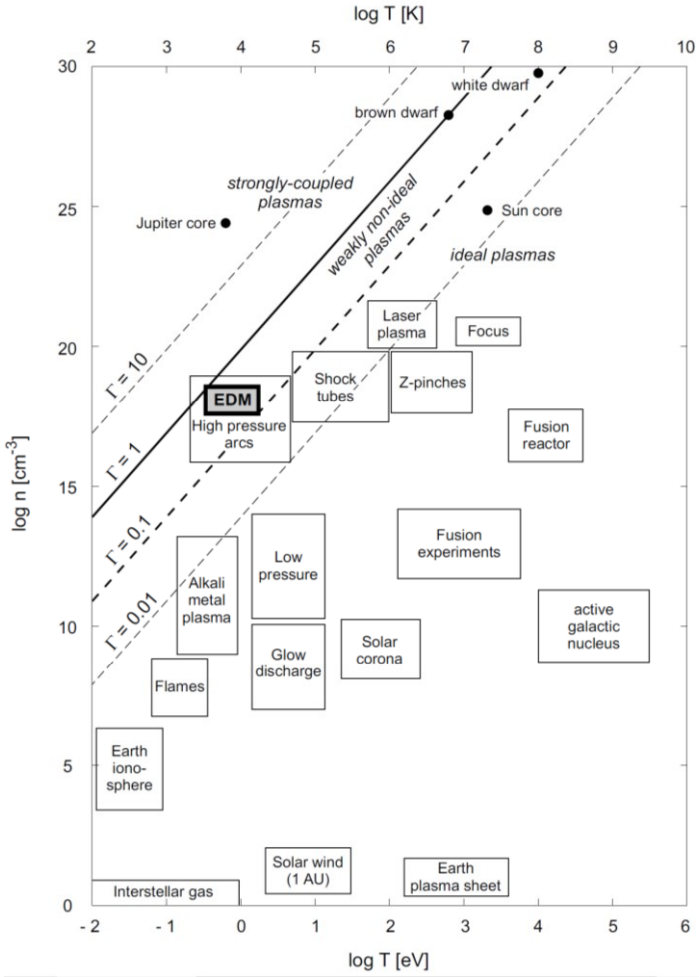

Fig. 2.3: Different plasma types according to their density and temperature [12]

The temperature of EDM plasma can reach tens of thousands kelvin. The density of those plasmas ranges roughly from 10^{15} cm^{-3} to 10^{19} cm^{-3}, therefore EDM plasmas are also described as high-pressure plasmas, as can be seen in Fig. 2.3. Thermal plasmas have equal electron and heavy particle temperature. Those plasmas have a high degree of ionization meaning the plasma is fully or nearly fully ionized.

The opposite are cold plasmas, non-ideal, non-thermal plasmas where the temperature and electrons and ions are strongly different. EDM plasmas are described as low-temperature plasmas. The individual properties and energy structure of the heavy particles define the plasma structure and the emission spectra. The energy distribution function (EDF) is often assumed as Maxwellian. In case all species have locally preserved the same temperature, the plasma is in a local thermodynamic equilibrium (LTE). This local equilibrium is mainly established because electron

collisions are much faster than ion collisions. Real thermal equilibrium (TE) over large volumes with all species having exactly the same temperature can only exist in extreme situations. Laboratory plasmas can be in LTE or even non-LTE as discussed for EDM plasmas in the dissertation work of Macedo [54]. Discharge plasmas used for material processing can be further distinguished in view of the discharge voltage and in the function of the discharge current as presented in Fig. 2.4.

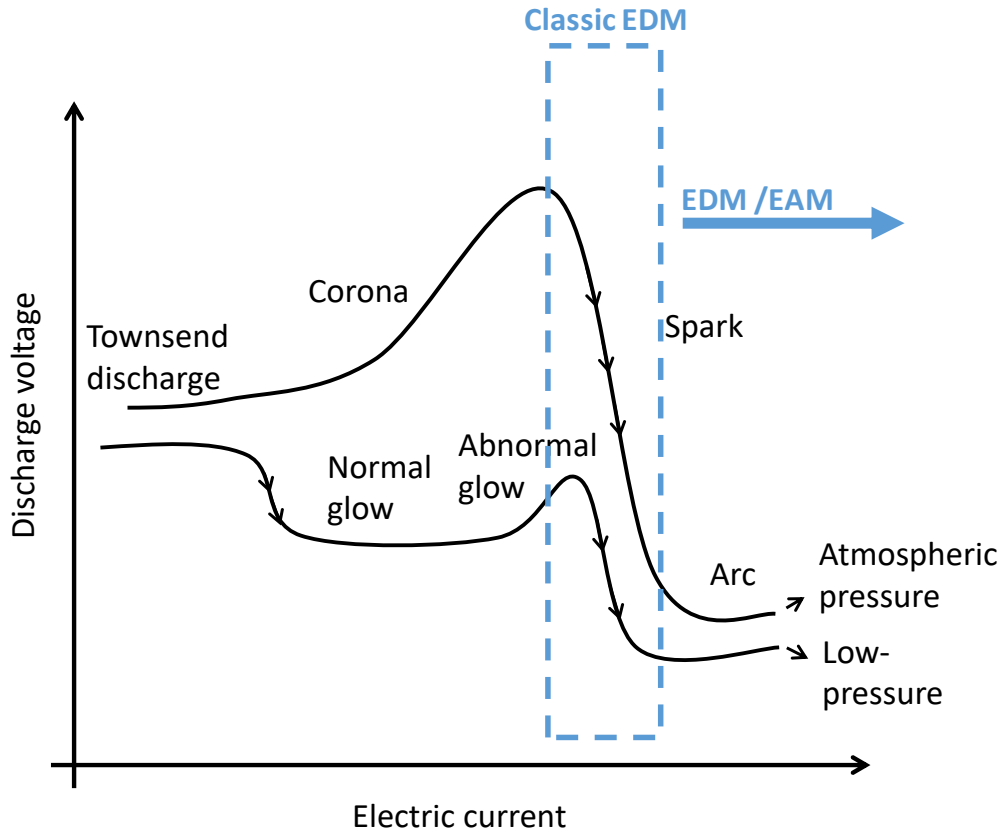

Fig. 2.4: Different discharge type characterized by voltage and current as adapted from [80]

Generally, EDM utilizes sparks and arcs, as described by Schumacher [86], where the spark is characterized by precise and good quality machining and arcs are “deteriorated”. Today, researchers distinguish between EDM, where sparks and short discharge duration which are usually preferred due to less surface damage and electrode wear, and EAM where arcs with high currents and long discharge duration are desired for high material removal rate as shown by Zhang et al. [97]. Blasting erosion arc machining (BEAM) goes even further aiming to blast away molten material explosively as shown by Zhao et al. [98].
A selection of different discharge types and their application can be found in Table 2-1

Table 2-1 Discharge types and its applications in EDM

Pulse duration	Pulse peak current	Application
Up to 3 µs	Up to 1,000 A	Wire EDM, high cutting speed
>0.5 ms up to several ms	>50 A	EAM [97] high material removal
50 ns	0.3 A	Super-finishing, high surface quality, in die sinking [64]
10-300 µs	1-40A	Regular die sinking, fast wire EDM, drill EDM

2.4 Anode and cathode phenomena

It is crucial to understand the processes that happen close to the electrodes surface to determine the thermal load onto the electrodes and the material removal. At the anode the situation is often less complex because electrons can just fall to the lower conduction band of the electrode material, therefore the anode is usually assumed to be mostly passive. Only at very high current the anode temperature rises, and the anode is actively involved in the discharge. At the cathode the situation is much more complex since the electrons must be pushed to a higher energetic level to overcome the barrier from the lower conduction band in the electrode to the higher potential in the inter-electrode space. Therefore, the situation on the cathode side is often the limiting factor for a discharge. The different situations and modes at anode and cathode are numerous and well described in Handbook of Vacuum Arc Science & Technology [8].

In EDM the situations are especially complex due to the use of very narrow gaps and due to the different dielectrics. The influence of the gap will be particularly important regarding material removal effects. Droplets and vapour can be deposited on the opposite electrode, strongly influencing the discharge and the electrode temperatures [18].

Cathode

In vacuum arcs literature the cathode phenomena are well investigated. As source of electrons, the cathode is usually highly active. The energy of the electrons must increase to overcome the lower conductive band of the electrode to the higher level of the inter-electrode space. There are several mechanisms, electrons can be elevated to the higher level singly e.g. by impact collisions or collectively with heating either by impact collision or joule heating.

Secondary electron emission describes a linear process where electrons leaving due to preliminary impacting particles. The electron emission depends among others on the impacting particle’s energy and the electrode materials respectively the work function. The emission current is proportional to the incident flux of particles and influenced by temperature and field strength.

Thermionic emission, where electrons with the highest energy leave the cathode is a non-linear process depending strongly on temperature and current.

The potential difference between inside and outside the electrode can also be lowered by an electric field enabling low energy electrons to leave the electrode. One already mentioned mechanism is an enhanced electric field caused by the presence of one or several ions at the electrode surface which significantly lowers the potential locally. Field emission of electrons is a collective effect and like thermionic emission non-linear. The most effective electron emission process is given by the combination of both thermionic emission and field emission, typically found in arcs.

In general, the situation on the cathode is described by active areas called cathode spots. There can be a single spot or multiple spots based on the spot spiting current, depending mainly on the electrode material. For the investigated materials and currents in this thesis, it can be assumed to observe one cathode spot maximum.

Spots reported in vacuum arc literature are generally non-stationary and move at high velocities ranging from 10-1,000 m/s. The spot motion is stochastic and influenced by the surrounding conditions like temperature and geometry of electrode surface. The reported internal spot pressures for vacuum arcs reaches values higher than 10 MPa. The radius of these spots is rather small and ranges from 1 µm to several tens of micrometre. After the discharge the observed crater radii are often larger that the observed spot radii during the discharge, because generally the crater is formed by material removal during the movement of the spot, point of impact of the discharge.

A detailed illustration of the cathode spot situation is given in Fig. 2.5.

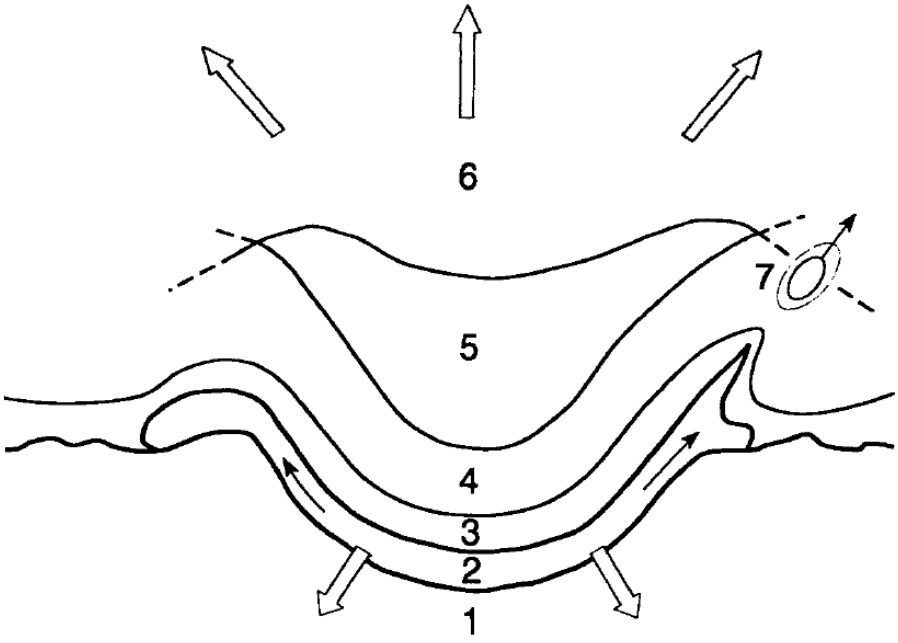

Fig. 2.5: From [29]: Schematic section of a cathode arc spot
(1) Solid metal cathode below the spot (arrows indicate current and heat flow);
(2) molten metal layer (3) space charge layer (4) ionization and thermalization layer of the spot plasma (5) dense central spot plasma; (6) plasma expansion region (plasma jet; arrows indicate plasma flow, current in opposite direction); (7) ejection of molten droplets.

Apart from vaporization and melt pool movement several explosive processes removing material of the cathode are reported. Mostly discussed is the so called “Thermal runaway”. If the deposited energy flux is larger than the heat transfer into the bulk, the surface temperature rises uncontrolled, and material can be directly vaporised and ionized resulting in explosions removing material and forming a crater. A phenomenon which also can be observed are plasma jets, a stream of exited or ionised atoms ejected from the electrode surface.

The cathode can be also spotless. In this case, the cathode must provide emission of atoms (evaporation) and electrons at the same time. At high cathode temperatures, steady-state thermionic emission could fulfil this requirement strongly depending on material properties like work function.

Anode

Normally, the anode situation is simpler because there is no potential barrier. Compared to the cathode, less research has been done. Nevertheless, anode activity can be observed in EDM by material removal or spectroscopy [42]. Based on spectroscopic results with dominating anode species in the plasma Macedo et al. [58] suggest, based on spectroscopic results, that dry EDM discharges are similar to hot anode vacuum arc (HAVA). Based on observations three “active” anode modes are described in the literature and a summary is presented in Table 2-2.

Table 2-2 Electrode phenomena adopted from [66]

Modes		Anode spot	Intense arc	HAVA
Specials		Highly ionized species	Narrow gaps very bright luminosity fills interelectrode gap.	Low cathode activity
Luminous Areas on Anode	Spot number	1 - few	1	1
	Size	Medium to large	Large	Large
	Brightness	Bright	Bright	Bright
	Temperature	Boiling	Boiling	Melting - boiling
Erosion	Anode	Moderate	High	Moderate
	Cathode	High	High	Low up to negative erosion / build up

The modes presented can change during the discharge, either caused by erosion or external influences. E.g. the mode can change from the anode spot mode to the intense mode or HAVA, this usually involves an anode jet striking the cathode as reported by Boxman and Goldsmith [6,7].

Cathode and anode interact with each other e.g. by particle exchange and thereby also influencing the phenomena observed on each of the electrode surfaces. One can assume that on small gap discharges these phenomena are even more influenced by

the electrode activities like vaporisation and particle removal and might differ from what is observed in large gap discharges.

2.5 EDM plasma and optical emission spectroscopy – OES

Optical emission spectroscopy is a widely applied tool to analyse plasmas in various disciplines. Especially in stellar plasmas or microplasmas where measurement devices like the Langmuir probe are not an option. Plasmas are emitting photons with characteristic energy, the observation of these characteristic spectra of the light reveal properties of the plasma, like density of ions, temperature, species and many more.

Among other methods OES is also a well-established method in EDM research and used by many researchers as reported in the overview over of visualization techniques for EDM by Kunieda et al. [43]. Already 1965 this method was used to estimate the energy consumed by ionization and researches tried to find a physical formula describing the EDM process with the removed material in gram/discharge as possible output parameter depending on the energy input [47].

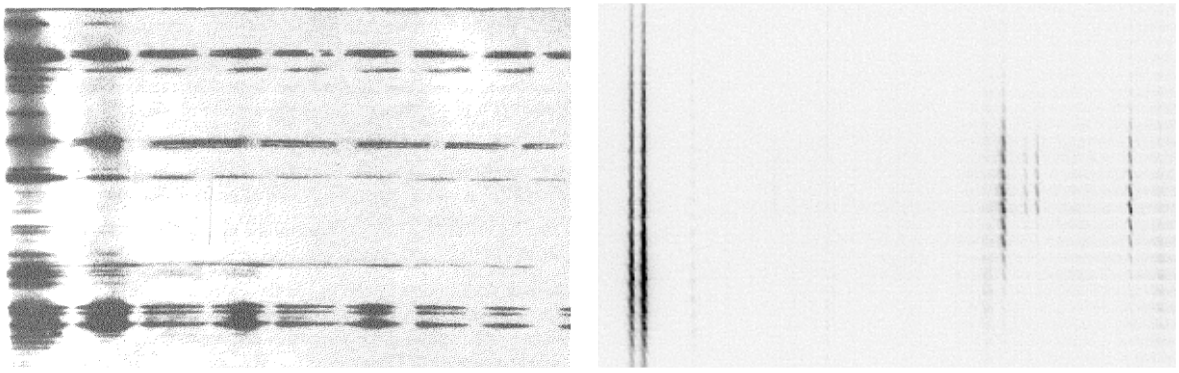

Fig. 2.6: Photographic recordings of a EDM discharge spectra between aluminium electrodes Right: Lazarenko and Krasyuk [47] (1964), axes labelling unknown. Left from this thesis (2020) x-axis wavelength y-axis spatial resolution.

Optical emission spectroscopy in EDM is generally used to estimate the plasma properties like temperature and density or the elementary composition of the plasma.

Generally, researchers use this method to characterize EDM plasmas in respect to other plasmas observed and researched in physics. In addition, a connection of plasma physics to material removal and crater formation or an estimation of heat sources is targeted. Results are often supported by high-speed imaging.

Although the analysis of EDM by spectroscopy was not new in 2004, A. Descoeudres under the guidance of C. Hollenstein initiated a restart of this research topic at the EPFL in Switzerland, which several researchers from IWF at the ETH Zürich have followed. The plasma was analysed by spatially and time-resolved spectroscopy and pre-breakdown phenomena were investigated. Descoeudres [12] describes EDM plasmas with low temperatures of approximately 8100 K and high electron densities at the beginning of $2 \cdot 10^{18}$ cm^{-3} and lower values of 10^{16} cm^{-3} at the

end of the discharge. He describes the EDM process and his physics involved as astonishingly complex with extreme physical properties.

FTB. Macedo and M. Wiessner published several papers about discharges in liquids and especially gaseous media using emission spectra simulation as a tool to identify plasma parameters and investigate the discharge phenomena. Among others, a theory of hot anode vacuum arc (HAVA) [58], the possibility of non-LTE plasma condition [56] and a model to estimate the anode power deposition [59] are discussed.

Several researchers under the guidance of M. Kunieda investigated EDM discharges in the past years. Kunieda and Kobayashi [42] used OES to estimate the copper vapor density in the EDM arc plasma. This information was used to explain the wear phenomena on copper electrodes for discharges in oil. When copper is used as cathode, evaporation of material is lower than when used as anode. Especially with short pulse duration evaporation of anode material dominates. This was explained with a protective carbon layer on the anode.

Natsu et al. [72] used spatial OES to describe EDM plasmas with different currents and discharge gaps. Smaller electrodes and larger gaps and higher currents showed higher plasma temperatures. A radial temperature profile was observed. The crater formation was linked to a fast expanding plasma derived by Natsu et al. [73] from high-speed imaging. He based on the fast-expanding plasma and the temperature profile he assumed a normal distributed heat source profile for carter generation.

Kojima et al. [39] continues the research, investigating the heat sources and erosion results. The researchers also observed an increasing arc plasma diameter with larger gaps and stated that this the reason for lower material removal rate and smoother surface roughness. Based on the almost uniform plasma temperature distribution he observed, the heat source was assumed to be a radial uniform but expanding over time. The plasma itself was found to be five times larger than the crater.

Maybe the most famous approach is the analysis of the EDM discharges with transparent electrodes by Kitamura and Kunieda [32-34,41]. With this technique the plasma diameter and molten area could separately observed with highspeed imaging. The researchers state that expansion of both the plasma and crater diameters is much quicker in the early stage of discharge duration, and the expansion speed is higher with discharge in air than in liquid. Theoretical heat conduction analysis showed that the heat source diameter must be significantly smaller than the plasma diameter, otherwise melting temperature cannot be reached. The spatial plasma temperature was classified as relevant and the heat distribution cannot be uniform but concentrated at the centre of the plasma.

Nagahanumaiah et al. [71] tries to separate micro EDM from EDM and like other researchers identifying electrode size and spark gap as important influence factors which are inevitably small in micro EDM.

Gu et al. [26] investigated EAM discharges respectively blasting erosion arc machining with OES and high-speed imaging. The calculated arc temperature values fluctuate largely even under the same discharge condition with planar workpiece and point tool electrode. For those long 10 ms discharges the positive polarity shows larger and deeper craters on the workpiece than those generated in negative polarity.

The most ambiguous approach was recently published by Mujumdar modelling the whole physical process of EDM in water considering plasma chemistry, power balance and Bubble dynamics [69]. The plasma model can estimate the plasma composition, pressure, temperature and the heat flux to the electrodes, with this information a second model estimates the crater formation [70]. Later he also investigated the plasma experimentally and confirmed higher temperatures estimation for CR models than in with the two-line Boltzmann method [68].

Apart from dielectric and electrode materials many researchers agree that gap and current have major influence on the EDM process respectively the EDM plasma and link this observation also based on the observed plasma temperature. Table 2-3 shows the plasma temperatures estimated by several researchers and their setups in respect to current and discharge gap. The temperatures are very similar when using the two-line Boltzmann method even though the setups are different. Plasma temperature estimated by the two-line Boltzmann method alone do not seems to be a very good key indicator to quantitatively describe and differentiate the EDM process under different conditions.

Table 2-3 Plasma temperatures in EDM estimated by several researchers

Researchers	**Current [A]**	**Gap [µm]**	**Plasma temperature [K]**	**Dielectric**
Descoeurdes et al. [13-16]	0.5 – 64	10 – 100	8,100 ± 1,750	Water, liquid nitrogen, oil
Natsu et al. [72,73]	20 – 40	500 – 1500	3,500 – 8,000	Air
Kojima et al. [39]	4 – 53	50 – 500	8,000	Air and oil
Nagahanumaiah et al. [71]	2 – 3	50 – 3000	6,170	-
Kitamura and Kunieda [32]	20	-	5,000 – 8,000	Air and oil
Macedo and Wiessner et al. [55-59,94]*	2 – 40	5-40	10,000 – 25,000	Air, oil, argon
Gu et al. [26]	50 – 200	Large	7,000 – 10,000	Water-based dielectric
Mujumdar et al. [68]*	-	1	10,000 – 12,000	Water with different conductivities

*Researchers used additional CR Models for temperature estimation

Because of the already mentioned complex situations and the many mechanisms in electric discharges it is often not possible to make a simple comparison, not only because of the many different experimental setups, electrode shapes and discharge conditions that exists but also because of the used measurement equipment. As already stated by Kojima et al. [39] results depends strongly on equipment's settings.

In general researchers and their publications agree to the following states and facts of the EDM process plasma:

- It is generally assumed that EDM plasmas are LTE Plasma
- To be able to observe the small gap discharges usually the gap is artificial enlarged, and the discharge is ignited with the help of a liquid droplet, thin wire or particles in the gap.
- In some publications radial temperature profile are observed in others not
- Plasma temperatures roughly around 8,000 K when the temperature is estimated by the so-called two-line method and up to factor two higher with plasma simulation but usually not higher than 25,000 K.
- Electron densities are reported roughly in a range from 10^{16} cm^{-3} - 10^{18} cm^{-3}
- The change of the polarity has not only an influence on electrode wear but also on the plasma composition
- Plasma expansion and crater formation do not match. The plasma is most likely not homogenous, a point to be discussed with this thesis.
- In general, observations and plasma parameters can change based on the electrode material and shape, the used dielectric and electrical parameters used.

EDM process simulation

As for other manufacturing technologies, EDM is a process which is often modelled and simulated to improve and understand the process.

Several researchers developed different models to describe how single craters or even entire surfaces are generated by EDM discharges. The single discharge models are physically complex as schematically shown in Fig. 2.7. Most of the models and simulations only deal with the power deposition onto one electrode and the resulting melt pool. Plasma models of the EDM discharge are rather rare and not very much developed. The not well-known plasma properties lead to unknown and speculative boundary conditions.

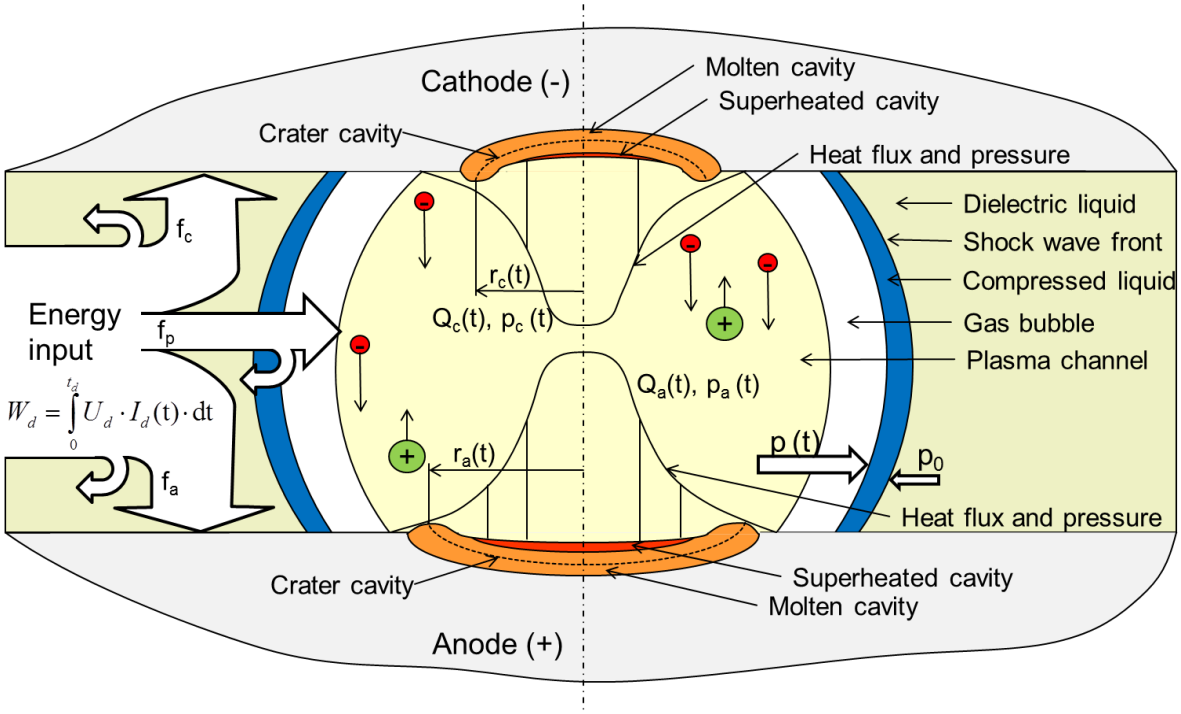

Fig. 2.7: Energy balance, crater formation, heat flux and pressure distribution during single discharge in EDM [35]

The boundary conditions for single crater models are usually taken from observations, which are either post-discharge analysis like the crater formation or real-time measurements like current and voltage as well as high-speed footage or spectroscopic observation of the plasma. Table 2-4 shows a summary of thermal EDM single crater models with respect to their heat source design. Most of these models are based on a gaussian heat source, as this is well accepted. Comparable processes like laser or welding have shown good results using this heat source design in simulation. Even though some models from researchers seem to match the experimentally observed craters precisely, most of the crater's models fail in the real prediction because many models are only fitted to individual craters. The reason for this is the complexity of the process, the seemingly random crater size and the lack of knowledge about the heat source.

It is important to know where simplifications are allowed, e.g., simplifying the heat source to a disc with constant energy. Currently it is not uncommon that researches observe different phenomena in very similar setups. Natsu et al. [73] developed a model with a fast expanding cylindrical gauss heat source with is constant after a few microseconds, whereas Kojima et al. [39] continues with a uniform model. Further investigations are needed to also increase the knowledge and solve questions like why for the same parameters and setups large differences in crater geometries are observed.

Table 2-4 Comparison of different single crater numerical models from 1971 to 2019 adapted from [35]

	Fraction of energy	Heat flux distribution	Dimension of the heat source	Expansion of the heat flux
Van Dijck's model [91]	$F = 0.5$	Uniform heat flux	Disk heat source	Constant heat flux
DiBitonto's model [17,76]	$F_c = 0.18$	Point heat source	Point	The plasma radius remains small during the discharge
Das's model [11]	$F_c = 0.18$	Gaussian heat flux	Disk heat source	Constant heat flux
Yeo's model [96]	$\mathrm{F_a} = 0.39$ $\mathrm{F_c} = 0.14$	Uniform heat flux equivalent to Gaussian	Disk heat source	Experimentally defined expanding heat source
Weingaertner's model [93]	$\mathrm{F_c} = 0.35$	Uniform heat flux equivalent to Gaussian	Disk heat source	Heat source expands from 5 µm to 80 µm
Tao's model [89]	$\mathrm{F_a} = 0.39$	Gaussian heat flux	Disk heat source	$\mathrm{r_c} = 0.788\,\mathrm{t_d^{3/4}}$
Mujumdar's model [70]	Calculated from plasma	Gaussian heat flux	Disk heat source	Time dependent heat source radius (from plasma model)
Kliuev's model [36]	Fitted	Uniform heat flux	Disk heat source	Experimentally fitted heat source

2.6 Predecessor works in the field of EDM

This thesis has some important EPFL/ETH predecessor works in the field of EDM shortly described in the following:

Descoeudres (EPFL, 2006) Characterization of electrical discharge machining plasmas [12]

This work gives a deep insight into the plasma physics for the EDM process, from the perspective of a physicist. From breakdown to plasma, with tools like optical emission spectroscopy and high-speed imaging, the processes were investigated involving various materials and dielectrics. This thesis has become a standard reference for the plasma physics of the EDM processes.

Maradia (ETH, 2014) Meso - Micro EDM [61]

Closing the gap between industrial application and fundamental research this thesis does not only deal with challenges in micro EDM but also analysed the EDM plasmas with tools like high-speed imaging and Optical emission spectroscopy (OES). Optical emission spectroscopy was introduced the first time to the IWF as a diagnostic tool for plasma analysis.

Raoul Roth (ETH, 2015) Trockene Funkenerosion [83]

In this the work dry EDM is thematized. The process has been studied in detail to investigate the suitability of different gases and process parameters on the material removal rate for different materials. Despite some advantages, dry erosion is rare in industry and more common in EDM micromachining.

Macedo (ETH, 2018) Fundamental investigation of dry EDM plasmas [54]

This thesis continues the research at IWF in dry EDM with the goal of better understanding of the fundamentals by introducing time-resolved emission spectroscopy of dry discharges and optical emissions spectra simulation as a tool for EDM discharge analysis. Furthermore, the hypothesis of an inhomogeneous, non-LTE plasma produced from an anode dominated discharge behaviour was discussed.

3 PROBLEM DESCRIPTION AND OBJECTIVES

Several researchers developed different models to describe how single craters or even entire surfaces are generated by EDM discharges; however, none of such models is widely accepted by the research community due to their very limited application range, since EDM can be performed under many different parameters and working conditions. Standard methods to estimate material removal rates, heat affected zones or workpiece surface roughness generated by EDM are currently lacking due to the complexity of the process. Therefore, to formulate theories that are more sophisticated and to develop models with correct boundary conditions, observation and analysis of the physics of the process are necessary.

Electric discharge plasmas must be observed in-situ, so that its physics can be properly described. During the last decades, a relatively small amount of investigations was published concerning in-process observations of EDM plasmas. The reason for the small number of publications is the fact that EDM discharges are very difficult to diagnose due to their small dimensions and short duration.

Optical observations require cameras and optical systems able to record with high frame rates, low shutter times, high sensitivity, high resolution and magnification. Visual access to the process is limited due to the small gaps in which the discharge occurs, within a typical range between 4 and 50 µm. This either requires an endoscope or a special design of the optical experimental setup. Regarding the plasma analysis, in-situ probes cannot be used as a diagnostic method due to space restrictions. Therefore, other alternative plasma diagnostic methods need to be applied, such as high-speed imaging and optical emission spectroscopy.

The presented thesis has the following two main directives:

1. Improve EDM discharge diagnostics

To investigate small gap discharges a special experimental setup and special measurement equipment is needed. This setup must also deliver data in an unprecedented temporal and spatial resolution of the discharge plasma within the gap to discuss and verify recent published theories and develop new plasma models. Ideally the setup should be able to cover high-speed imaging and spatial and time-resolved optical emission spectroscopy. The comparison of results from both methods substantiates the presented theories.

A software automatically post-processing the raw data is an absolute prerequisite for the analysis of the immense number of spectra. In addition, the experimental setup should ideally allow the plasma to be axisymmetric in order to apply properly methods getting correct radial emission line spectra. For plasma parameter identification a method must be developed to extract information from the many emission profiles and the plasma parameter profiles. This is done by inverse parameter identification with PrismSPECT, a collisional-radiative (CR) code for optical emission spectra simulation. Investigations suggest that CR-Models deliver more reliable results. The possibility to

investigated also non-single Maxwellian energy distributions is another reason why the use of a CR-Model is preferable over simple mathematics using e.g. two lines comparison for plasma analysis.

2. Advanced physical understanding of the process

To improve the physical understanding of the EDM process the setup and methods for analysis of micro gap discharges developed within this work are used to investigate typical EDM discharges between aluminium and copper electrodes.

Profiles of different plasma parameters, such as electron density and temperature, should be evaluated and compared with the results deduced from emission spectra simulations reported in the literature. The characterization of the plasma properties as function over radial coordinates should also improve the understanding of inter-electrode plasma and the cathode and anode phenomena. The following questions are to be addressed in this context:

- Do EDM plasmas exist in local thermodynamic equilibrium?
- Do EDM plasmas have homogenous properties over the whole discharge area, or do radial profiles exist e.g. for the temperature?
- How do plasma properties behave spatially and over time, and what can be the reasons for changes of those properties?

Additionally, recently reported investigations with non-spatial resolved OES suggesting that EDM discharges performed in air are similar to hot anode vacuum arcs (HAVA). Anode and cathode phenomena are investigated with newly developed methods in detail and estimated whether common discharge theories can be applied to micro gap discharges or not.

The thesis is divided into 8 chapters. Chapter 1 to 3 covering the state of the art and the objectives. Chapter 4 is focusing on measurement setup and analysis procedures. Chapter 5 addresses the open question of the plasma equilibrium in EDM-like discharges. Additionally, several plasma properties and their spatial profiles are discussed. Following, an overview of the plasma properties with different currents can be found in Chapter 6. Chapter 7 gives a deeper insight into anode and cathode phenomena observed and several annotations of influencing factors. Finally, in chapter 8 the reader can find summarized conclusions and an outlook for further research.

4 EXPERIMENTAL SETUP AND ANALYSIS TOOLS

This chapter describes all setups and measurement equipment used in the experiments. The data processing and all numerical methods used for interpretation of the measurements are explained in detail.

4.1 EDM machine and electrical parameters

For the single spark experiments, an AgieCharmilles Form 1000 is used. This machine was modified to create singly controlled capacitors and transistor discharges.

Fig. 4.1: AgieCharmilles Form 1000 with an axis resolution of 0.1µm

In this work only transistor discharges are investigated with a square wave shaped current profile. The most important EDM process parameters are given in Table 4-1.

Table 4-1 Process parameters

Variables of the process	Working conditions
Open voltage (U_{open})	250 V
Electric current (I)	20 A, 15 A, 10 A, 5 A and 2A
Pulse duration (t_{on})	100 µs
Electrode geometries	Point-type
Electrode polarity	Positive and negative
Dielectric media	Air at atmospheric pressure;

The electrical discharge parameters are measured using voltage and direct current probes with a LeCroy Wave Runner 44MXi-A oscilloscope. Typically used voltage and current forms are shown in Fig. 4.2

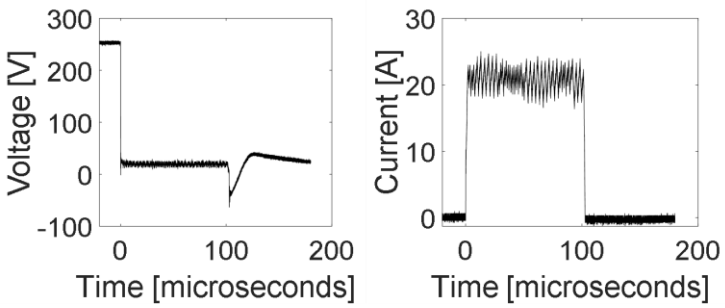

Fig. 4.2: Typical 20 A 100 µs discharge, measured electric voltage (left), discharge current (right)

4.1.1 Electrode configuration and materials

The major problem of in-situ observations in EDM are the very small gaps. The light created by electrical discharge is mostly absorbed, reflected and scattered by the electrode surfaces. The very short time span in which the discharge occurs also limits the observability. To maximize the observation window, to receive a maximum of light and to minimize noise several point electrode configurations were tested. Sharply tipped electrodes yield the best observability. The electrodes are machined by turning or laser ablation. The tip shape and sharpness was improving the repeatability. The best geometrical quality was achieved by picosecond laser ablation with an Amphos 200 laser, as seen in Fig. 4.3, right electrode. With the laser machined tips therefore the most repeatable and reliable results can be obtained.

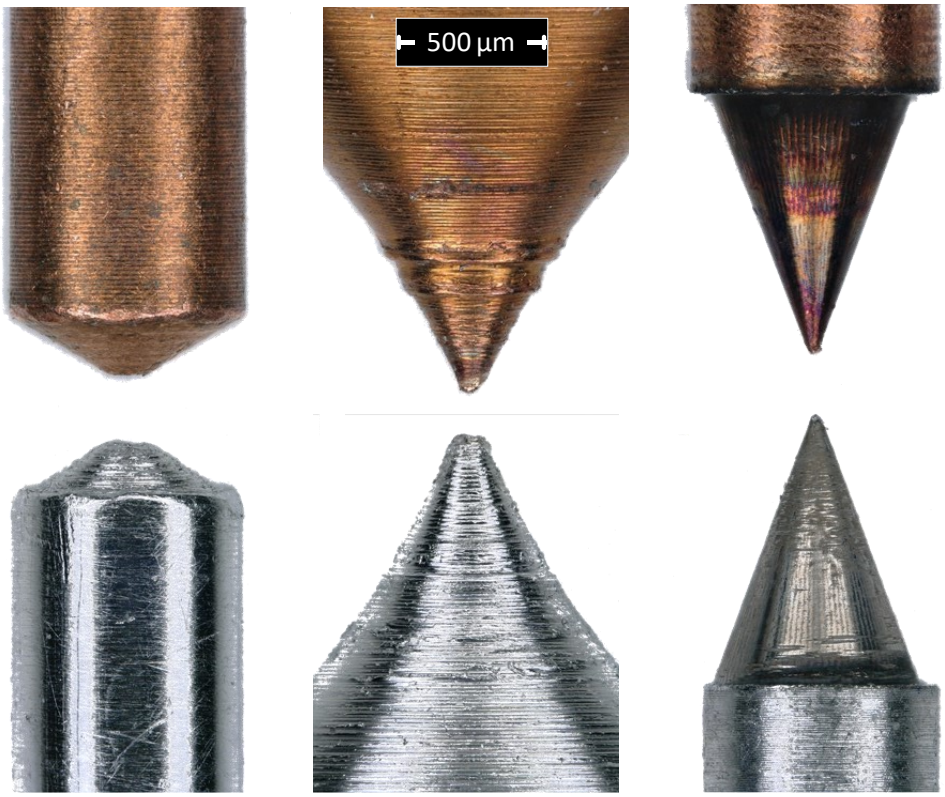

Fig. 4.3: Example of different point electrodes used, from left to right: conical tip (disc plane, radius 70 µm) and sharp tip machined by turning (sphere like tip, radius 30 µm) , and very sharp (sphere, radius 10 µm) tip machined by laser ablation. Images acquired and measured with Keyence VHX-5000

The electrode configuration used is point to point, with copper as tool, clamped always as top electrode and aluminium as the workpiece, clamped as bottom electrode. Both materials have well known and investigated emission lines which is important for the plasma analysis. The material properties for copper and aluminium, which are important parameters for the EDM process, are given in Table 4-2. The work function describes the energy needed to extract electrons from the bulk material and the spot splitting current describes how many spots (Table 2-2) will exist on the electrode surface. In the case of 20 A maximum one cathode spot can be expected.

Table 4-2 Properties of the used materials [8,85]

Properties	**Copper**	**Aluminium**
Element number	29	13
Melting point [K]	1356	832
Boiling point [K]	3150	2621
Density [$g \cdot cm^{-3}$] @ 298 K	8.92	2.71
Melting enthalpy [$kJ \cdot mol^{-1}$]	13	10.6
Evaporation enthalpy [$kJ \cdot mol^{-1}$]	325.7	303.4
Specific heat capacity [$J \cdot kg^{-1} \cdot K^{-1}$]	385.43	902.78
1.Ionisation energy [eV]	7.72	5.98
2.Ionisation energy [eV]	20.29	18.82
Thermal conductivity [$W \cdot m^{-1} \cdot K^{-1}$] @ 298 K	406.0	237.5
Electrical conductivity [$A \cdot V^{-1} \cdot m^{-1}$] @ 293 K	$58.8 \cdot 10^6$	$38.2 \cdot 10^6$
Work function [eV]	4.4 (solid) 5.5 (liquid)	4.25(solid)
Spot splitting current [A]	75-100	30-50

4.2 High-speed imaging

For high-speed and spatial resolved optical emission spectroscopy and for high-speed imaging a Phantom v12.1 high-speed camera is used. The most important key features of the used camera are shown in Table 4-3.

Table 4-3 Technical specification of the high-speed camera

RAM	32 GB
Timing	20 ns
Maximum resolution	1280x800
Frame rate at 1 Megapixel	6,242 FPS
Pixels size	20x20 µm
Grey levels	12 bit
Maximum framerate	10^6 fps at 128x8 pixels

The high-speed camera is triggered by the oscilloscope via the rising current signal. The high-speed images are continuously recorded and stored in a ring buffer,

while the trigger just indicate the first frame. Hence the time point of the first image cannot be controlled and the time between the trigger respectively current rise and the exposure time varies for each recording. The saving time is 300 ns constant, for 10^6 fps the minimum exposure is 700 ns. For lower frame rates the pause and exposure can be controlled, within the range of the frame rate as illustrated in Fig. 4.4.

Best high-speed imaging results are obtained with a 5x ultra macro objective with a focal length of 24 mm and an aperture of f/2.8 from Venus Optics. This allows still high working distance from the discharge of 4 cm at maximum level of magnification as well as the high light accumulation due to large lenses compared to microscope lenses. With this combination of magnifying lens, images with a frame rate of $4 \cdot 10^5$ fps (exposure 2.2 µs) and resolution 4.25 µm/pixel could be achieved.

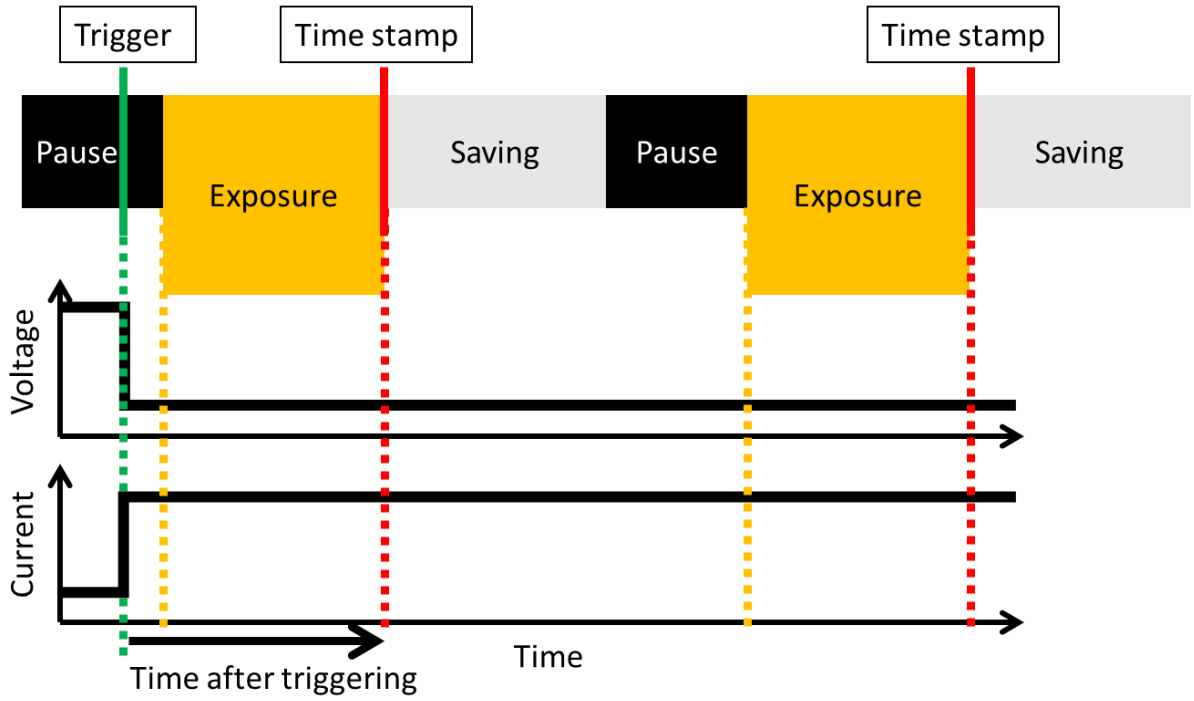

Fig. 4.4: Schematic of the triggering and time stamp in high-speed observations. The oscilloscope is triggering the high-speed camera at the rising edge of the current and thereby marking the first frame in the discharge. The time stamp reflects the time passed from triggering after each frame's exposure time.

This allows insights into the erosion process, the plasma development and the crater formation. The plasma diameter and plasma expansion are obvious parameters to observe. But as Kojima et al. [39] already mentioned the sensitivity for each camera sensor is different. Therefore, overexposed images are not a good tool to make quantitative statements about the plasma because the. Those results from high-speed images are difficult to compare between researchers. Much worse, results from overexposed images lead to incorrect assumptions regarding the plasma diameter and the area where the plasma is mainly interacting with the electrode material. Therefore sometimes erroneously the final crater shape is directly defined by the plasma diameter.

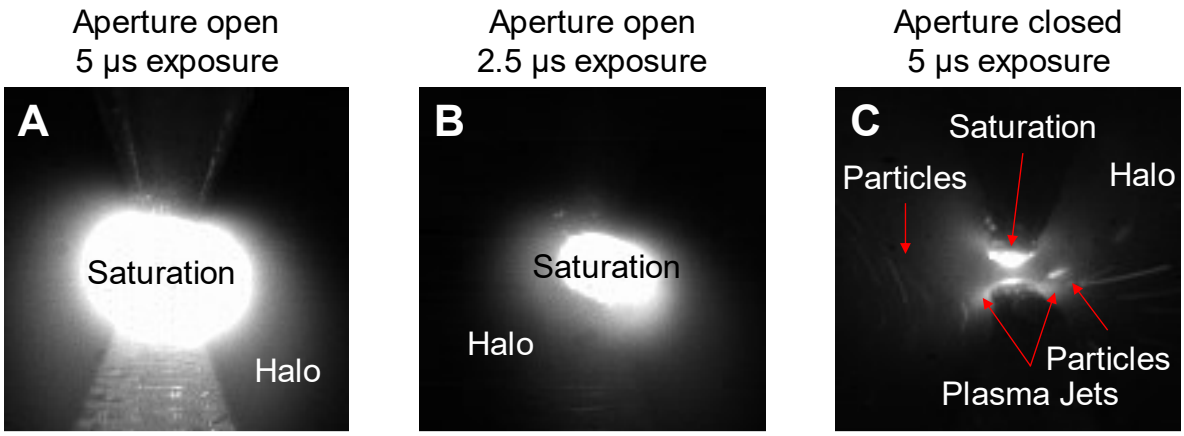

Fig. 4.5: High-speed imaging of a 5 A discharge with different camera settings

The influence of exposure time and aperture setting on the plasma radius measurements can be seen comparing Fig. 4.5-A and Fig. 4.5-B. A quantitative plasma radius analysis is not reasonable. Observations of discharge details can be achieved at low exposure time and small aperture as seen in Fig. 4.5-C. Much more details can be observed. The strongest light emission is not coming from the gap as one might interpret from Fig. 4.5-B but originates from the electrode tips in this observed case. Besides, plasma jets, halo and moving particles can now be observed. To further increase details and extract more information from the images the use of artificial colouring is helpful. In Fig. 4.6 the same 5A discharge is visualized applying different colourmaps.

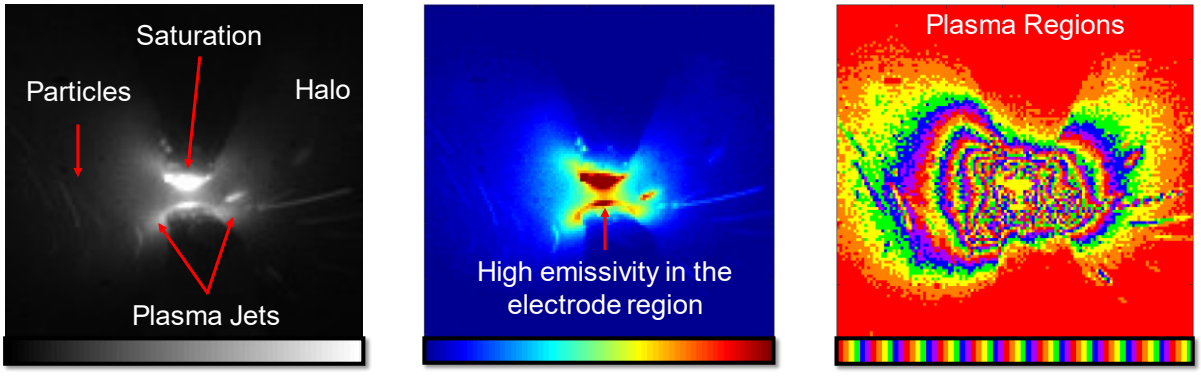

Fig. 4.6: High-speed imaging of a 5 A discharge with different colouring, right grayscale, middle jet scale highlighting the emission intense regions, left prism scale indicating the gradient of emissivity and the size of the plasma

The greyscale colouring shows particles, plasma jets and the halo. The colouring the same image with colormap jet, seen in the centre illustration in Fig. 4.6, highlights the high emissive regions at the electrode tips. The colormap prims, illustration on the right, is particularly suitable to visualize the plasma and the plasma expansion as well as the light emission gradient of the plasma by the different coloured contours. This illustration leads to similar observations for the plasma as the saturated image in Fig.

4.5-A. With artificial colouring a larger scale of observations can be covered than only with normal grayscale and overexposure images.

Plasma movement

At very high time resolution, also the movement of the plasma and plasma root can be observed. This is an important information because mathematical methods to convert the axial observations of the plasma to a radial information require symmetry.
Additionally, the information gained by optical emission spectroscopy might be blurred at high exposure times through this movement.a
Therefore, for the used spatial resolved optical emission spectroscopy (OES) setup, the exposure time was lowered to 10 µs to ensure a good signal to noise ratio. A saving time of 32 µs is chosen which is necessary to have a sufficiently high image resolution resulting in a frame rate of 23809 Hz or one frame each 42 µs.

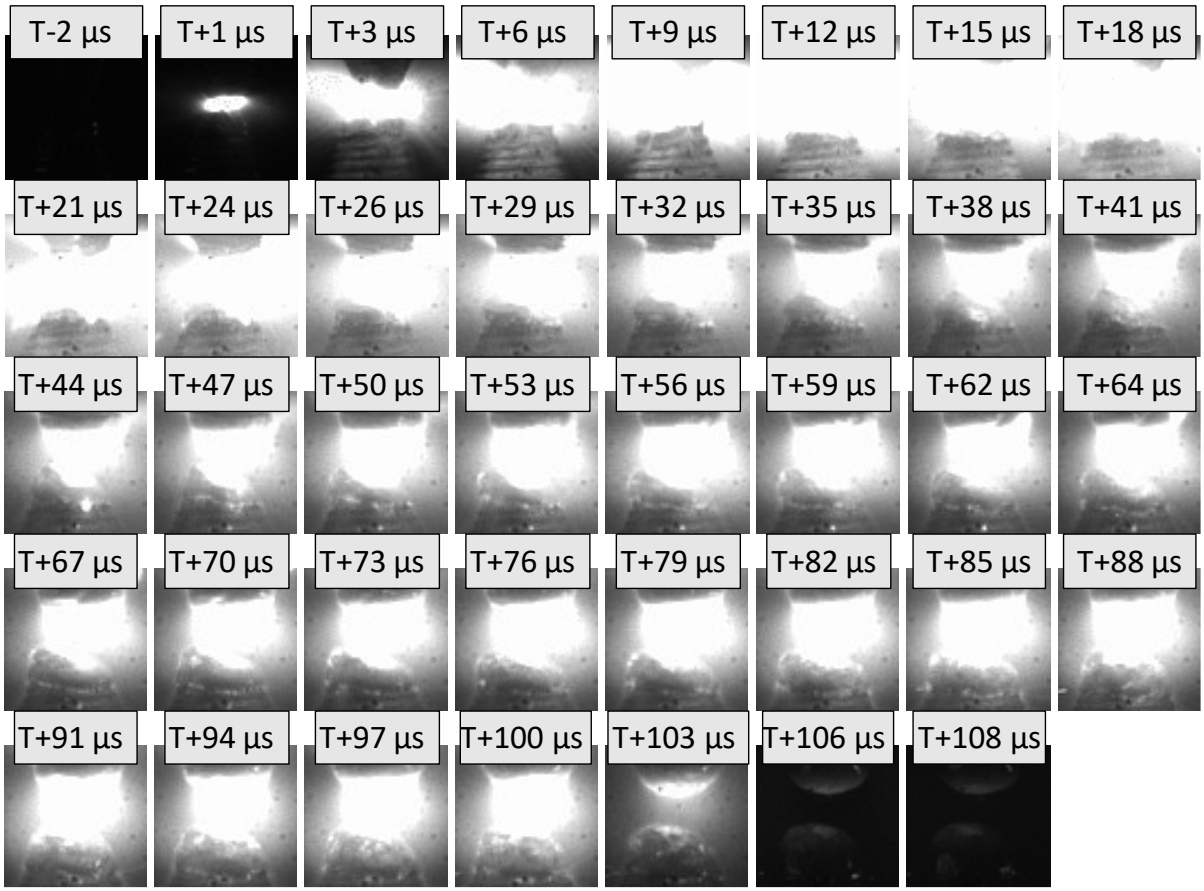

Fig. 4.7: High-speed imaging of a 20 A and 100 µs discharge between two sharply turned electrodes top aluminium bottom copper, the index shows the time after the trigger signal

The observation time series of images for 20 A and a 100 µs discharge presented in Fig. 4.7 shows that a stable and nearly axisymmetric plasma over nearly 100 µs of the discharge is found between sharply tipped electrodes. In contrary, Fig. 4.8 shows a less defined point electrode, the plasma channel is heavily moving. In both figures, Fig. 4.7 and Fig. 4.8, the formation of the melt pool and crater can be observed.

Particularly in Fig. 4.8 for 15 µs until 47 µs the flow and ejection of the liquid material and an arc movement can be seen.
The sharply tipped electrodes machined with laser-ablation, introduced in Fig. 4.3, showed the best results and repeatability and were used in optical emission spectroscopy analysis.

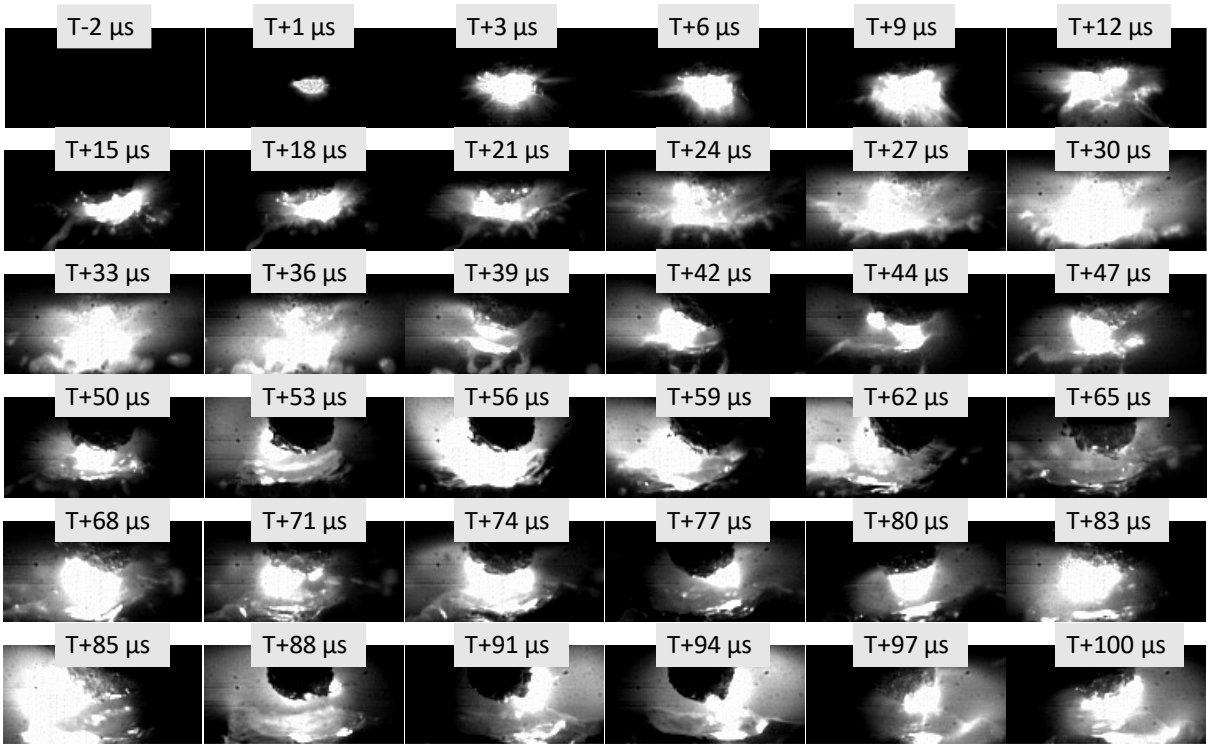

Fig. 4.8: High-speed imaging of a 20 A and 100 µs discharge between point electrodes worn after several discharges and thus geometrically undefined, top electrode copper negative, bottom aluminium, the index shows the time after trigger

4.3 Optical emission spectroscopy OES

For high-speed optical emission spectroscopy (OES) an Acton Research spectrograph SP2556, Czerny-Turner setup, was used with three installed gratings on the turret, technical details see Table 4-4. Mainly the 150 g/mm grating was used due to the wide observation area of 351 nm.

Table 4-4 Spectrograph SP2556 specifications

Focal length	500 mm
Aperture ratio	f/6.5
Wavelength scan range	0 - 1400 nm
Focal plane size (front exit port)	25 mm wide x 10 mm high
Astigmatism (at focal plane edges)	250 - 300 µm
Slits	10 µm to 3 mm
Wavelength accuracy	± 0.2 nm
Repeatability	± 0.05 nm
Drive step size	0.005 nm
Gratings:	Resolution - Range
150 g/mm	13.1 nm/mm - 351 nm
600 g/mm	3.2 nm/mm - 85 nm
1800 g/mm	0.94 nm/mm - 25 nm

The experimental setup is shown in Fig. 4.9. An oscilloscope is used to trigger the high-speed camera and observe the electrical discharge conditions. A computer is needed to control the high speed camera and another computer is used to observe and adjust the small electrodes with a USB microscope in the form 1000 EDM from GFMS machine. This is necessary since the electrode are very fragile and the adjustment of the point tipped electrodes must be very precise. Additionally, optics for the observation must be adjusted carefully in all three spatial directions: In the direction of the optical axis of the setup the plasma channel must be in the focal plane and in the middle of the fibre array to obtain as much light as possible from the plasma centre.

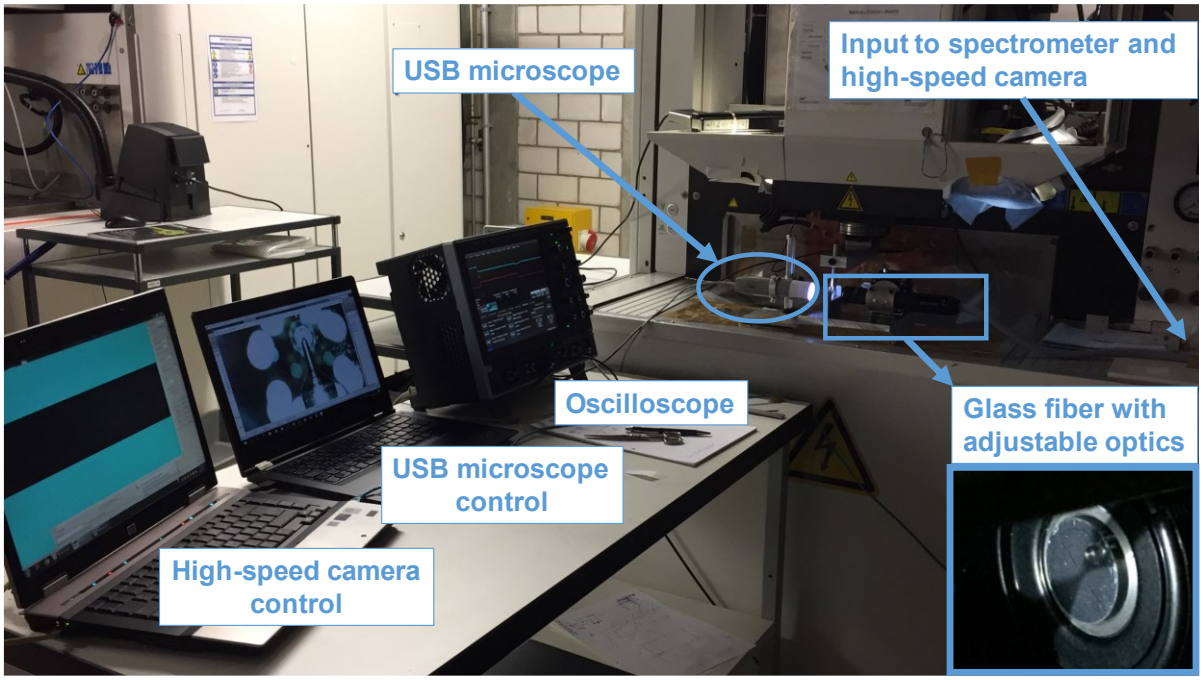

Fig. 4.9: Experimental setup in the lab showing in the right bottom corner the electrode positioning in the fibre array

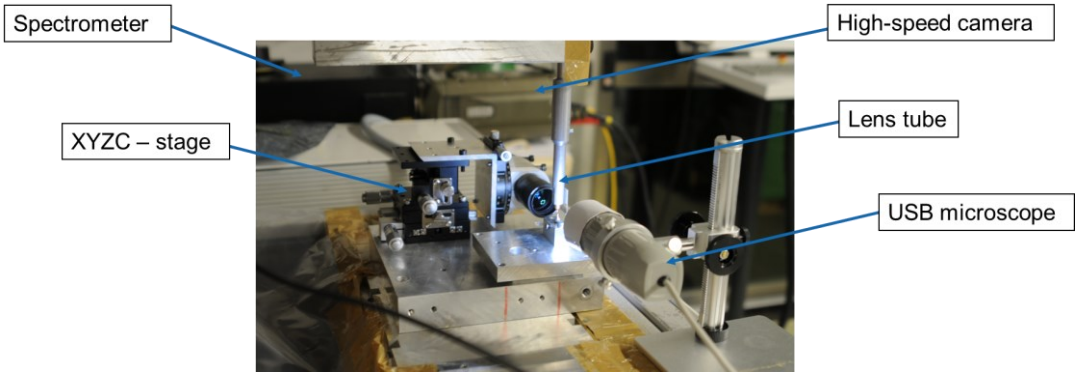

Fig. 4.10: Experimental setup in the lab showing fixation of the lenses tube with the fibre array on a manipulation stage

The light from the plasma must pass through lenses and fibres into the spectrometer and is ultimately detected by the CMOS sensor of the high-speed camera, illustrated in Fig. 4.11. The fibres, arranged in a line orthogonal to the electrode axis, are used to guide the light into the spectrometer. The spectrometer and the high-speed camera are too large in this setup, so that direct guidance of the light, e.g. with mirrors, is impractical therefore the light is guided by a flexible glass fibre tube.

The optical setup has two purposes, first, the plasma is magnified to illuminate as many fibres as possible. A decent amount of light with a reasonable amount of 21 illuminated fibres could be achieved with a magnification factor of 3.8. The second purpose of the optics is to ensure a small angle of incidence on the fibres and therefore achieve a good acceptance rate. This was realized with a Thorlabs setup with

achromatic doublet lenses. The optical system is mounted on a manual high precision XYZC stage allowing even more flexibility.

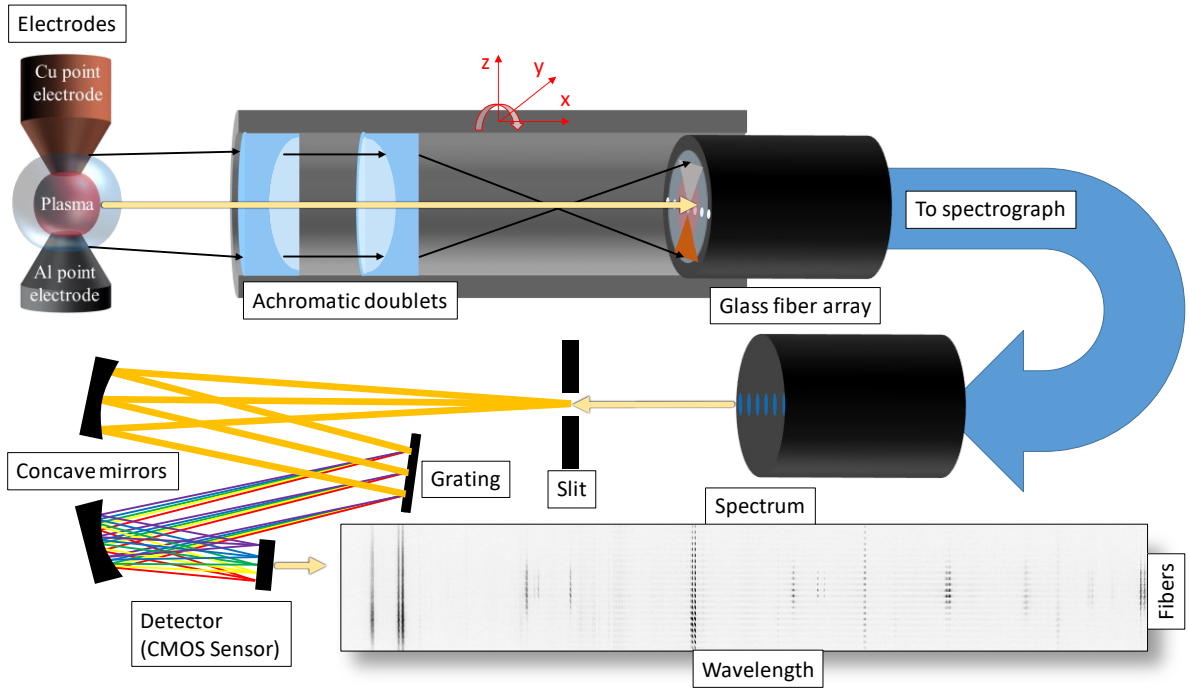

Fig. 4.11: Schematic diagram of the optical path of the light emitted by the discharge between the electrodes

4.4 Treatment of spectral data

Each optical element illustrated in Fig. 4.11, lenses, mirrors and fibres, influences the wavelength-dependent light intensity. The grating and the slit influence the resolution of the spectra, the final crucial parameter is the CMOS sensor efficiency. To obtain meaningful emission spectra several correction steps must be considered.

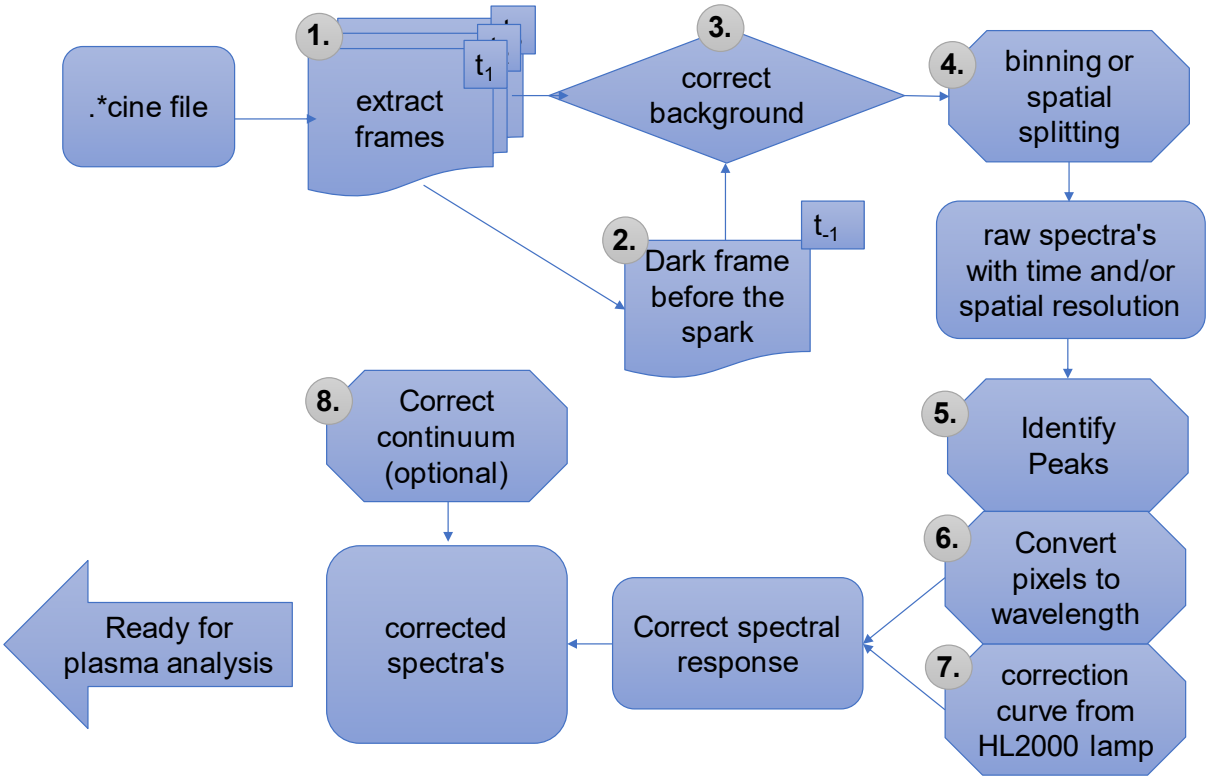

Fig. 4.12: Schematic of the image processing – correction steps from raw cine video to emission spectra

1. All frames and metadata have to be extracted from the Phantom V12.1 raw *.cine movie file.
2. The full movie file also contains some dark pictures just before the discharge. They have to be separated from frames with the discharge.
3. The frame just before the discharge, without any discharge light, is subtracted from frames with the discharge light. This background subtraction reduces the noise, e.g. from photons that come from other sources than the plasma or general noise of the CMOS sensor.
4. In the fourth step either all pixels are binned along the fibre axis to extract one spectrum or the pixels are binned for each fibre to get spatially resolved spectra. This must be done for each frame to get time-resolved spectra.
5. **& 6.** In the following peaks can be identified and their species automatically assigned based on the expected emissions for the electrode species. Thereby the pixel scale is converted to wavelength. In earlier works, this was transformed in wavelength scale using a HG-1 mercury argon calibration light. This method comes with the disadvantage that small deviations in the setup cause a shift of all and new reference spectra with the calibration lamp must be acquired frequently. The new method to determine the wavelength automatically. The spectral range under investigation is first roughly defined by the central wavelength of the spectrometer. Then, based on the elements involved, the experimental lines in this area are compared with those from a

database, either PrismSPECT [60,92] or the atomic database from the National Institute of Standards and Technology (NIST) [40]. The experimental spectrum with its most prominent peaks is compared with some known prominent lines of the species involved in the plasma and the wavelength is adjusted to the pixels accordingly, as illustrated in Fig. 4.13. This is especially possible since no line shifting phenomena are expected.

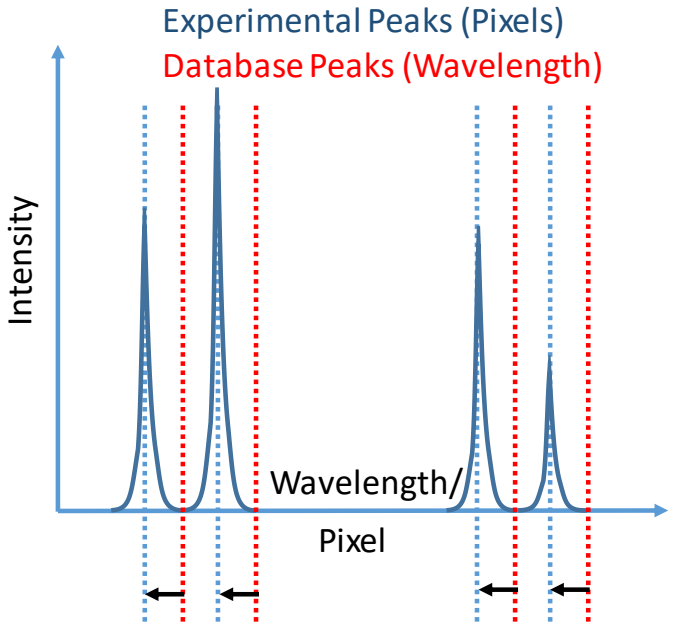

Fig. 4.13: Illustration of the wavelength axis adjustment. Lines in blue (experimental) and red (database) must match.

7. After identifying the wavelength axis, the intensity must be corrected. In high-speed imaging with the Phantom v12.1, the colour fidelity of the CMOS sensor is not of great importance. Whereas in optical emission spectroscopy the colour fidelity of the CMOS sensor plays a significant role in the spectra analysis since the relative heights of emission lines with different wavelength respectively colours is highly important. The acquired images are influenced depending on the wavelength by the spectral responsivity of the sensor, seen in Fig. 4.14. The black curve indicates the total spectral response. The CMOS sensor performs best in the range between 400 nm and 800 nm. Especially the waviness of the response curve introduces irregularities in the acquired data and must be corrected when OES is carried out. In comparison to the thesis of Maradia [61] and Macedo [54] the correction curve, seen in Fig. 4.15, was newly created with an Ocean Optics HL2000 calibration light, which covers a larger range of wavelength and ensuring that ageing of the sensor or other influences does not affect the measurement quality.

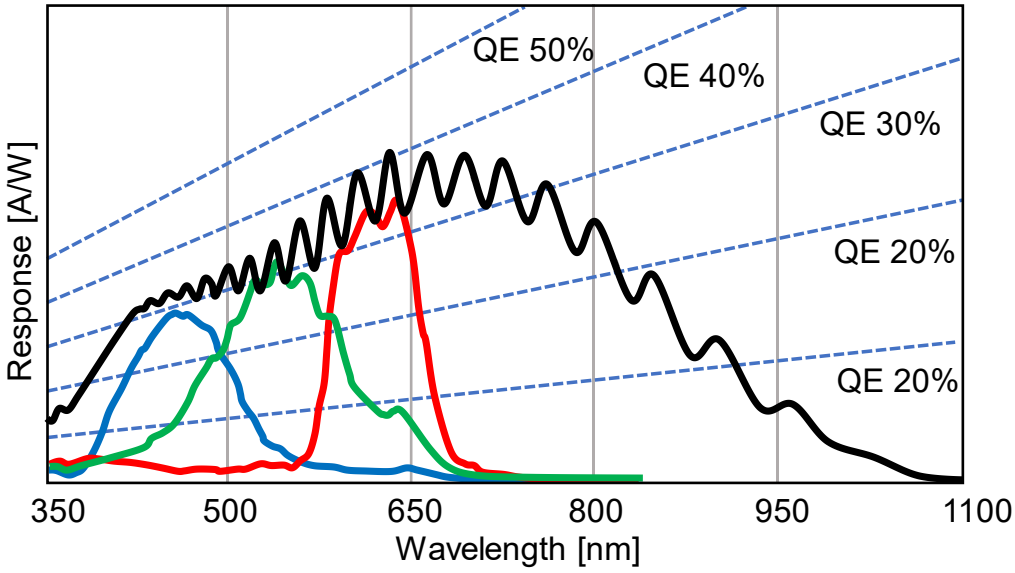

Fig. 4.14: Spectral response of the Phantom v12.1 CMOS sensor

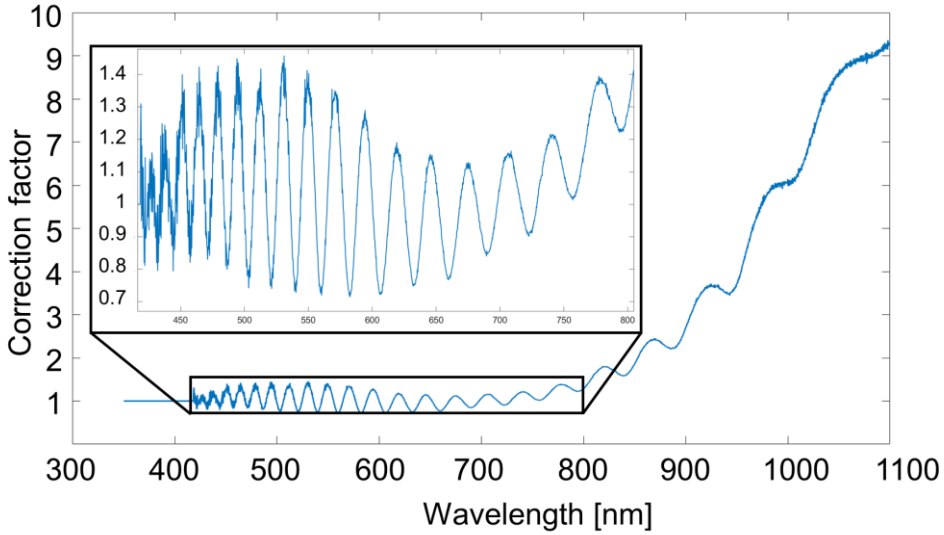

Fig. 4.15: Calibration curve for the Phantom v12.1 CMOS sensor created with the Ocean Optics HL2000 calibration light

8. Finally, in case of strong continuum e.g. blackbody radiation must be corrected (subtracted), but this phenomenon has not occurred in our experiments.

The spectra are now corrected from instrumental errors and can be further processed, which is addressed in the next chapter

4.5 Abel Inversion

The acquired emission spectra always represent an integration over space and time of the measured plasma. The time integration is controlled by the exposure time settings of the high-speed camera. The spatial integration is defined by the optical

system respectively the arrangement of the optical fibres and the size of the plasma. The information in each fibre is an integration of the plasma along the x-axis as visualized in Fig. 4.16. The used optical setup, which is explained in chapter 4.3 uses a 1D array of 40 fibres. Due to the arrangement of fibres and lenses, a spatial resolution of 50 µm along the y-axis is realized.

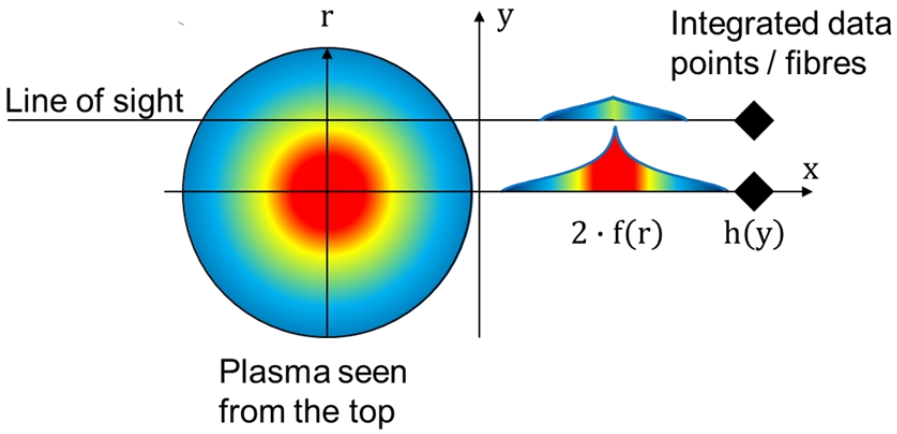

Fig. 4.16: Illustration of the Abel inversion problem

If the plasma has a symmetrical profile, the radial emission intensity can be calculated by the Abel inversion as described for instance in Kunze [45]. In 1823 Niels Henrik Abel developed for a mechanical problem with an inverse relationship a method to derive the original function from the resulting integrated observed function. This formulation has become generally known as Abel inversion. Nowadays the Abel inversion can be found in numerous applications like tomography applications or more specific in astrophysics e.g. to derive the radial mass distribution of a galaxy. In manufacturing, this method has been used to analyse technical plasmas like in EDM e.g. by Natsu et al. [72]. Assuming an axially symmetric plasma the Abel inversion can be used, to determine the local emission $f(r)$ out of the observed emission $h(y)$:

$$h(y) = 2\int_{y}^{R} \frac{f(r)\,r}{\sqrt{r^2 - y^2}}\,dr \tag{4.1}$$

$$f(r) = -\frac{1}{\pi}\int_{r}^{R} \frac{dh(y)}{dy}\frac{1}{\sqrt{y^2 - r^2}}\,dy \tag{4.2}$$

Where r is the radial distance, R is the radius e.g. of the plasma, y is the position of the measurement points, in this case the fibres. There are few polynomials and functions h(y) and $f(r)$ for which the Abel inversion can be analytically solved, one such an example is a Gaussian distribution as shown below.

$$\mathrm{f(r)} = \exp\left({}^{-r^2}/_{\sigma^2}\right) \qquad \mathrm{h(y)} = \sigma\sqrt{\pi}\exp\left({}^{-y^2}/_{\sigma^2}\right), \quad \sigma > 0 \tag{4.3}$$

In some cases, an analytic function exists which describes the experimental data $h(y)$ sufficient and the function $f(r)$ can be directly calculated. However, in most cases, Abel inversion must be used with a numerical formulation. In literature, several algorithms to perform Abel inversion numerically are given and discussed in detail. For the sake of consolidation, only two are described in detail, namely the Nestor-Olsen method [74] and the Fourier-based approach according to Pretzler [78].

Nestor-Olsen approach:

$$f(r) = -\frac{2}{\Delta y \pi} \sum_{n=k}^{N-1} h_{y_n} B_{k,n} \tag{4.4}$$

Where k and n are the integer position indexes for radial and axial intensities, whereas Δy is the width between two adjacent experimental data and h is the intensity observed at each fibre and f is the calculated radial intensity.

The coefficient $B_{k,n}$ is calculated by:

$$B_{k,n} = -A_{k,n} \qquad \text{for: } n = k \tag{4.5}$$

$$B_{k,n} = A_{k,n-1} - A_{k,n} \qquad \text{for: } n \geq k+1 \tag{4.6}$$

$$A_{k,n} = \frac{[n^2 - (k-1)]^{1/2} - [(n-1)^2 - (k-1)^2]^{1/2}}{2n-1} \tag{4.7}$$

Fourier approach:

$$f(r) = \sum_{n=N_l}^{N_u} A_n f_n(r) \tag{4.8}$$

$$f_0(r) = 1\,, \qquad f_n(r) = 1 - (-1)^n \cos\left(n\,\pi \frac{r}{R}\right) \tag{4.9}$$

$$h(y) = 2 \sum_{n=N_l}^{N_u} A_n \int_y^R \frac{f_n(r)\, r}{\sqrt{r^2 - y^2}}\, dr \tag{4.10}$$

Both numerical approaches have been benchmarked with two analytical functions, a polynomial with a saddle point at the zero, and a Gaussian distribution, seen in Fig. 4.17. The Nestor-Olsen method is known to be strong for a low amount of measurement points, $n \leq 15$. The disadvantage is that the result has one data pointless the axially observed. The Fourier approach outperforms the Nester-Olsen method when it comes to more data points. Additionally, there is no loss of datapoints after inversion.

Even though the Nestor-Olson method shows a slightly better performance in the benchmark (Fig. 4.17.), for the present work the Abel inversion based on Fourier transforms is applied. This is since all measured points can be transformed.

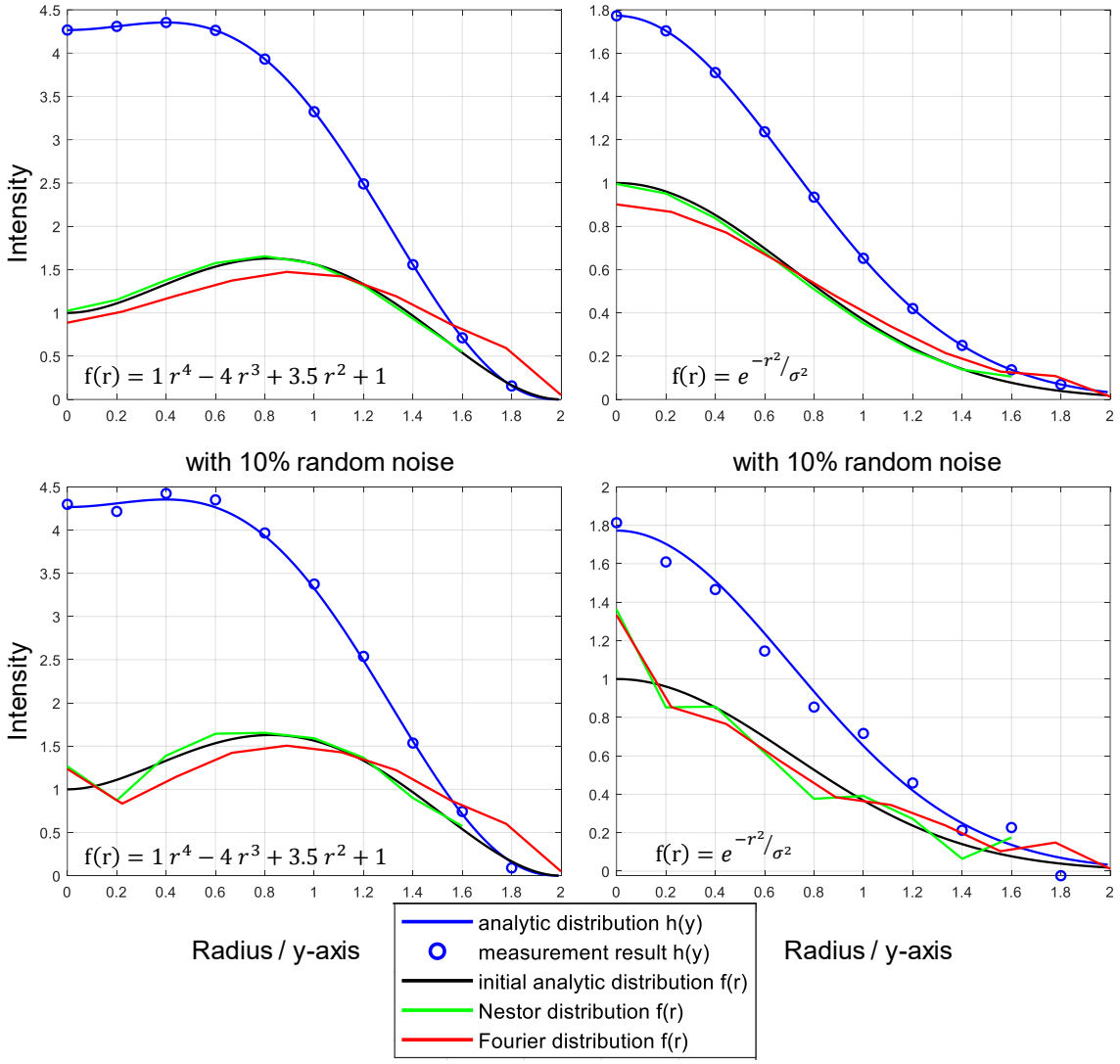

Fig. 4.17: Comparison of Nestor-Olsen (green) and Fourier (red) numerical methods based on 10 artificially created measuring points (blue circle) derived from analytical functions (blue and black). To imitate measurement error, in the lower graphs the measurement points multiplied by a random deviation error of 10%

Abel inversion applied to optical emission spectroscopy

Fig. 4.18 shows an acquired emission spectrum at a point of time after data preparation according to the scheme given in Fig. 4.12. In this case, the time between frames was set to 42 µs to reach sufficient resolution covering all fibres. The exposure time was set to 10 µs of and the pause time is 32 µs. In the radial emission line profile such as presented in Fig. 4.19 and the following, only the most important emission lines are analysed. These emission lines are given in Table 4-5.

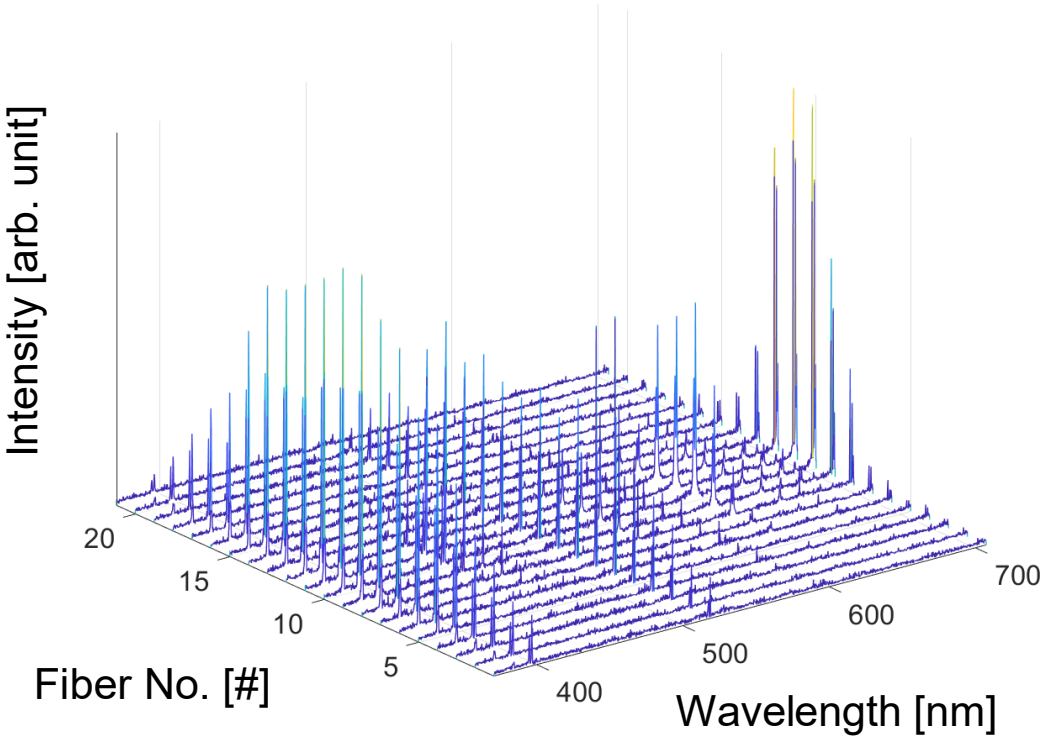

Fig. 4.18: Optical emission spectra spatially resolved with 21 fibres for a typical EDM discharge at one point of time and one cross section height through the plasma channel.

Table 4-5 Atomic emission lines

Species	Atomic	1. Ionization	2. Ionization
Al	394.48 nm	466.4 nm	451.36 nm
Cu	515.32 nm	490.97 nm	

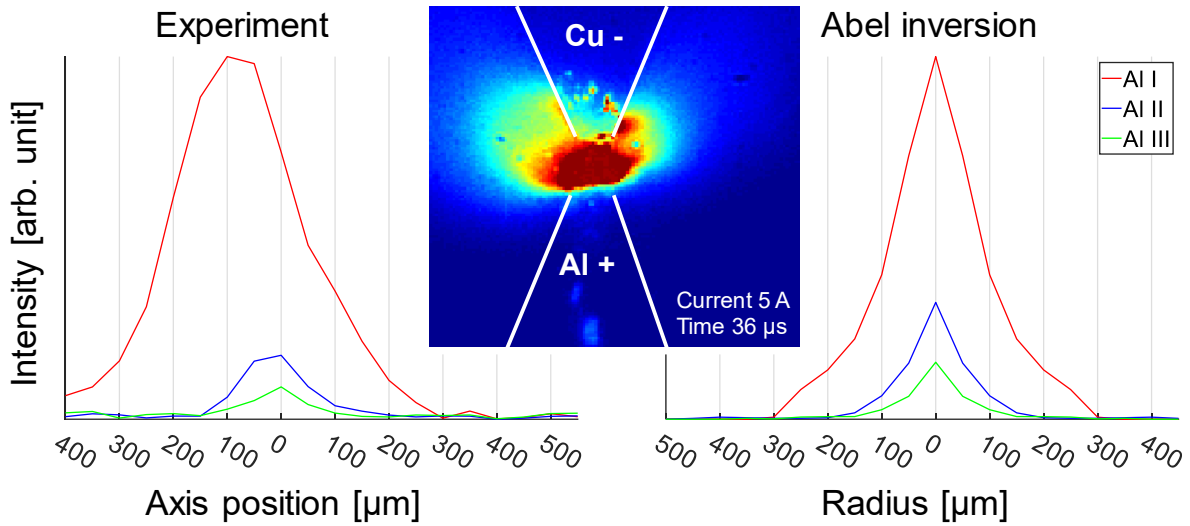

Fig. 4.19: Comparison of experimental measured intensity (left) with results of the calculated intensity by Abel inversion (right) of a 5 A discharge together with a high-speed image of such a discharge in jet colour code

Gaussian-like shape profiles for the measured intensity have a similar shape after inversion for the emitted intensity. The Gaussian type of emission line profile can be observed especially in low current discharges such as 5 A, as seen in Fig. 4.19.
Profile shifts, e.g. of Al I, are no longer observable after inversion. This problem appears especially at higher currents as can be seen in Fig. 4.20.

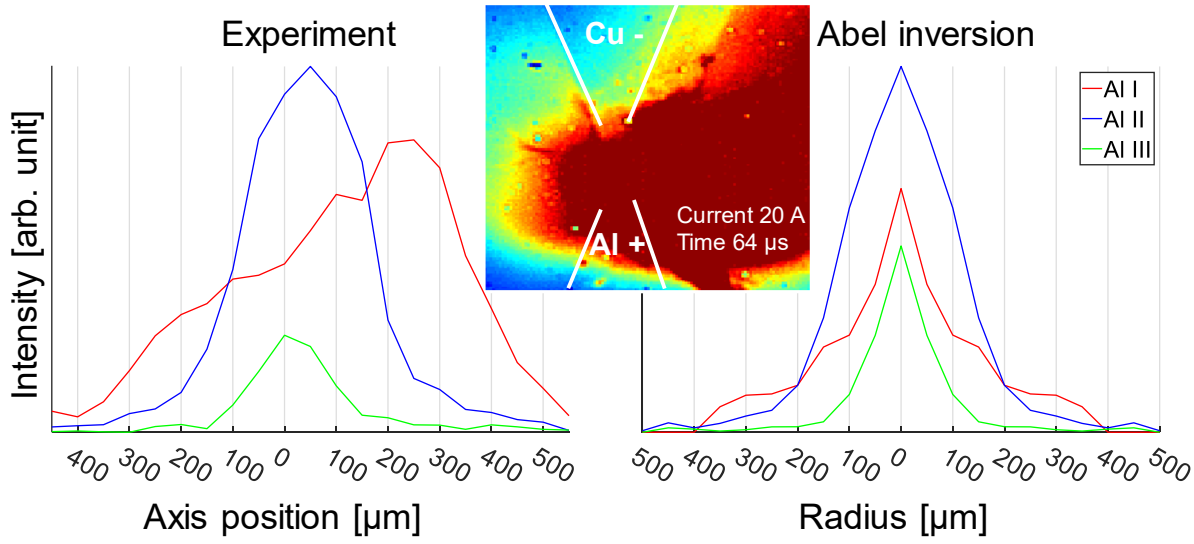

Fig. 4.20: Comparison of experimental measured intensity (left) with results of the calculated intensity by Abel inversion (right) of a 20 A discharge strong profile asymmetry together with a high-speed image showing strong plasma asymmetry

The presented 20 A seen in Fig. 4.20 discharge shows not only a displacement of the profile and also, but also a strong emission line profile asymmetry, which is clearly visible in the Al I profile as well as in the high-speed image. After inversion, this asymmetry appears as a bumpy profile. This makes the analysis difficult and the Abel

inversion less reliable. Nevertheless, only the inverted profiles can be interpreted appropriately since only the represent correct intensity values. The time resolved analysis results of a 20 A discharge can be seen in Fig. 4.21.

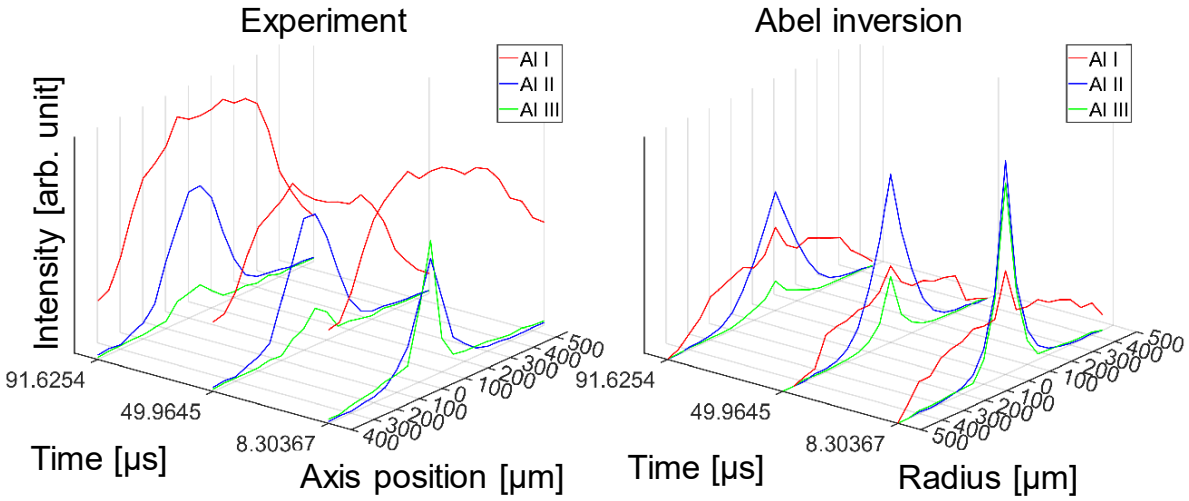

Fig. 4.21: Comparison of Experimental results with Abel inversion of a 20 A discharge time-resolved (see Fig. 4.20)

In this case, the impact of Abel inversion on the emission spectra interpretation can be seen clearly. In the raw experimental data (Fig. 4.21, left) it can be erroneously assumed that Al I is dominant. After inversion (Fig. 4.21, right) true plasma structure becomes clear, Al I occurs mainly at the edges, while in the centre higher ionised species are visible. Al II and Al III show a very symmetric behaviour.

4.6 EDM discharge plasma analysis

To interpret the emission spectrum and deduce statements about the plasma properties some assumptions are required and must be verified.
The most important plasma parameters and properties are introduced in short in the following.

Plasma density

A plasma consists of ions and electrons. The electron density n_e $[cm^{-3}]$ of plasmas in LTE can be estimated from the full width of a half maximum (FWHM) $\Delta\lambda_W$ $[nm]$ of the spectral line. Gigosos and Cardeñoso [23] established the following formula to calculate the electron density using the spectral line H_α:

$$n_e = 8.8308 \cdot 10^{16} \cdot (\Delta\lambda_W)^{1.6005} \tag{4.11}$$

The broadening of H_α is dominated by the Stark effect, which is very sensitive to the electron density. The broadening of metallic lines, on the other hand, is much less sensitive to the Stark effect. But they are an alternative, if H_α cannot be used, such as the aluminium line at 446 nm [10].

The density of ions n_i [cm^{-3}] is usually of secondary importance since the movement and density of electrons have greater impact on the emission spectra.

The ratio of electron density n_e and ion density n_i is called mean charge Z

$$Z \cong \frac{n_e}{n_i} \tag{4.12}$$

and indicates the degree of ionisation which is an important parameter to characterize the plasma. Form emission spectra simulation the electron density, ion density for each species and mean charge can be derived by line-broadening of several peaks, and by emission intensities.

Plasma temperature

To calculate the plasma temperature T_e [K] a fast and very common way used already by many researchers is the two-line Boltzmann method. Assuming an optically thin LTE plasma, this method can be applied. The intensity ratio of two selected spectral lines I_{R_1}/I_{R_2} emitted by atoms or ions of the same element is directly related to the plasma temperature. Griem [1] describes the calculation of the electron temperature T_e of a plasma as follows:

$$T_e = \frac{E_{L_2} - E_{L_1}}{k_B} \cdot \left[\ln \left(\frac{I_{R_1} \lambda_1 g_2 A_2}{I_{R_2} \lambda_2 g_1 A_1} \right) \right]^{-1} \tag{4.13}$$

where E_{L_1} and E_{L_2} are the energy levels of the species from the two selected spectral lines, k_B is the Boltzmann constant and λ_1 and λ_2 are the wavelengths of the chosen lines. The statistical weights g_1 and g_2 of the excited level and A_1 and A_2 are the transition probabilities are needed as well. E_L, λ, A and g are parameters of the selected spectral lines, which are available online in the atomic database of the National Institute of Standards and Technology (NIST) [40]. The relative intensity I_R must be measured.

The accuracy of this method is decisively influenced by the choice of lines. The lines must be clearly visible, without overlapping and close together to minimize continuum errors. Their energy level E_L, must also be significantly different, the greater the difference the better.

The measurement uncertainty alone results in an error of at least ±10%, as discussed by Griem [25]. The calculation of the plasma temperature is rather an estimation, which depends strongly on the measured line quality and the plasma specification. Moreover, Griem already proposed to improve the temperature estimation by considering CR (Collisional Radiative) models.

If the plasma is not in thermal equilibrium, the energy respectively temperature of the species in a plasma is not uniform but normally distributed. The probability for a particle to have a certain energy is described by an energy distribution function (EDF). In general, those energies are often assumed to be Maxwellian distributed which is here

out of simplicity assumed as well. However, other distributions may also occur, these are the subject of current plasma research.
For two temperature plasma the hotter respectively faster fraction of electrons is described as hot electron fraction [%] and hot electron temperature [eV].

Optical depth

An important parameter is the optical thickness or optical depth of the plasma τ. For optical emission spectroscopy, an optically thin plasma is a requirement, i.e. $\tau \ll 1$. It is generally assumed that EDM plasmas fulfil this. The wavelength-dependent optical thickness of the plasma can be calculated to prove this statement. The PrismSPECT software, introduced below, allows the calculation of the optical thickness. Calculations are carried out for aluminium, as these emission lines are predominantly investigated in the plasmas generated in the experimental setup. Table 4-6 shows a better overview of optical thickness in the range of temperatures from 5,000 K – 20,000 K and ion densities from 10^{16} to 10^{18} where EDM plasma properties can be expected. The wavelength dependent absorption appears for EDM plasmas dominantly for excited Al I lines.

Table 4-6 Optical thickness τ for Al I lines at different plasma parameters

	$T_e = 5{,}000$ K	$T_e = 10{,}000$ K	$T_e = 20{,}000$ K
$n_i = 10^{16}\ [cm^{-3}]$	0.08	0	0
$n_i = 5 \cdot 10^{16}\ [cm^{-3}]$	0.5	0.02	0
$n_i = 10^{17}\ [cm^{-3}]$	1	0.04	0
$n_i = 10^{18}\ [cm^{-3}]$	11.25	1.37	0.02

In general, it can be expected that the plasma will be well visible. Even for Al I lines the requirement, $\tau \ll 1$ is generally fulfilled for EDM plasmas. With Table 4-6 this can be controlled individually during the experiments.

Parameter identification with PrismSPECT

PrismSPECT [60,92] is a commercial software to simulate the spectral response of plasmas using collisional-radiative models and photoionization cross-sections. This enables analysis beyond electron temperature and density, estimation of several plasma parameters, such as atom and ion densities, fraction of ionic species, plasma composition and application of different energy distribution functions, other than Maxwellian. Kunze [45] listed a series of equations to describe the plasma based on possible radiative and collisional transitions.

The density n_z of species for the charge z in the upper energy level p is proportional to their transition probability form the upper to the lower energy level q described as:

$$-\frac{dn_z(p)}{dt}\bigg|_{p\to q} = A_c(p \to q)n_z(p) \tag{4.13}$$

where $A_c(p \to q)$ is an atomic constant for this transition. Also known as atomic transition probability or Einstein coefficient of spontaneous photon emission. At each transition one or more photons are emitted. The emission coefficient ε of a given line is given by:

$$\varepsilon(p \to q) = \frac{h\nu_{pq}}{4\pi} A_c(p \to q)n_z(p) \tag{4.14}$$

The kinetics of local populations of atomic states s of ions of charge z are described by coupled rate equations of the type

$$\frac{dn_z(s)}{dt} = -C_z(s \to) + C_z(\to s) + \Gamma_z(s) \tag{4.15}$$

$C_z(s \to)$ and $C_z(\to s)$ described the sums of all rates of possible radiation and collision transitions out of the energy level s and into the energy level. The external flux is $\Gamma_z(s)$ for all level-s population by diffusion and convection. Eq. (4.15) with all transitions, some of them with unknown parameters, is practically impossible to solve.

To simulate emission spectra, PrismSPECT uses a CR code based on the physical principles of Eq. (4.15) with a reduced set of coupled rate equations that consider only the most relevant processes and time scales. The software uses a database with photoionization cross sections (ATBASE of PrismSPECT), and among others line broadening mechanisms are also considered in the calculations. PrismSPECT can calculate collisional excitation and ionization rates for plasmas with a Maxwellian, double Maxwellian or custom EDFs. Simulated emission spectra are generated with the formulation proposed by Chung et al. [9]:

$$\frac{dn_q}{dt} = -n_q \sum_{j\neq i}^{N_L} W_{qp} + \sum_{j\neq i}^{N_L} n_p W_{pq} \tag{4.16}$$

$1 \leq q \leq N_L$

for upward transitions from level q to level p

$$W_{qp} = B_{qp}\bar{J}_{qp} + n_e C_{qp} + \beta_{qp} + n_e\gamma_{qp} + \sigma_{qp} + I_{qp} \tag{4.17}$$

for downward transitions from level p to level q

$$W_{pq} = A_{pq} + B_{pq}\bar{J}_{pq} + n_e D_{pq} + n_e\alpha_{pq} + n_e\kappa_{pq} + n_e^2\delta_{pq} \tag{4.18}$$

where N_L is the number of the levels included in the calculation and $\bar{J}$ is a frequency-averaged mean intensity, which is relevant to the transition. The rate coefficients of the atomic processes can be seen in Table 4-7.

Table 4-7 Rate coefficients of the atomic processes adopted from [9]

A_{pq}	spontaneous emission	α_{pq}	radiative recombination
B_{qp}	stimulated absorption	β_{qp}	photoionization plus stimulated recombination
B_{pq}	stimulated emission	γ_{qp}	collisional ionization
C_{qp}	collisional excitation	δ_{pq}	collisional recombination
D_{pq}	collisional deexcitation	κ_{pq}	electron capture
I_{qp}	beam and non-thermal electron collision	σ_{qp}	autoionization

Radiation emitted by an electrical discharge can be reabsorbed in its plasma. This phenomenon depends on the optical depth of the plasma, as described by Kunze [45]. The change in spectral radiance $dL_\lambda(x,\lambda)$ through a thin layer of a plasma due to absorption in the direction x is given by

$$dL_\lambda(x,\lambda) = -\kappa(x,\lambda)L_\lambda(x,\lambda)dx \tag{4.19}$$

where $L_\lambda(x,\lambda)$ is the spectral radiance for a specific wavelength λ and $\kappa(x,\lambda)$ is the wavelength-dependent absorption coefficient. Considering emission $\varepsilon_\lambda(x,\lambda)$ and absorption of a thin plasma layer the total change of the radiance is defined as

$$dL_\lambda(x,\lambda) = \varepsilon_\lambda(x,\lambda)dx - \kappa(x,\lambda)L_\lambda(x,\lambda)dx \tag{4.20}$$

The equation can be reformulated by the division of dx, which leads to the equation

$$\frac{dL_\lambda(x,\lambda)}{dx} = \varepsilon_\lambda(x,\lambda) - \kappa(x,\lambda)L_\lambda(x,\lambda) \tag{4.21}$$

Kunze [46] introduces the optical depth τ of the thin slab shown as

$$d\tau = -\kappa(x,\lambda)dx \tag{4.22}$$

Thus, the optical depth along a certain distance within the plasma can be calculated to

$$\tau(x,\lambda) = -\int_0^x \kappa(x',\lambda)dx' \tag{4.23}$$

In PrismSPECT, the optical depth is assumed to correspond to the number of mean-free paths of a photon along the line of sight, as described by Chung et al. [9]. As mentioned earlier emitted from plasma with $\tau > 1$ are optically thick, whereas lines with $\tau \ll 1$ are optically thin. Considering the integration along the line of sight l of the plasma, (4.21) can be written as

$$\frac{dL_\lambda(x,\lambda)}{d\tau} = L_\lambda(x,\lambda) - \frac{\varepsilon_\lambda}{\kappa(x,\lambda)} = L_\lambda(x,\lambda) - S_\lambda(x,\lambda) \tag{4.24}$$

where $\varepsilon_\lambda(x,\lambda)/\kappa(x,\lambda) = S_\lambda(x,\lambda)$ is called the source function. Finally, the radiance at the plasma surface can be obtained by

$$L_\lambda(0,\lambda) = \int_0^{\tau(-l,\lambda)} S_\lambda(\tau,\lambda) e^{-\tau} d\tau \tag{4.25}$$

Simulated emission spectra

EDM plasma properties mentioned earlier are estimated from a fit between the peaks of emission spectra calculated by PrismSPECT and the observed EDM plasma optical emission spectra. Fig. 4.22 shows a comparison between optical emission spectra and simulated spectra of an EDM discharge in oil.

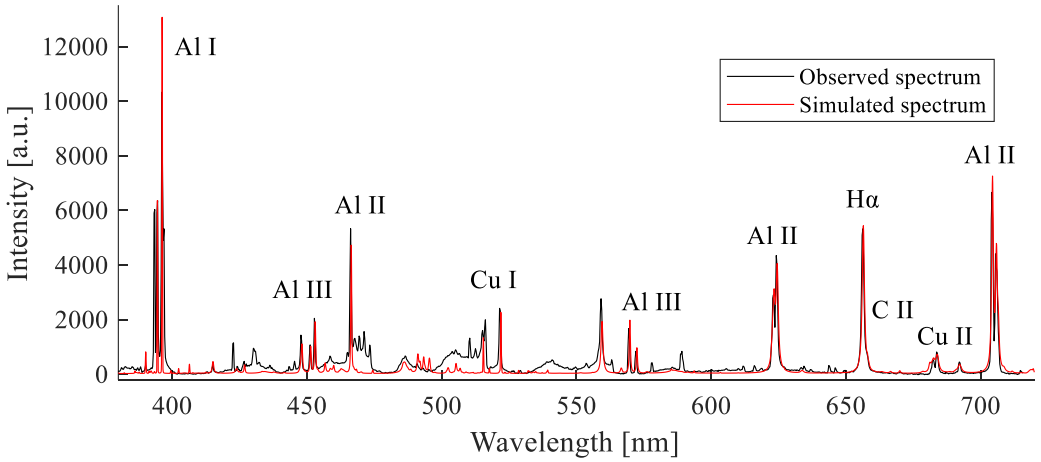

Fig. 4.22: Experimental and simulated spectrum for copper anode and aluminium cathode

The commercial software Matlab and C++ are used for the evaluations and plot generation. For a fast and provisional analysis, the LIBS database from NIST [40] is also a very useful tool and delivers for LTE cases comparable results to the commercial tool PrismSPECT seen in Fig. 4.23.

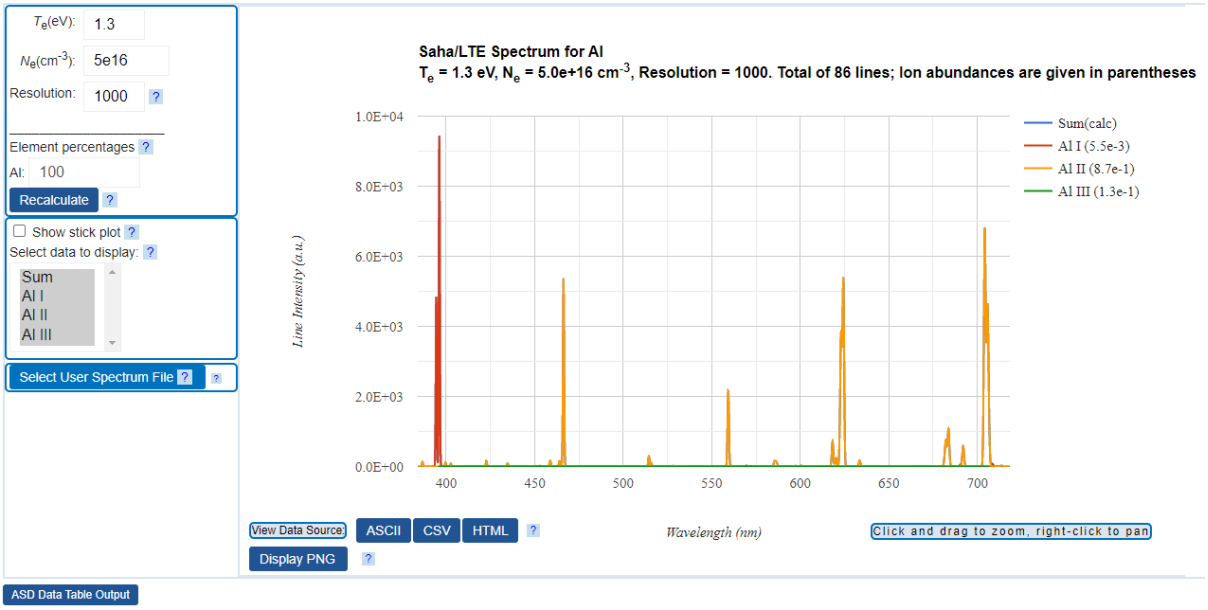

Fig. 4.23: Result from LIBS database [40] for an aluminium spectrum at T=15600 K with an electron density of $n_e=5\cdot10^{16}$ cm^{-3}

Reverse parameter identification by emission spectra simulation

Each experimental observation of an EDM discharge in this thesis consists of several spectra for the spatial and timely resolution. The plasma parameters of the discharge are calculated by reverse parameter identification with emission spectra simulation. Simulated emission spectra are fitted to experimental emission spectra by emission intensity to obtain the plasma parameters like electron density or electron temperature. Several dimensions between the simulated and experimental spectrum must match. First, inside one emission spectrum, the peak height of all simulated and experimental lines have to be the same, e.g. the intensity of a simulated Al I peak has to be the same as the experiential counterpart: $I_{sim\_Al\,I} = I_{exp\_Al\,I}$. Additionally, the FWHM of those peaks shall match. The ratio between different peaks in an emission spectrum shall be the same. This is required especially for selected spectral lines with different energy levels and line ratios between different ionic species. E.g. the ratios between Al I and Al II lines have to be equal in simulated and experimental emission spectra: $I_{sim\_Al\,I} \Big/ I_{sim\_Al\,II} = I_{exp\_Al\,I} \Big/ I_{exp\_Al\,II}$.

The spatial experimental emission spectra have also to match the spatial simulated emission spectra in relative intensity also between different fibres. A normalization of the simulated spectra for each fibre is not allowed. All those correlation are illustrated for better comprehension in Fig. 4.24.

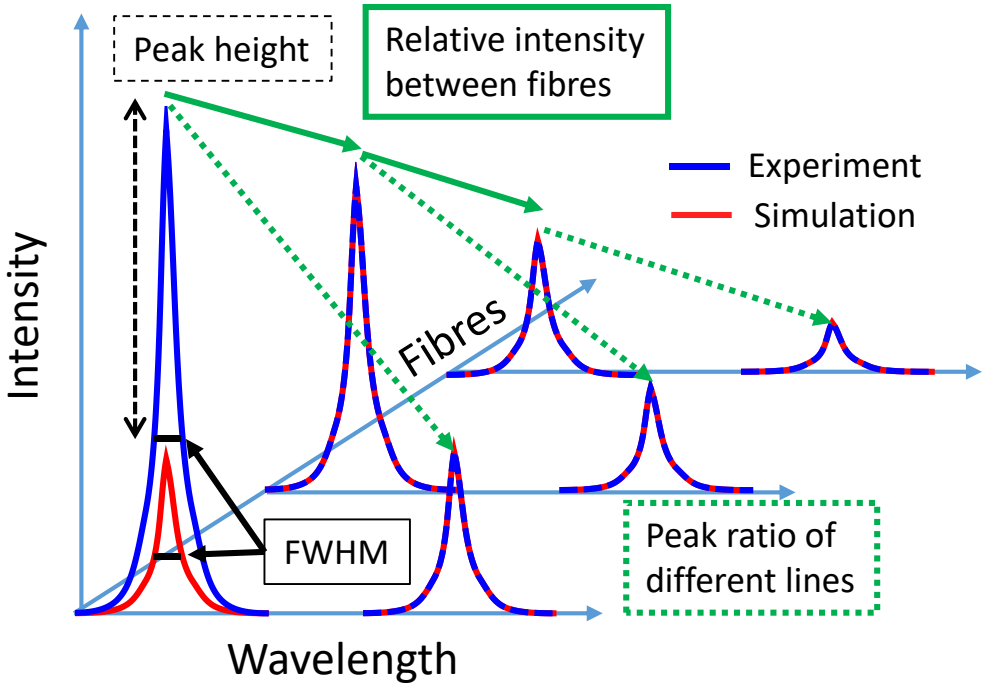

Fig. 4.24: Important intensity values to match between simulated and experimental spectra, peak to peak ration of different lines in one fibre respectively spectrum, FWHM of the same line, peak hight of the same line and peak to peak ratio of the same line between different fibres.

To get an idea of the fitting quality the error R between a simulated and an experimental spectrum is calculated for as presented below:

$$R = \sqrt{\sum (I_{i_{sim}} - I_{i_{exp}})^2 + \Delta FWHM_{466}{}^2} \tag{4.14}$$

With I_i being the line intensity for the observed experimental line and its simulated counterpart. And $\Delta FWHM_{466}$ being the difference in line broadening of the 466 nm Al II line. This value is chosen because it is also a good indicator for the density as reported earlier and therefore should fit in both spectra.

To find matching simulated spectra to the experimental one's different approaches are possible. Fitting simulated spectra based on experience can be done manually but is not practicable due to the high number of spectra to fit, roughly 60 per discharge. To speed up this process a database with of 50,000 simulated spectra is created. These spectra are simulated with PrismSPECT covering a large field of plasma parameters, as illustrated in Fig. 4.25. Those boundary conditions were chosen based on the plasma parameters expected for EDM plasmas as mentioned in the introduction. To investigate non-LTE plasma additionally, emission spectra with an electron beam are simulated. The values for temperature are fixed at 6 eV and a variable number of fast electrons between 0-50% is covered. These values are chosen based on observations by Rakhovsky [80]. Further information on this can be found in chapter 5.

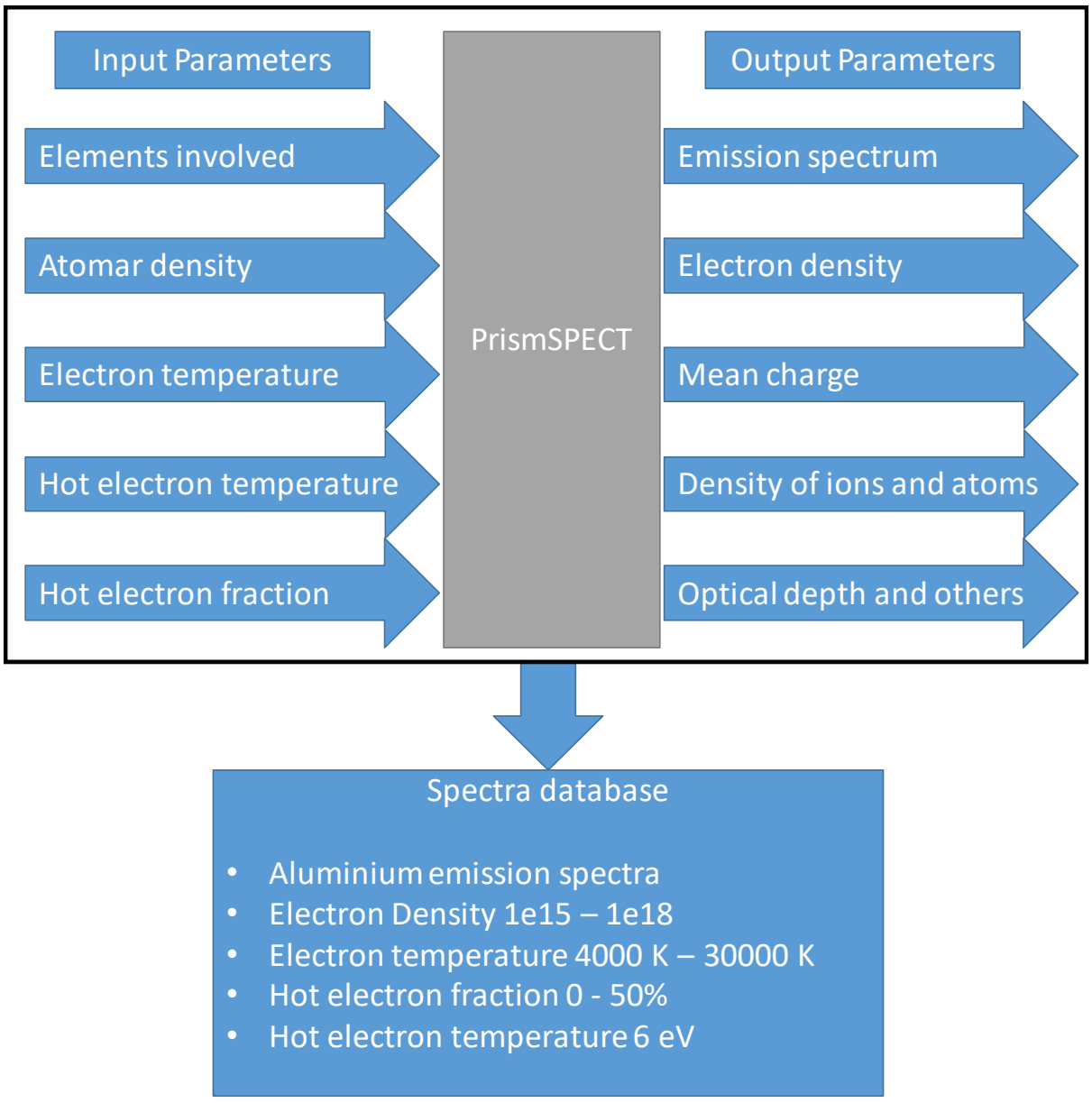

Fig. 4.25: Illustration of the simulated spectra database created with PrismSPECT

From this database, for each experiment, the error R is calculated for each fibre resulting in a multidimensional matrix from which, the best fit is chosen. This is illustrated exemplarily for a single emission spectrum for the parameter's electron density and temperature in Fig. 4.26. Blue colour suggests a good agreement between simulated and experimental spectra and yellow a bad fit. A large yellow region on the left side at low temperature can be observed, where it is impossible to fit spectra. This is because at low temperature only two Al I lines appear, namely lines 394 nm and 396 nm. For temperatures below 12,000 K these lines do not strongly change with varying plasma parameters hence the calculated R-value is not changing at lower temperatures and no optimum can be found. It can only be stated that plasma with

emission spectra where no ionized lines are visible have plasma temperatures roughly lower than 12,000 K.

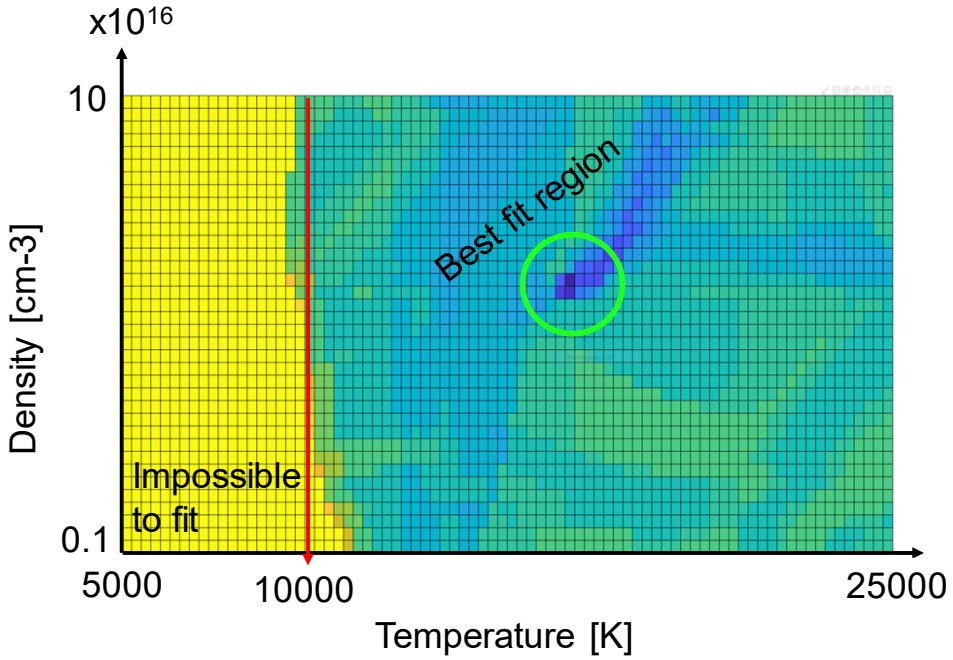

Fig. 4.26: 2D Map to identify the best-fit region simulated and experimental spectra over electron density and temperature. The yellow area indicates an impossible fit region because higher ionized lines are missing due to too low temperature. Deep blue shows the best fit.

The result in Fig. 4.27 shows the experimental data after the final steps described in chapter 4.5 and the artificial simulated plasma of a discharge. In general, the artificial emission spectra match very well. Sometimes small differences can be observed which are caused either by a lack of resolution of the simulation or by the Abel inversion of the experiments which can have slight deviations from real possible plasmas.

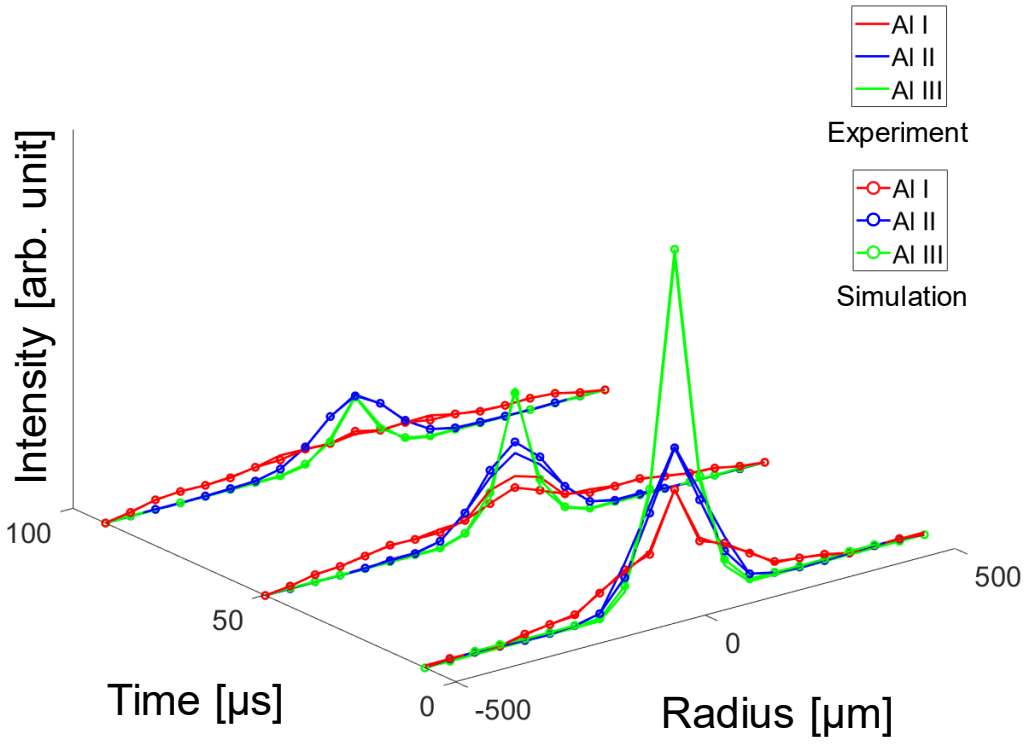

Fig. 4.27: Experimental line profiles and simulated ones by PrismSPECT

Measurement uncertainty and error bars

Graphs from measures in this thesis usually do not show error bars. As already previously discussed calculations depend strongly on the observed lines. Even more, the measurement setup is the measuring instrument which has some weaknesses and measurement errors of ±10% and higher must be considered. Additionally, reverse simulation and the fitting of emission spectra is complicated due to the many parameters involved. Following Table 4-8 shortly summarises qualitatively the sources of errors.

Table 4-8 Rated sources of influence and errors on the final emission spectra analysis

	Risk of influence (+ minor / +++ major)
Measurement setup	
Optics like lenses fibres and mirrors	++
Gratings of the spectrometer	+
Calibration lights for intensity and wavelength	+
CMOS sensor sensitivity and resolution	++
General repeatability of experiments (electrode shapes etc.)	++
Calculations	
Preparation of the experimental data like background corrections continuum correction	+
Abel inversion	+++
PrismSPECT simulations	+

5 PLASMA PROFILES IN EDM LIKE DISCHARGES

In EDM literature it is mostly assumed that EDM plasmas are in LTE. Plasma parameters like density and temperature are calculated based on this assumption using the relative peak height of two or several emission line intensities for temperature calculation or the FWHM for density estimation. Recent investigations on spatially resolved emission lines already indicated a temperature or density distribution. Temperature profiles were already observed by Natsu et al. [72] via the two-line Boltzmann method, whereas Descoeudres [12] observed density profiles for discharges in oil based on the FWHM of H_α.

Recently OES investigations of EDM plasma without spatially resolution in combination with emission spectra simulation have shown that the observed emission spectra cannot be explained assuming a single electron temperature [56]. Assuming two plasma regions a reasonable agreement between simulated and experimental emission spectra was achieved. This situation can be explained theoretically with a hotter region in the plasma centre and a colder region forming a plasma shell. Fig. 5.1 shows the two mentioned regions with experimental and corresponding simulated synthetic emission spectra. Colder region is defined by the measured outer plasma diameter while the hotter region is defined by observation from literature as explained by Macedo et al. [56].

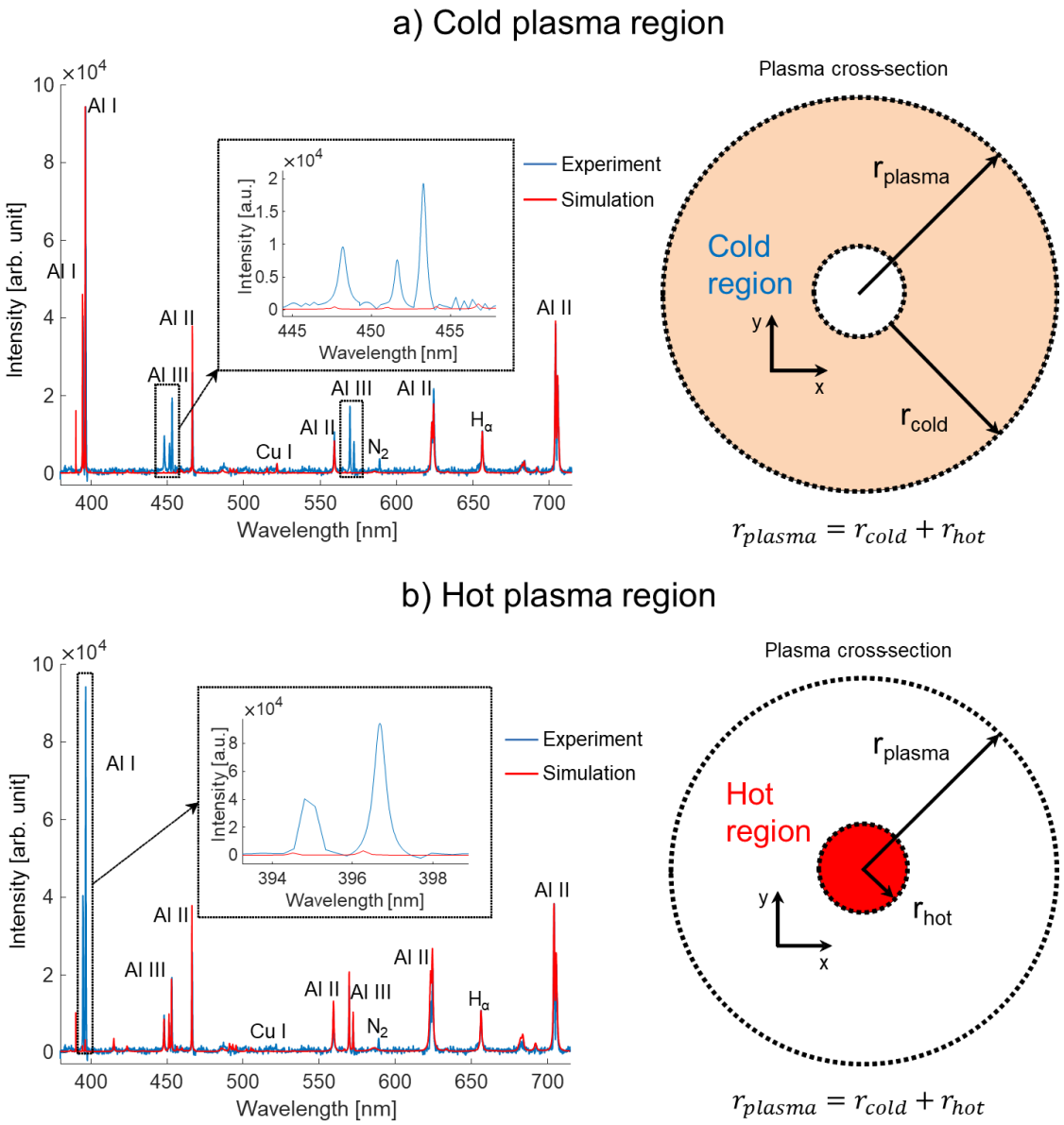

Fig. 5.1: Theory of cold (a) and hot (b) plasma region in a typical small gap EDM plasma. The corresponding observed and simulated optical emission spectra are shown as inlets adapted from [56]

Only with several regions of different plasma properties the correct simulation of Al I, Al III and Al III lines as observed in the optical emission spectra can be explained.

Alternatively to the theory of a temperature profile, the hypothesis of an electron beam formed in the plasma centre was proposed by Macedo et al. [56]. In this case, the EDM plasma is not in LTE and in the centre of the plasma an electron beam with a certain fraction of fast electrons might exist. Up to now this is only theory based on observation of a single spectra.

Spatial and time-resolved optical emission spectroscopy is necessary to clarify the nature of these observed emission spectra and finally to determine if a temperature profile, peaking in the plasma centre, or an electron beam exists in the discharge plasma, a main objective of this thesis. To show which theory applies the most the

EDM plasma should be spatially investigated. This can be realized by the setup and measurement procedures developed and introduced in chapter 4.3 of this work.

Plasma parameters along the radius of the plasma can be calculated by reverse simulation with PrismSPECT as explained prior. In this chapter first, the spatially resolved emission spectrum is analysed in detail followed by an estimation of plasma parameters and concluded with a final evaluation of the models.

5.1 Profile analysis

As a typical case, an electric discharge performed with I = 15 A is investigated in detail. In this experiment, the copper electrode is negatively polarised, whereas aluminium is positive. The spatially resolved OES setup made it possible to illuminate 21 fibres of the experimental arrangement. The spatial and time-resolved spectra of this discharge is presented in Fig. 5.2.

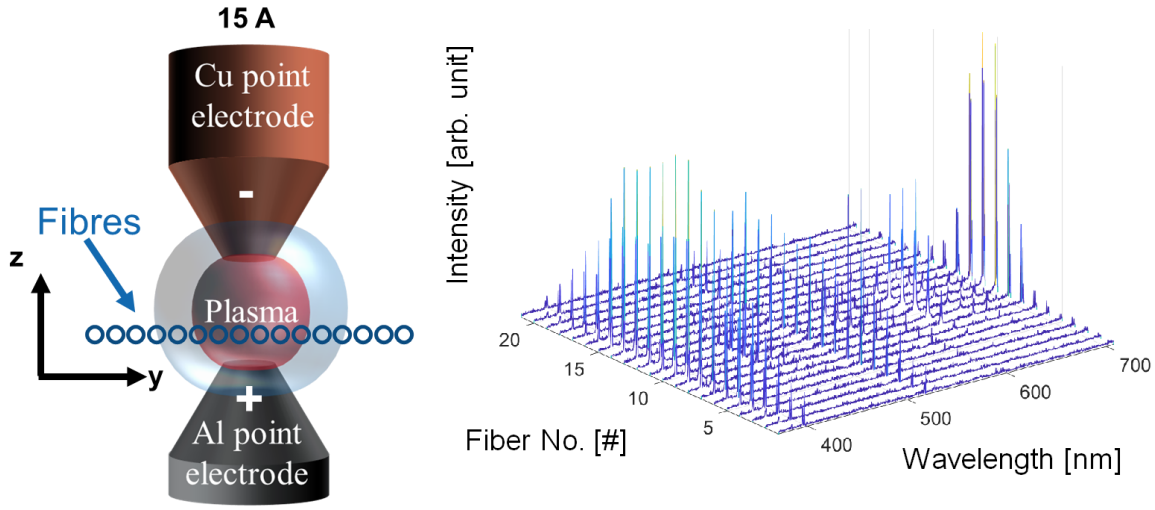

Fig. 5.2: Electrode configuration and spatially resolved emission spectra for a 15 A discharge

The existence of a temperature profile can be already identified due to the presence of neutral and ion emission lines at wavelengths 396 nm (Al I) and 704 nm (Al II) wavelengths.

Fig. 5.3 shows the line emission spectra at three selected regions within the plasma. The first spectrum, obtained from the plasma edge, contains only Al I emission lines. In the second spectrum, emitted from a region between the plasma centre and the plasma edge, some ionic Al II lines are appearing. While strong Al III emission lines are emitted from the third region, located at the centre of the plasma, clearly indicating that the ionisation increases towards the centre of the discharge. This now spatially resolved spectra match with observations and models previously proposed, which indicate that EDM plasmas do not have homogenous but characteristic profiles. Nevertheless, the experimental results leave room for the existence of an electron beam at the centre, a hypothesis that is investigated later in the present work.

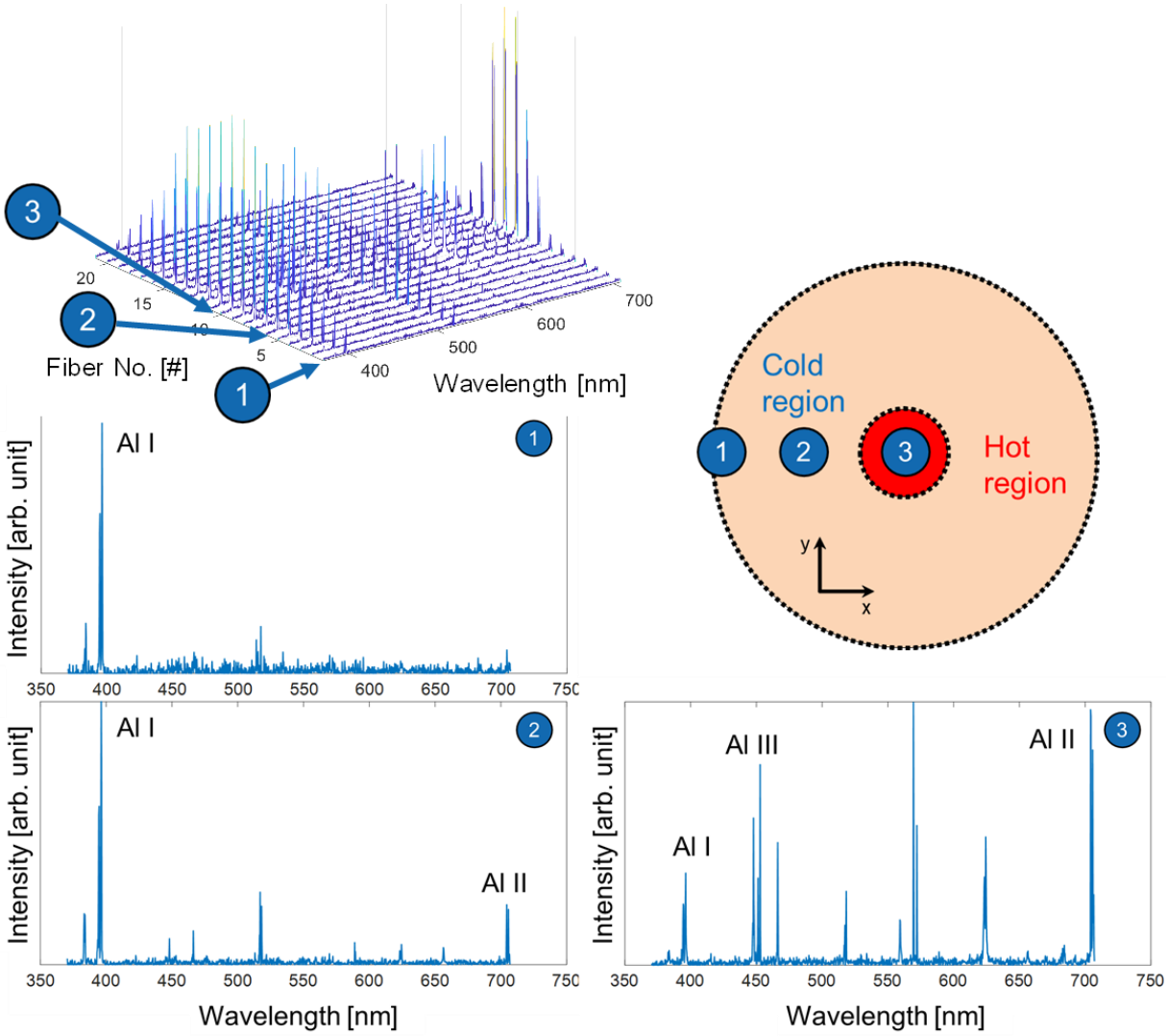

Fig. 5.3: Abel inverted emission spectra observed from different regions of the plasma compared to the theory of a colder and hotter plasma part.

Abel inverted emission lines selected from Table 4-5 are shown over time and space in Fig. 5.4 in addition high-speed imaging of similar discharge performed also with I = 15 A are visualized.

Observation of time and spatially resolved optical emission spectroscopy gives indications on the time-dependent emission line profile development. For the 15A discharge, the Al I lines emission show a strong spatial expansion over time, while the Al II lines only slightly increase as shown in Fig. 5.4. This matches well with the observations of high-speed imaging where the halo around the electrode tips expands over time, whereas the intense core region only slightly changes. Comparing the data of both acquisitions, it can be assumed that the halo is mostly composed of Al I species. In contrast to the plasma centre which shows a strongly ionised plasma. This plasma region is located close to the electrode tips, emits strong light and is mainly composed of Al II and Al III species according to the measured optical emission spectra. Furthermore, the very centre of the plasma is characterized by strong Al III lines emission.

The temporal profile development shows that the intensity of Al III decreases over time, whereas the intensity of Al II lines increases. This observation could be explained by the thermalization of the plasma. To further investigate this question, detailed information about the plasma parameters is necessary. Also, a detailed view also on copper species, as well as the electrode polarity, is important to discuss phenomena such as hot spots, topics which are addressed in chapter 7.

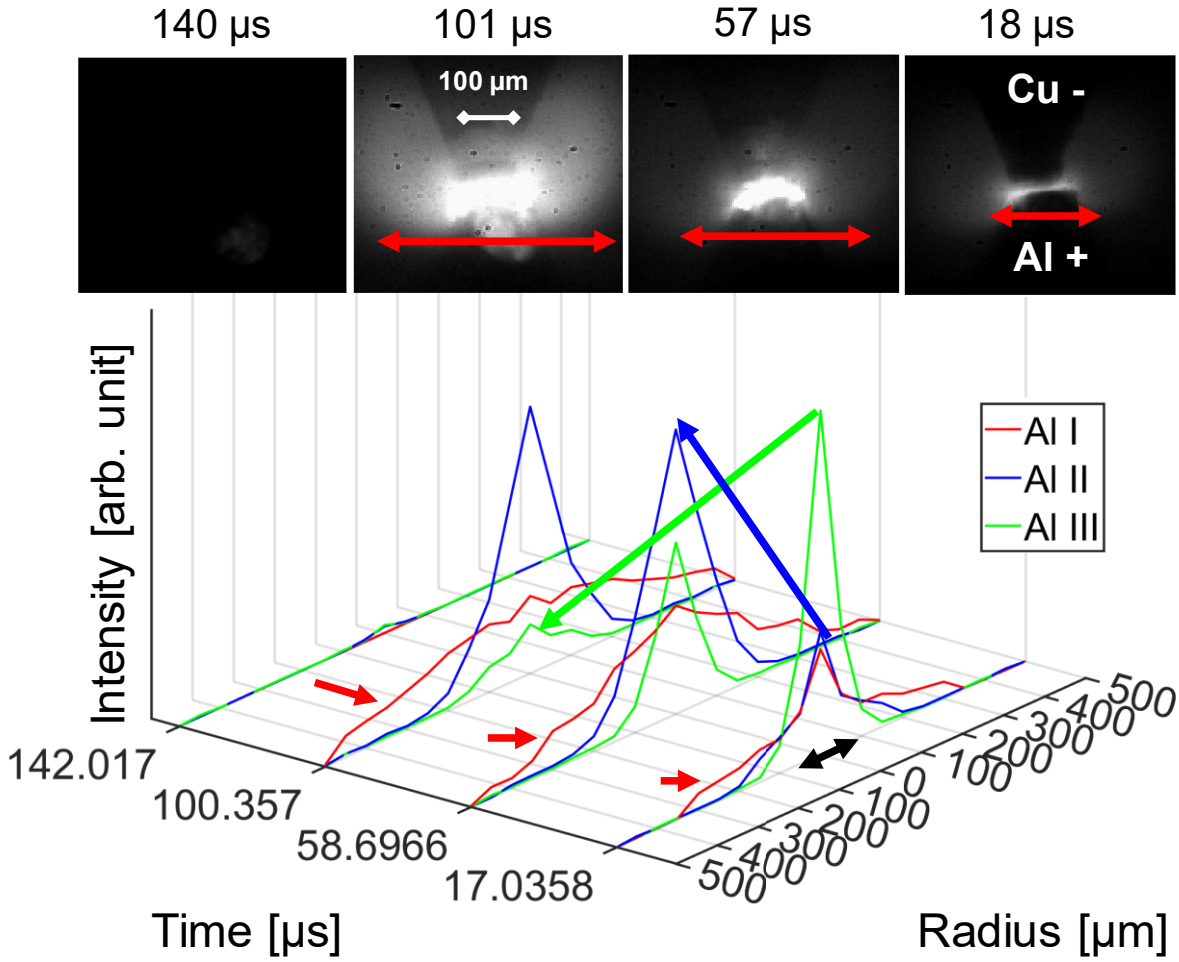

Fig. 5.4: 15 A discharge time and spatially resolved plasma with corresponding high-speed observations. Arrows highlight details: Red arrow - plasma plume expansion; Blue arrow - increase of Al II; Green arrow - drop of Al III; Black arrow - plasma channel approx. 100 µm.

For plasmas formed in discharges with electric currents from 25 A to 100 A, it has been previously reported by Jüttner et al. [29], that hot regions can be observed with radial sizes between 10 µm and 100 µm. Besides, current densities of 10^9 A/m^2 and higher flow within the hot plasma region occur. For the referred EDM plasma (I = 15 A), an average current density of $1.9 \cdot 10^9$ A/m^2 can be calculated, estimating a plasma core diameter of 100 µm as deduced from the Al III emission line profile observations in Fig. 5.4. In the introduction of this work, it was reported that usually EDM plasma temperatures of 8,000 – 20,000 K are observed. Such a high current density, of at around $1.9 \cdot 10^9$ A/m^2, cannot be transported by plasma with such low temperatures, as reported by Rakhovsky [81]. However fast electrons can lead to high current

densities. To explain the high current densities in the hot plasma region an electron beam might be considered. Rakhovsky suggests fast electrons temperature T_e varying from 5 to 6 eV and a surrounding LTE plasma with a temperature $T_i = T_e$ between = 12,000 and 24,000 K. Thus, the highly accelerated electrons could be responsible for the current in the plasma centre.

5.2 Plasma parameter profiles of EDM plasmas

This situation, having two electron temperature distributions in the plasma can be numerically simulated with PrismSPECT by adding a second energy distribution for fast electrons. In Fig. 5.5 Maxwell distributions with different temperatures are illustrated, where the black line shows the combination of the two temperature distributions blue (1 eV) and red (6 eV).

It is clearly recognizable that the number of fast electrons does not need to be high to stimulate the excitation of some Al III lines with ionization energies of 18.82 eV highlighted as green line in the figure. In a 1 eV (12,000 K) plasma with an additional fast electron fraction of 5% at 6 eV (dashed line in Fig. 5.5) 10^4 times more Al III ions are stimulated than in a comparable LTE plasma with an electron temperature of 1.25 eV (yellow line) or 1 eV (blue line). A very hot, 6 eV plasma (orange line) on the other hand has a too low probability to excite Al I.

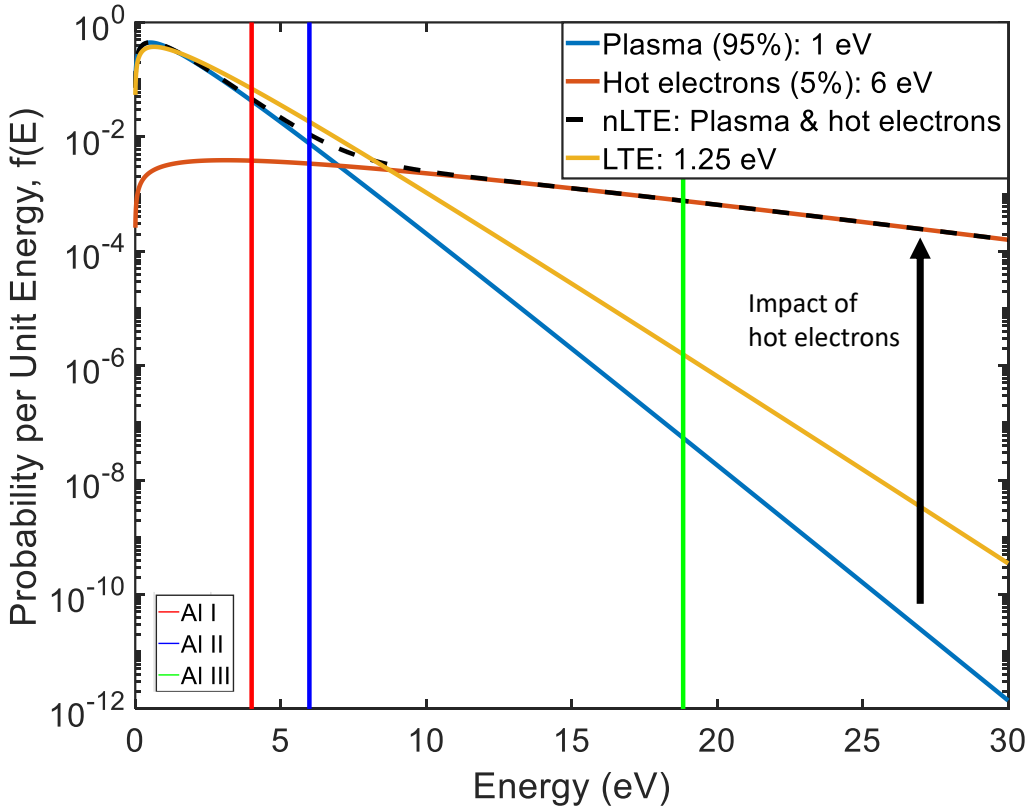

Fig. 5.5: Different Maxwellian energy distributions, with some aluminium excitation energy (red) and ionisation energies (blue and green) highlighted.

Considering all the reported observations, one can conclude that the existence of a different EDF or as presented an electron beam with a second Maxwell distributed energy is necessary. One or more non-Maxwell electron energy distributions can exist within the discharge, and in this case, the assumed two Maxwellian EDF would only be an approximation. There could also be one or more non-Maxwell distributions. One prominent candidate could be a Kappa distribution which is stronger in the region of higher energic electrons. The number of publications considering the Kappa distribution is rising [51]. According to Livadiotis [52], an important point about the Kappa distribution is that the plasma under this condition is not in thermodynamic equilibrium, but it also has a low density and is collisionless. It is also known that a superposition of two Maxwell distributions, such as reported in this thesis, can lead to a Kappa distribution [4].

The development of the electron density profile, including electrons with all temperatures, over time can be seen in Fig. 5.6. The results indicate that the electron density slightly grows during the time. Changes in the density over the time of erosion might be a result of the arc root moving irregularly removing material, or from the plasma expansion.

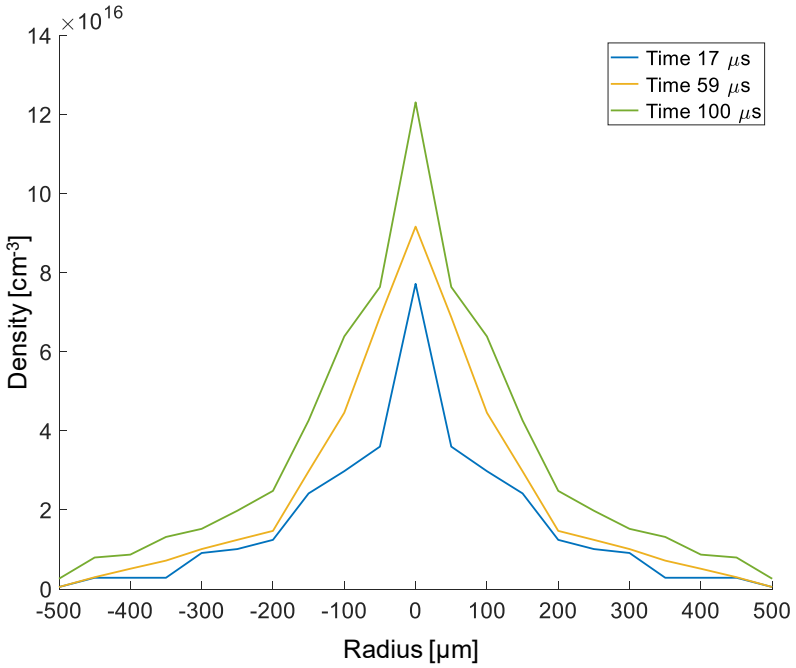

Fig. 5.6: Electron density distribution over time of the discharge presented in Fig. 5.4

The electron density is sharply peaking in the discharge centre in particular at early times the density gradient is strong. The high radial density drop could be explained by the high energy electron beam leading to a strongly localized ionisation and therefore an electron density peaking in the centre of the discharge. It is reported that the plasma density decreases rapidly at radial distances >20 µm from the spot, as

described in the literature [8] an approximation of r^{-2} fits roughly to the observed profile.

The spatially and time-resolved plasma temperatures for a selected discharge (Fig. 5.4) can be seen in Fig. 5.7.

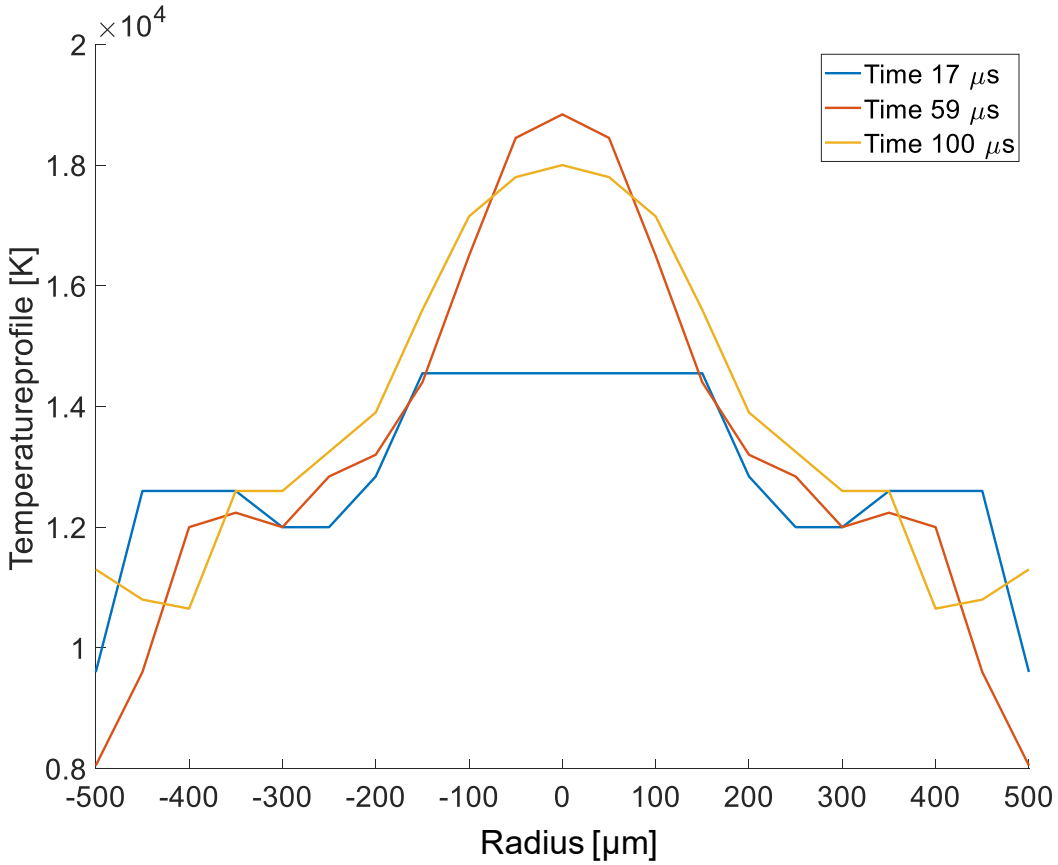

Fig. 5.7: Radial temperature profiles in the function of the discharge time for the discharge presented in Fig. 5.4

Similar to the electron density, the electron temperature shows a profile that expands and increases over time. In general, the temperature in the middle of the plasma is slightly higher. As mentioned before, Al II and Al III emission lines are not present in the plasma edge spectra for r>300 µm. As mentioned before this makes temperature estimation at the plasma edge difficult. Also, with the so-called two-line Boltzmann method temperature estimation is nearly impossible because the energy levels are very similar. This absence of Al II and Al III also indicates that the temperature must be low enough to not ionize those species (T_e < 12,000 K).

Natsu et al. [72] observed temperature profiles for discharges in air using the two-line Boltzmann method and Abel inversion. The results show a twice lower temperature in the plasma edge than in the centre with values up to 8,000 K for copper lines. In the present case applying the Boltzmann two-line method, 12,000 K +/-6% could be calculated in the present case using the Al II lines 559 nm and 704 nm wavelength, within a wide central part of the discharge. The difference between the

temperature values estimated by emission spectra simulations and two-line method has been observed earlier. Among others Mujumdar et al. [68] have shown that emission spectra simulations give indications on higher temperatures, concluding that this type of calculation is more accurate since several emission lines from different species can be involved having more support points. However, the emission spectra simulation is a much more complex method costly software and the involved calculations of the emission spectra. On the other side this method allows not only determination of the electron temperature but also many other properties and parameters important for the understanding of the discharge.

As explained earlier the determined electron temperature shown in Fig. 5.7 alone does not describe the emission spectra. In the centre of the plasma, a fraction of fast electrons exists, with an second electron temperature of 6 eV based on observations from Rakhovsky [81]. According to the emission spectra simulations, seen in Fig. 5.5, the best agreement between simulated and experimental spectra exists when an electron beam is assumed in the centre region of the plasma with electron fraction from 0-10%.

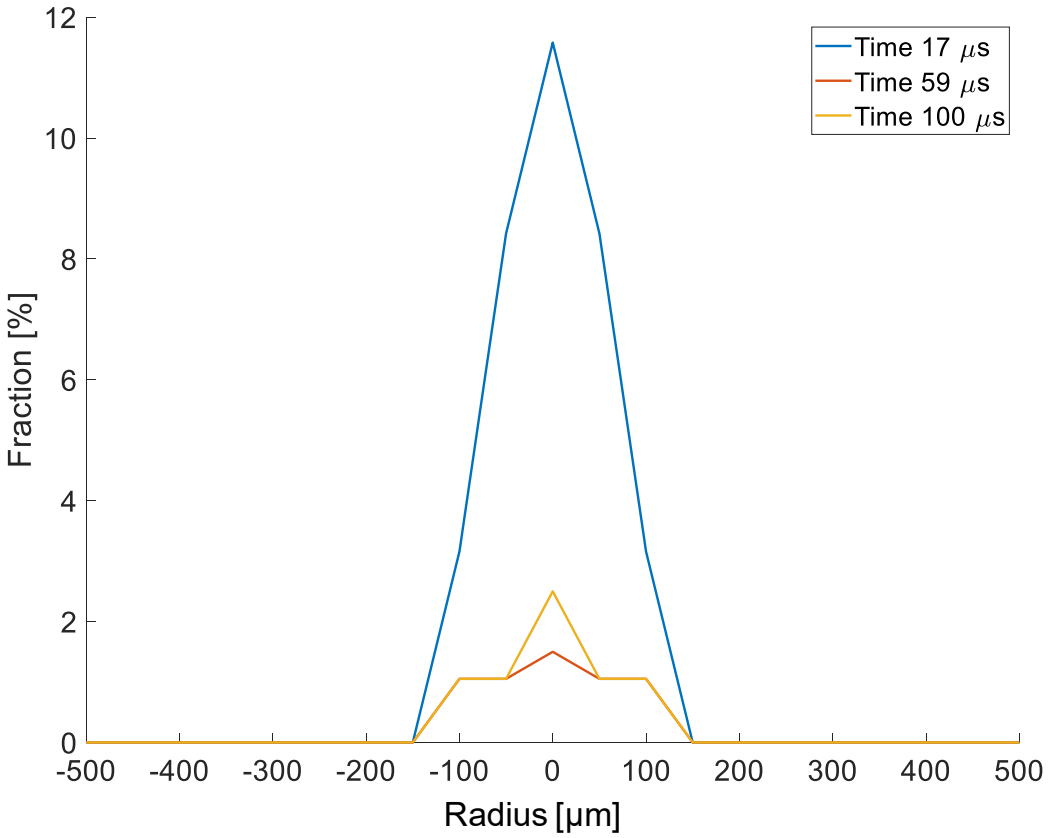

Fig. 5.8: Hot electron fraction (electron energy 6eV) in the centre of discharge determined from emission spectra simulations

Fig. 5.8 shows that in the beginning, the number of hot electrons is decreasing over time. Al II and Al III species in the central plasma region indicate the presence of a sufficient number of fast energy electrons. However, assuming a single electron temperature, the also present Al I species cannot coexist with the ionic.
The degree of ionisation and the population of Al I, Al II and Al III species are shown in Fig. 5.9. Since the mean charge is around 1 or lager ($n_e > n_i$) the plasma is called fully ionised. It can be observed that especially in the middle the number of electrons is far larger, peeking up to Z = 1.75. The mean charge is important information for further interpretation, the major number of electrons is in the centre. The population of ions Al II and Al III is increasing towards the inner plasma, with Al III dominating the plasma centre. Exited Al I species exist but far less. It can be seen that not much exited atoms have to be present to have strong Al I lines appearing in the spectra.

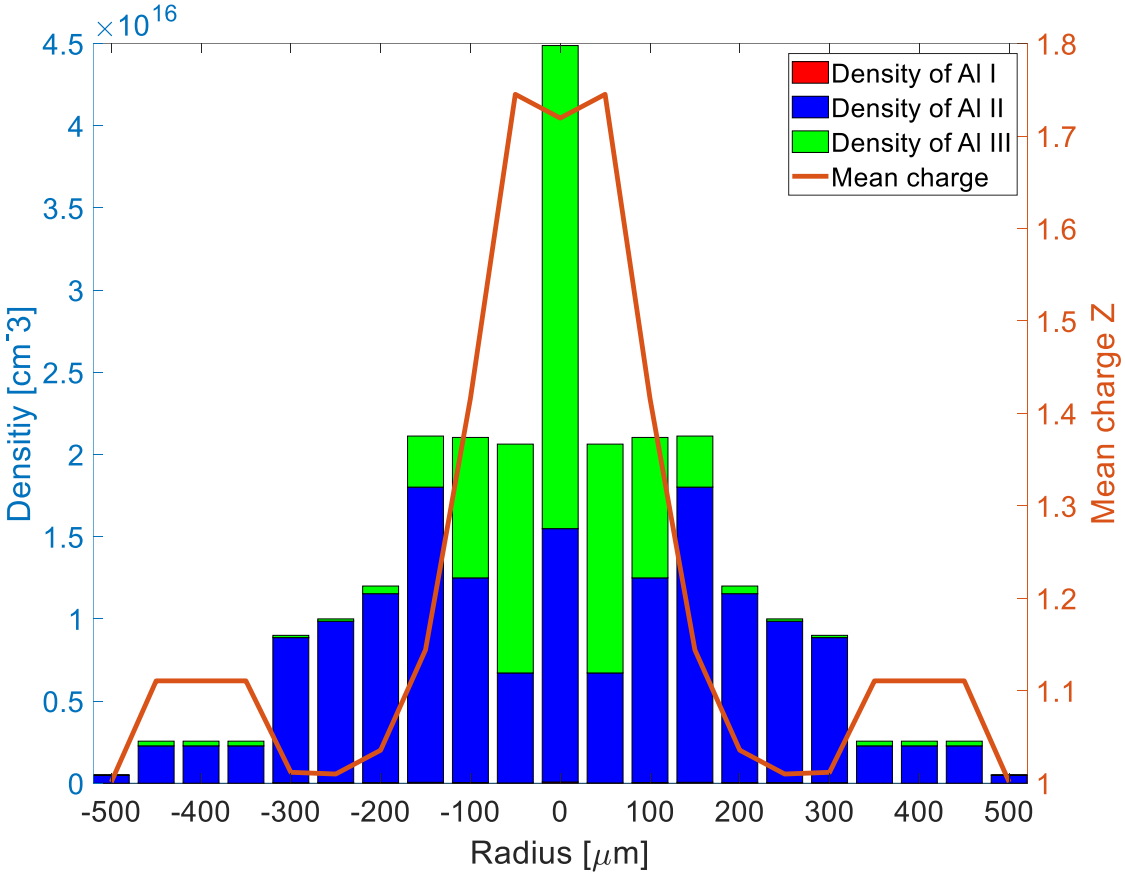

Fig. 5.9: Mean charge and ion density for the different Aluminium species form the first time point of the discharge presented in Fig. 5.4. Despite strong lines, the A I density is not present in a large amount compared to Al II and Al III

The mean charge is decreasing towards larger radii. At radii larger than 300 µm the parameters the fits are more difficult due to the fewer lines at the plasma edge, as discussed above, which means there are fewer support points for the simulation. As seen in Fig. 5.3 at the plasma shell only two lines in the emission spectra are left which reduces the number of support points drastically.

5.3 Summary

In this chapter a single 15 A discharge with a copper cathode and aluminium anode has been investigated by spatial and time-resolved spectroscopy supported by high-speed imaging of the discharge. The following information can be derived from the result achieved:

- Mean charge, density and temperature profiles of the plasma are measured and determined.
- With the observed values of density and temperature, the plasma can be considered with sufficient accuracy to be optically thin. The absorption is less as 4% per 100 µm and $\tau \ll 1$, the plasma is optically thin. Absorption appears only in the colder and less dense region in the plasma shell additionally this will only affect Al I lines in the centre. Spectroscopy for these discharges and plasmas is therefore applicable.
- In the centre (r <100 µm) of the plasma:
  - An electron population with a second Maxwell distributed electron temperature must be assumed to explain the observed spectra.
  - This is not only necessary to mimic the emission spectrum correctly but is also necessary to explain the very high current densities of $1.9 \cdot 10^9$ A/m^2.
- Electron densities of $n_e=10^{17}$ cm^{-3} in the centre and $n_e=10^{16}$ cm^{-3} at the plasma edge are observed.
- Temperatures higher than 10,000 K were calculated by CR simulation with PrismSPECT.

6 INFLUENCE OF CURRENT ON EDM PLASMA OVER TIME

Electric discharges performed with currents from I = 2 A to 20 A are investigated in this thesis and discussed in the following chapter. Due to the sharply tipped electrodes and air as dielectric medium dissipation of the heat generated by the discharges is very limited. The electric current has a major influence on the discharge properties. Discharges made with I = 20 A are characterized by strong electrode erosion and explosively expanding plasmas, while observations for discharges performed with I = 2 A are much more difficult and such effects are substantially less visible.

6.1 Discharges performed with currents of 2 A

Discharges made with current I = 2 A are investigated in the present work just by high-speed imaging, since their plasma light emission is insufficient for the OES equipment used. Furthermore, this type of discharge is very unstable and can be interrupted due to a collapse of the plasma channel. Fig. 6.1 shows two discharges made with I = 2 A and different polarities. Discharges performed with aluminium cathode and copper anode are even less stable than the ones made with the inverted polarity.

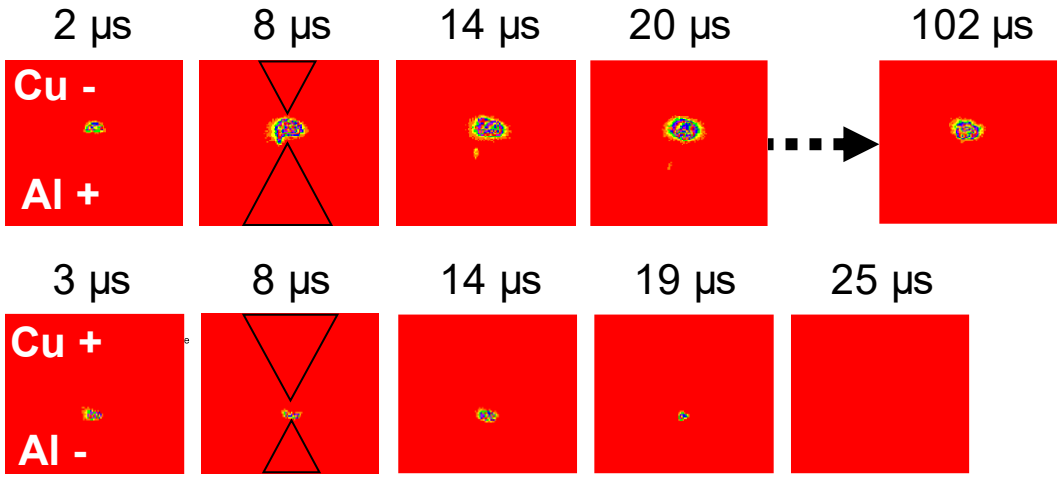

Fig. 6.1: High-speed imaging artificially coloured of discharges made with current I = 2 A at different polarities

The low stability for small currents and the different behavior of the plasmas with different polarity indicates that the current is not high enough to release the vaporize and ionize the electrode metal, which is essential to build up the metal plasma. This is confirmed by [56,94], who also showed that the plasma is dominated by the anode material. Discharges performed with aluminium anode are probably more stable due to the lower necessary energy to evaporate and ionize this material.

Literature [19] reports that discharges similar to the ones presented here have usually a cold cathode, while their stability is strongly linked to the electric current. In addition, the lifetime of the discharges can vary from experiment to experiment. The

discharge will be extinguished if the current becomes too low, even for a very short period in the nanosecond range. Usually, the current is shaped by several transistors in EDM machines. During the switching times, the current can slightly drop, causing instabilities in the discharge. The stability can be increased using an additional resistor-inductor circuit, which allows the EDM process to be performed properly with low current pulses (I = 1 and 1.5 A), as described by Maradia [61]. Apart from the current and electrical circuit the following facts about arc lifetime can be added according to Boxman et al. [8]:

- Electrode geometry: arc lifetimes are proportionally long for large electrode areas and small gap distances.
- Material: stronger metal vapor pressures lead to longer arc lifetimes.
- Surface condition: Arcs exist for longer time on rough electrode surfaces.

Other influences on the discharge stability are the electrode surface temperature and the presence of magnetic fields. Additionally, the prior breakdown mechanism could play a role yielding a relatively small quantity of particles, electrons and ions from the electrodes. Researchers like in [8] describe the breakdown process as an exchange of electrons and ions between the electrodes, whereby ions bombarding the cathode release electrons to the anode. The stability of the plasma channel depends on the yield of particles originating from the electrodes. Since the thermal properties and work function which are important for ion and electron emission, are different for these materials a change of the discharge stability by polarity is to be expected.

6.2 Discharges performed with currents from 5 A to 15 A

Discharges made with currents varying from 5 A to 15 A seem to be the most stable for the applied sharp tip electrodes. Nevertheless, the discharges differ in their appearance in terms of plasma size and flushing efficiency regarding erosion. Fig. 6.2 shows high-speed imaging of such discharges.

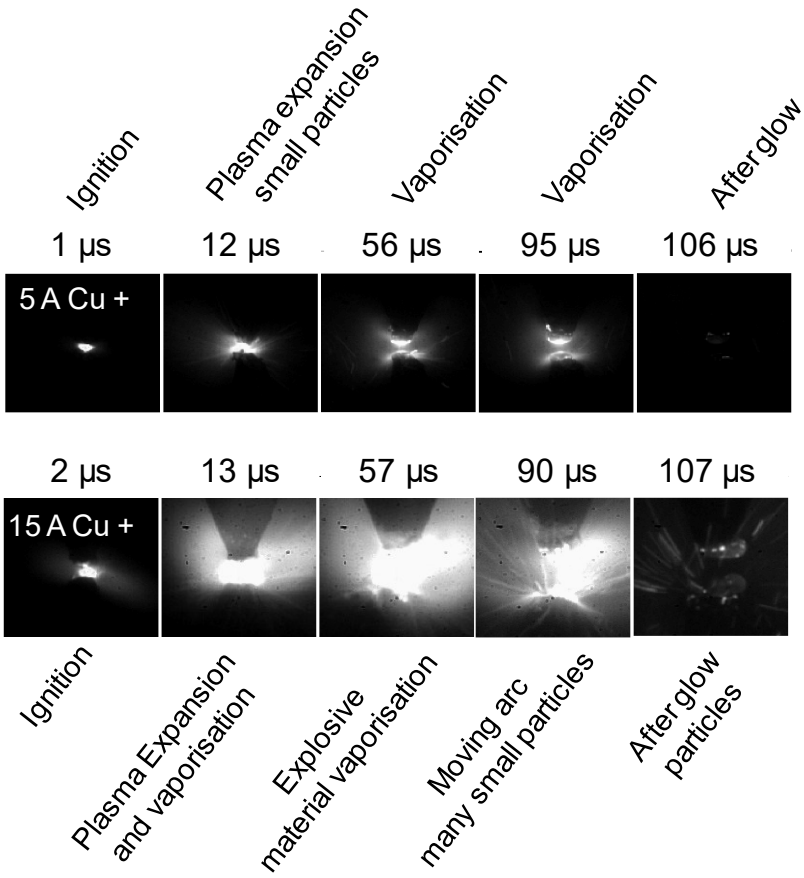

Fig. 6.2: Development of a discharge performed with current I = 5 A (top) and with I = 15 A (bottom)

After ignition, the discharge performed with current I = 15 A develops more rapidly, showing often explosive material removal. In contrast, the discharge made with I = 5 A leads less often to particle removal and more vaporization of the electrode material according to the high-speed imaging results. Furthermore, discharges made with I = 15 A have a stronger afterglow, emitting light 40 µs after the plasma channel collapse, which can be seen in Fig. 6.3. The prism colour code allows visualization the left-over plasma in the gap.

This is an important information for multiple discharges, since the breakdown for consecutive discharges can occur close to the previously discharge, hampering the EDM process. Unwanted side effects are locally high thermal load which can lead to cracks in the surface and bad surface quality. Additionally, a decreasing accuracy can be expected since the craters are not uniformly distributed and material is removed in specific regions.

This phenomenon has been also studied by Kitamura et al. [34] who shows that with small pause times the distance between two consecutive discharges shrinks. From these observations Morimoto and Kunieda [67] developed a model determining the discharge locations in liquids.

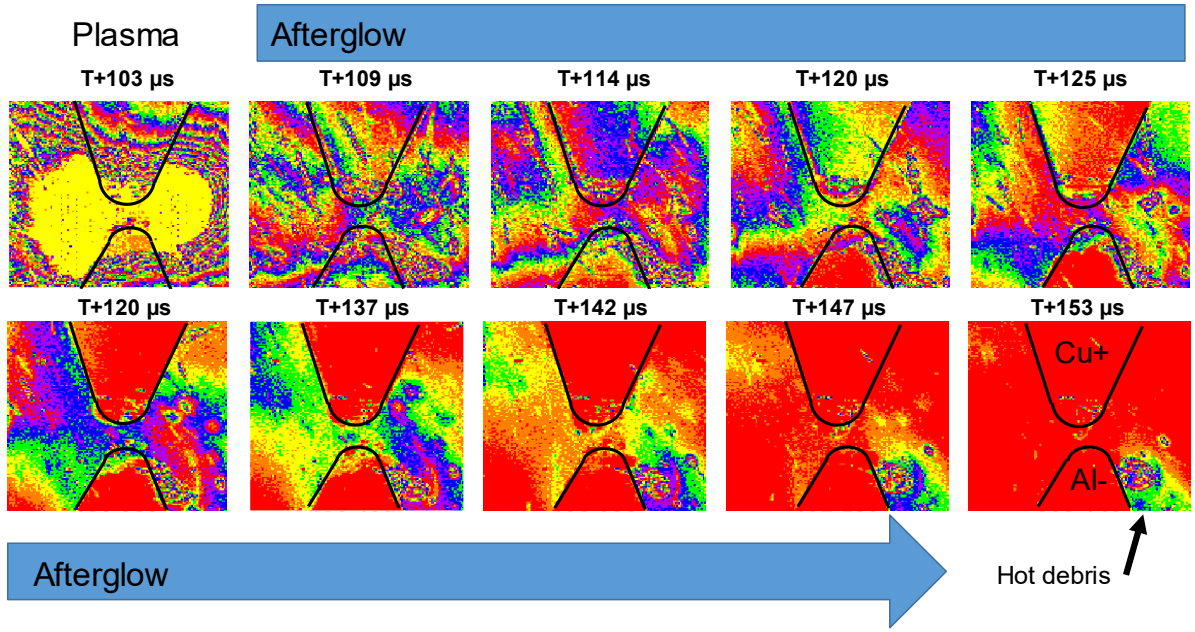

Fig. 6.3: High-speed imaging of a discharge performed with I = 15 A; afterglow can be visualised thanks to prism colour map

OES analysis and profile evaluation

Optical emission of electric discharges performed with currents varying from 5 A to 15 A can be well acquired by OES. High-speed imaging and OES of a discharge made with I = 5 A can be seen in Fig. 6.4.

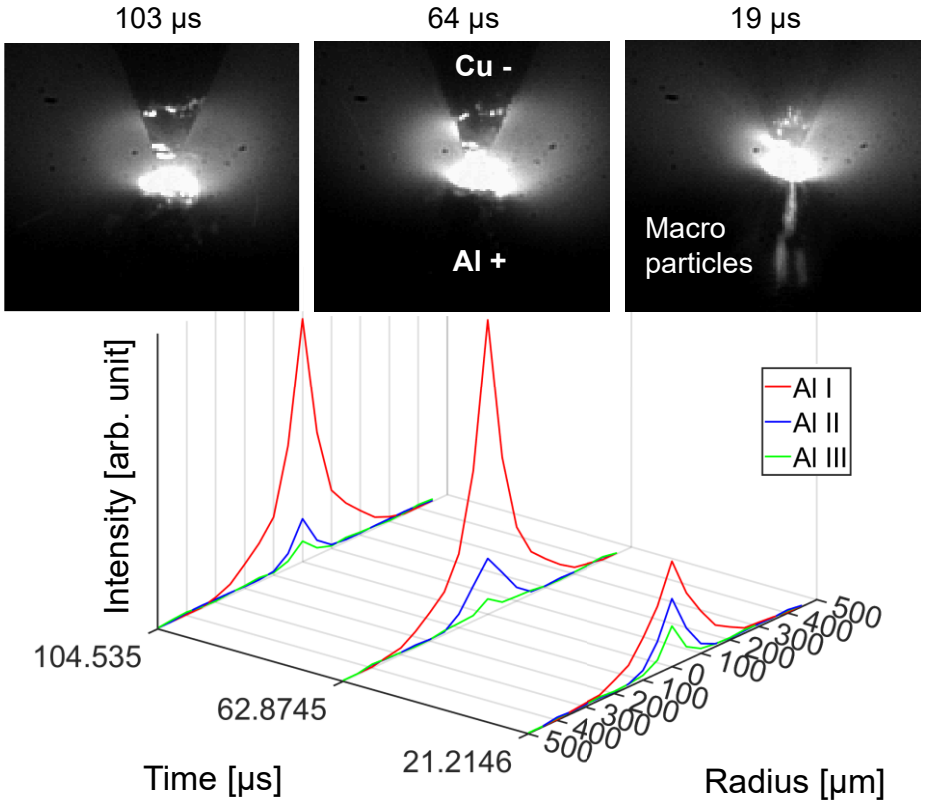

Fig. 6.4: Time and spatially-resolved OES together with high-speed imaging of a discharge performed with current I = 5 A

Discharges made with I = 5 A are very stable and do not move much, as seen in the high-speed images. The expansion of the plasma is also small during the time. Al I lines dominate the optical emission spectrum during the whole discharge, whereas Al II and Al III are rather weak and lose intensity over time. The emission profile shows a constant thin and slender shape border and peaks in the middle.

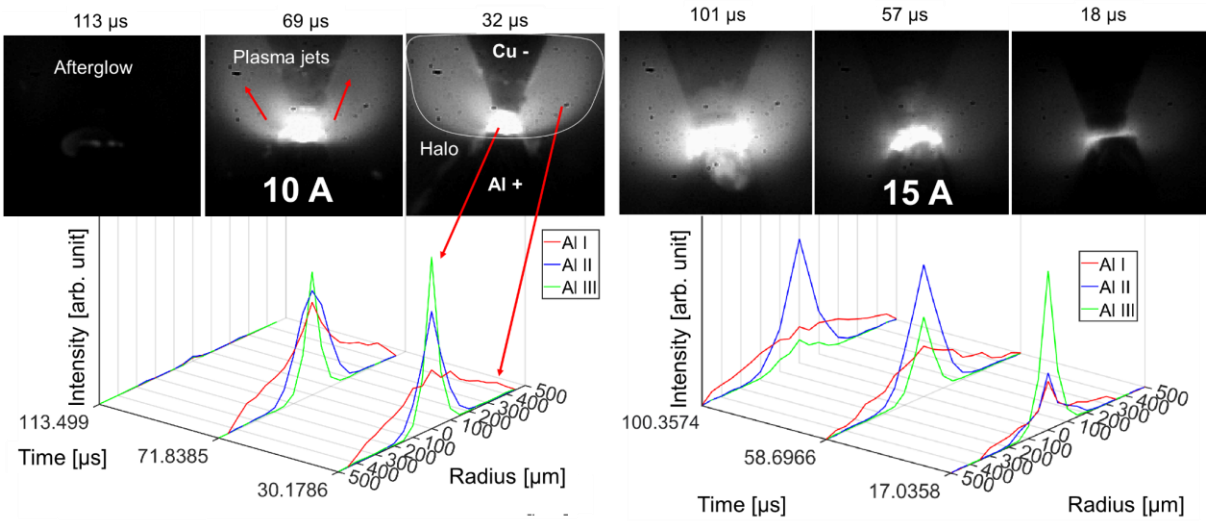

Fig. 6.5: Time and spatially-resolved OES together with high-speed imaging of discharges performed with I = 10 and 15 A

As shown in Fig. 6.5, discharges made with I = 10 A have a strong expansion of the plasma in the high-speed images, which is also visible in OES. This is in contrast to the discharges performed with I = 5 A. The spatial distribution of Al I lines is also different, showing a much wider profile. The same trend, even stronger, can be seen for the discharge performed with I = 15 A, as already discussed in Chapter 5 in detail.

Fig. 6.6 shows optical emission spectra acquired from discharges performed with different electric currents. A peak of emission lines from highly ionized species is always observed in the centre of the plasma.

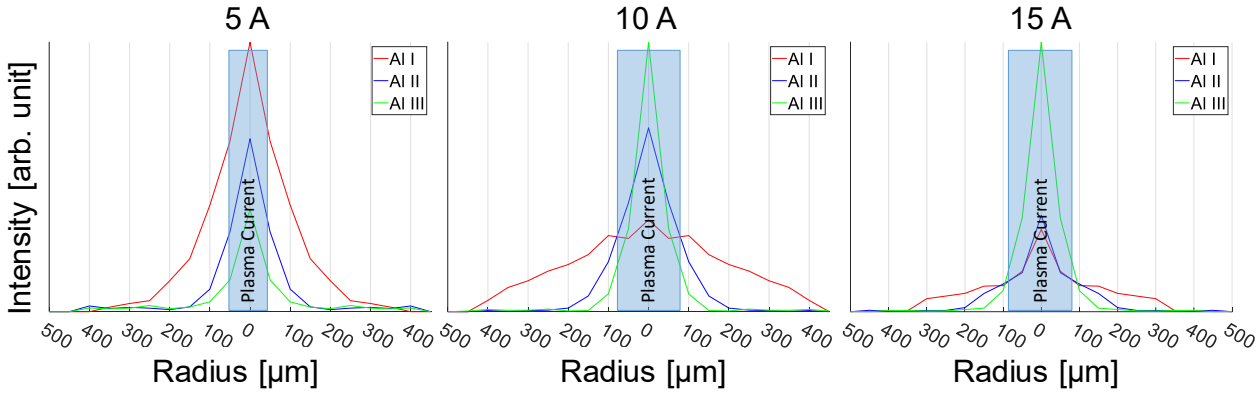

Fig. 6.6: Comparison of emission profiles for different currents with plasma channel, defined by Al III emission, highlighted at the first time point.

Although it is also possible to perform OES for discharges generated with higher currents, their plasma properties are highly influenced by electrode erosion. In general, such discharges also have strong emission of highly ionized species in their centre as can be seen in Fig. 4.21.

6.3 Plasma parameter analysis

In this chapter, previously the spatial distribution of optical emission lines of EDM discharges performed with different currents is observed. The profiles of Al I lines distribution show that the plasma plume expands as a function of the time and the applied electric current. The plasma centre, on the other hand, has strong Al II and Al III emission lines, for which their spatial distribution only slightly expands when a high current is applied. The profiles from ionized lines show an increase in intensity in relation to the Al I profile. This suggest an increasing degree of ionization with rising currents which could be caused by the increasing current densities.

Emission spectra simulation of EDM plasma can help to support this observation. Fig. 6.7 shows simulated values of the plasma composition and its mean charge. The red arrow indicates the point where the mean charge drops below Z=1. The region of high ionization increases with the current.

The radial region where the electron density is higher than the ion density increases with the discharge current. Furthermore, higher currents lead to an increasing amount of highly ionized species towards the centre of the plasma, while also slightly enlarge the region where ionic emitting species can be observed.

The results indicate that the density of hot electron increases in the centre of the discharge for higher currents. This observation supports the discussion reported in chapter 5 , since a large number of electrons should be available to carry the electric current. Due to the restricted area of the electrodes, the current density increase can only be explained by a rising number of hot electrons, assuming a constant electron temperature.

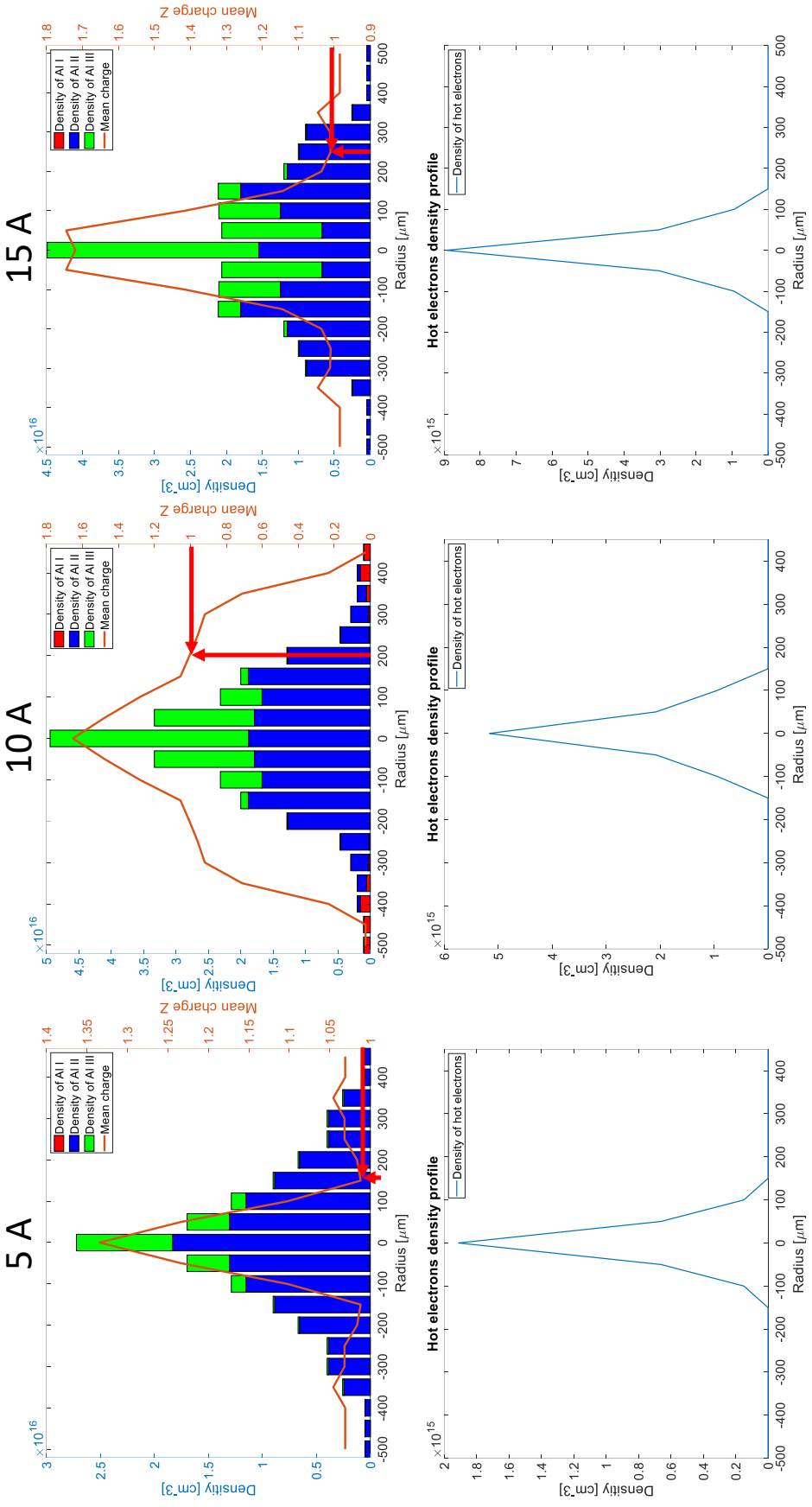

Fig. 6.7: Simulated profiles for the plasma properties: composition with atomic and ionic aluminium species and mean charge (top), and hot electron density for the profiles (bottom) shown in Fig. 6.6

Analysis of the discharges

Since each discharge behaves differently, the absolute values can vary significantly. This is known and very typical for EDM discharges. An example can be seen in single crater analysis reported by Maradia [61], shown in Fig. 6.8. The depth and radius of the craters is analysed over the discharge duration, showing very scattered data. Nevertheless, it can be shown that the crater radius and depth increase with the discharge duration.

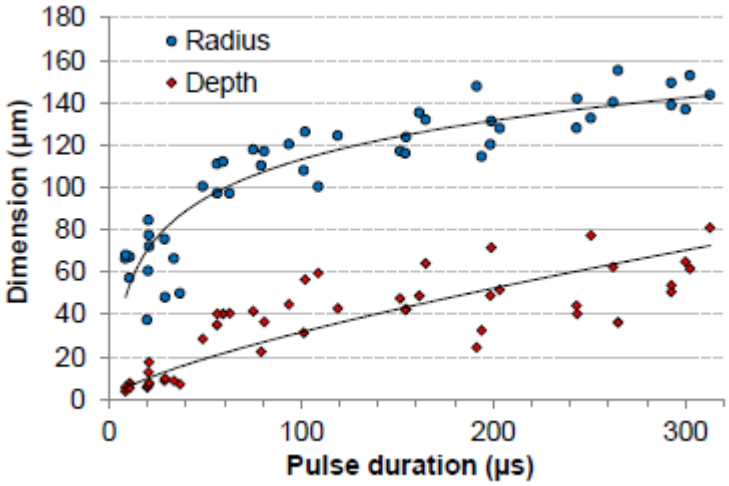

Fig. 6.8: Crater dimension over discharge duration for an I = 20 A pulse using a graphite anode and steel cathode with 1 mm diameter [61]

To analyse the influence of the behaviour of the plasma for currents, four experiments for each current are analysed over time. The different plasma parameters are presented with the respective standard deviation for I = 5, 10 and 15 A, over the discharge duration of 100 µs. The peak of the electron temperature profiles can be seen for different currents in Fig. 6.9. The discharges performed with I = 5 A have a lower temperature than the those made with I = 10 A and 15 A and showing a constant trend over time. In contrast, higher currents lead to rising temperatures over time.

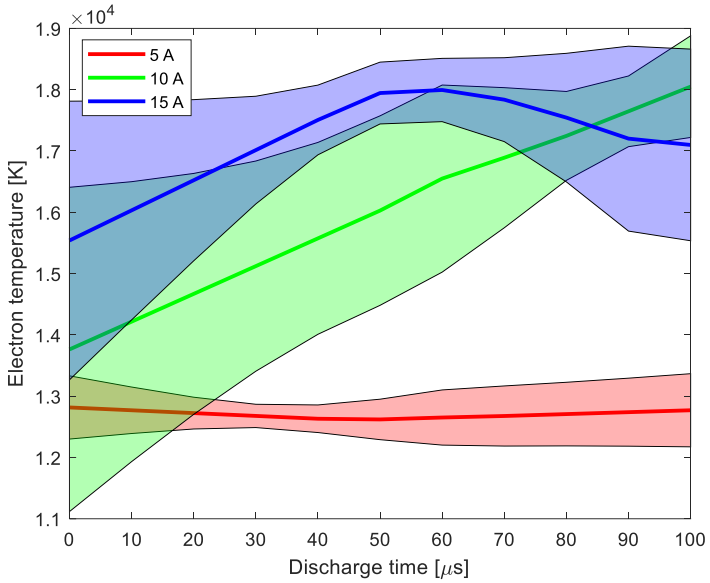

Fig. 6.9: Time behavior of the peak of the electron temperature profiles for different currents, shaded area illustrates the standard deviation.

The peak of the electron density profiles is shown in Fig. 6.10. Higher electron densities can be observed with rising currents. Like the observed temperature the standard deviation is larger at higher currents. The temporal behaviour of the electron density shows only slight variations.

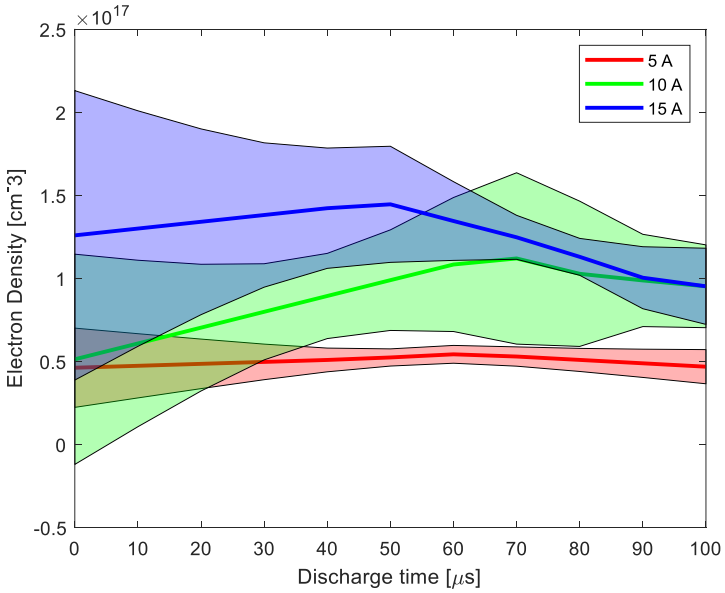

Fig. 6.10: Time behavior of the peak of the electron density profile for different currents; shaded area illustrates the standard deviation.

The development of the peak of the hot electron fraction profile over time and for different currents is shown in Fig. 6.11 . Discharges performed with I = 15 A show higher values, while in general the differences of the hot electron fraction between the currents is not clear. However, a clear trend for the discharge time is visible. The percentage of hot electrons decreases over time for all currents. The electron beam with fast electrons is heating the plasma. This is also in agreement with Fig. 6.10 which

shows rising temperatures. The transport of the current can be compensated by many slower electrons, still a decent fraction of fast electrons still exists at the end of the discharge.

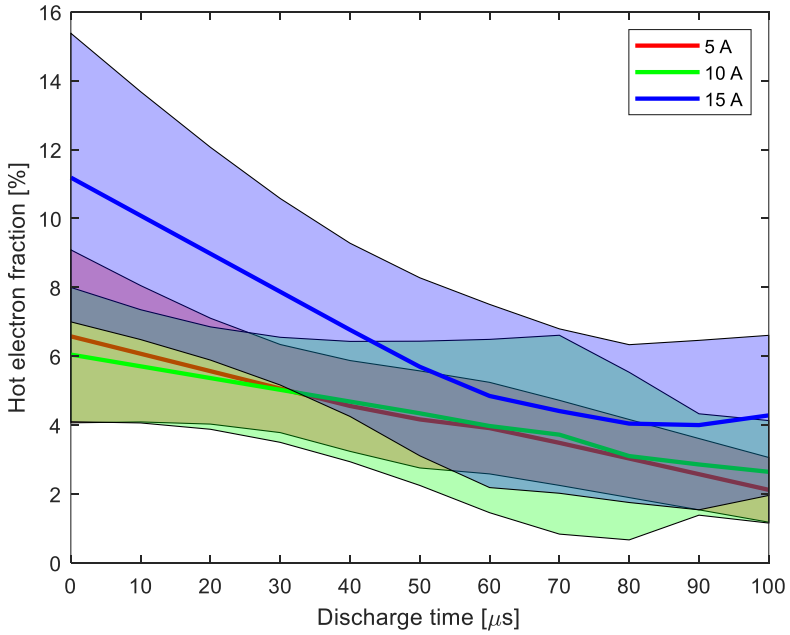

Fig. 6.11: Time behavior of the peak of electron temperature profile for different currents; shaded area illustrates the standard deviation.

Additional information could be gained looking at the broadening of the emission profile over time. The development of the Al I and Al III profile broadening over the discharge time is shown in Fig. 6.12. The difference between the profiles is more significant at the bottom of the profiles. Hence the radius at a fifth maximum of the profiles of Al I and Al III emission is represented.

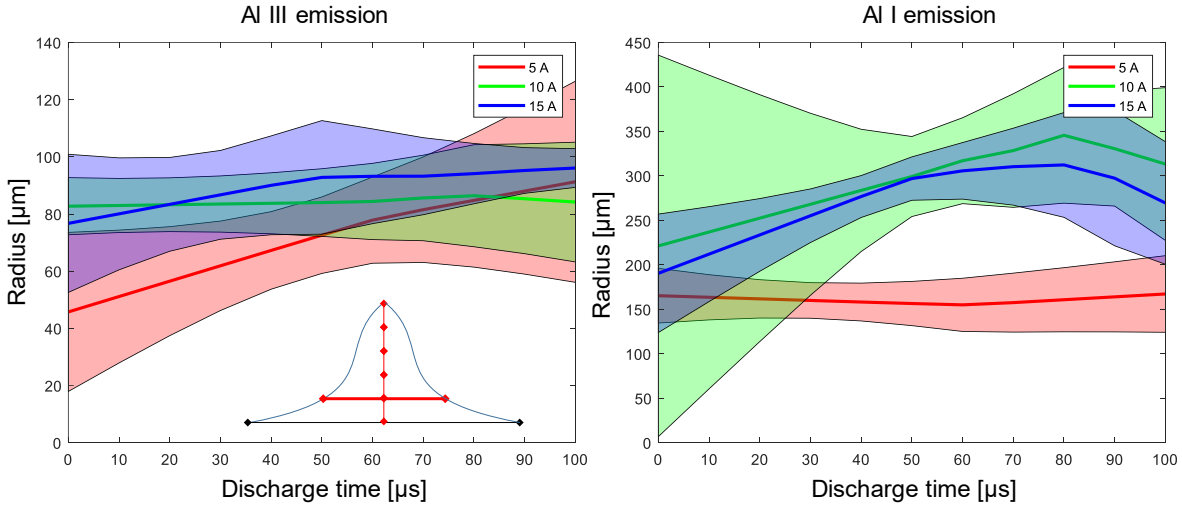

Fig. 6.12: Al III (left) emission line profiles at one fifth maximum of the profile peaks and half width of Al I (right)

The width of highly ionized Al III emission profiles shows increasing radius over time, especially for I = 5 A discharges. However, all current show a similar behaviour over time and the radius is not exceeding 100 µm much. The behaviour is comparable

to the hot electron density but with an inverse gradient, indicating that the fast electron component is restricted to the active area on the electrode tips.

Al I emission on the other hand, shows a different behaviour, 5 A discharges differ from those with I = 10 A and 15 A. Al I profiles expand much larger which could be already observed in the detailed analysis of emission profiles, as shown before in Fig. 6.13 to Fig. 6.6. The behaviour of the exited emission profiles shows a consistent behaviour with the electron temperature shown in Fig. 6.10, the rising temperature goes a long with an expanding plasma plume.

The different behaviour between 5 A discharges and discharges with higher current can be explained by the electrode geometry. All discharges start between similarly sharply tipped electrodes. After a few microseconds, the high load on the electrodes causes severe erosion. During the discharge duration, the electrode geometry, the discharge and the plasma is less affected by lower currents as can be seen in Fig. 6.14.

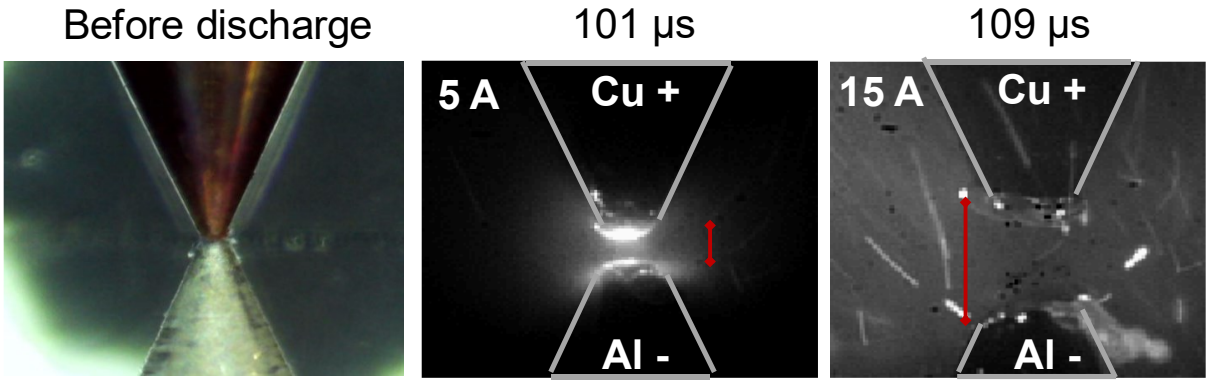

Fig. 6.14: Image electrodes unused (left) and after erosion 5 A and 15 A (right). After discharge the gap 3 times lager at 15 A compared to 5 A.

6.4 Summary

In this chapter single discharges with a copper cathode and aluminium anode with currents I = 5 A, 10 A and 15 A have been analysed in detail with spatial and time-resolved spectroscopy supported by high-speed imaging and emission spectra simulation. Discharges with I = 2 A were unstable and had not sufficient light. From Chapter 6 the following information can be derived:

- Profiles for light emission of different species as well as plasma temperature and density profiles are present for all currents
- Profiles are broader for higher currents
  - This applies particular to Al I emission line profiles
- The amount of highly ionizes species Al II and Al III in the plasma centre increases with increasing currents
- Time-resolved analysis of several experiments reveal
  - Hot electron fraction is decreasing over time for all currents
  - The width of the Al III profile is increasing over time for all currents

        - In both higher currents show slightly higher values
    - The width of the Al I profile is increasing only for currents higher than 5 A
        - This also counts for the peak height of the temperature profile
- From the observations it can be assumed that the plasma core behaves similar over time for the different currents
- Absolute numbers of plasma parameters like temperature and electron density as well as the emission intensity of lines are larger for higher currents
- The plasma plume develops differently over time for higher currents
    - This can be especially observed with the electron temperature and Al I emission lines.
- The erosion of the electrodes is increasing with increasing currents affecting the electrodes geometry over time and influencing the discharge plasma

7 ANODE AND CATHODE PHENOMENA

The strong influence of the electrode polarity on the EDM process properties is well known. In simulations this is described by different energy fractions deposited on the anode and cathode during machining. The main research is done to understand the material removal on the tool electrode (wear) and the workpiece (MRR) electrode under different electrical parameters and fro different electrode materials. Additionally, the chemical behaviour of the involved materials during the process is important, mainly because the electrode material properties can change drastically. This must be particularly considered when eroding in carbon-based dielectrics. The formation of carbon layers as reported by Maradia [61] or carbide layers as reported by Holsten et al. [27] and Wiessner et al. [95] among others, drastically change the erodibility.

In industrial applications, the electrode polarity is changed by experience based on the best result for tool wear, material removal rate and surface quality. In finishing strategies, copper electrodes with negative polarity are used while graphite electrodes are used for roughing usually with positive electrode polarity.

For discharges in air as a dielectric, most chemical influences can be neglected which simplifies the analysis of anode and cathode behaviour.

7.1 Optical emission spectroscopy

To contribute to this important research field, the newly developed methods in this work were used to investigate the influence of the electrode polarity on discharges performed with electric currents I = 5 A and I = 15 A.

When looking at the aluminium lines only, discharges performed with copper anode show similar behaviour like the ones made with the same material as cathode. Fig. 7.1 shows a 5 A discharge with a copper anode. In comparison to the already discussed copper cathode (Fig. 6.1) lines are very similar, showing constricted profiles with dominating Al I lines. Some differences can be identified between discharges performed with different polarities: Al I lines are decreasing over time compared to Al II and Al III. The exactly opposite behaviour is observed for OES of discharges that use aluminium as anode.

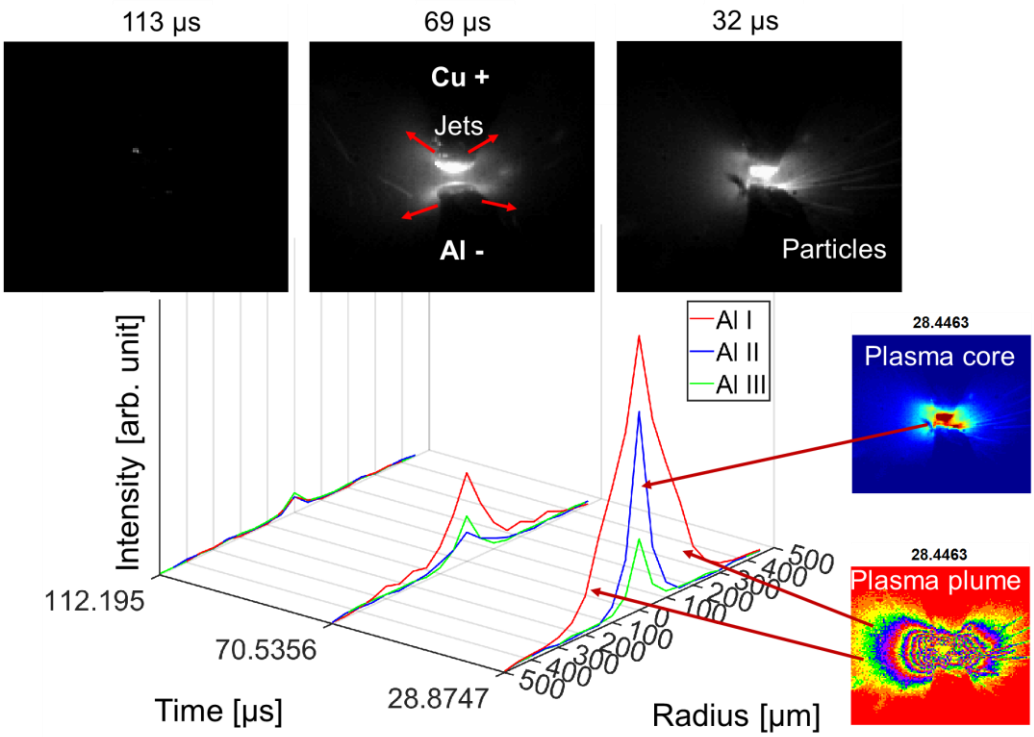

Fig. 7.1: OES resolved in time and space and high-speed imaging of a discharge performed with electric current I = 5 A, copper anode aluminium cathode

High-speed imaging shows strong light emission on the copper electrode with positive polarity. Similar trends regarding the polarity can be observed in the 15 A discharges. As observed before the higher current result in stronger emission of ionised lines like Al II and Al III. In Fig. 7.2 the 15 A discharge with copper anode shows stronger Al III lines In comparison to the other polarity, where a copper cathode is used, much less broadening over time for all observed profiles occur, seen in chapters before in Fig. 5.4 and Fig. 6.5. Furthermore, the total emissivity of all aluminium species is decreasing.

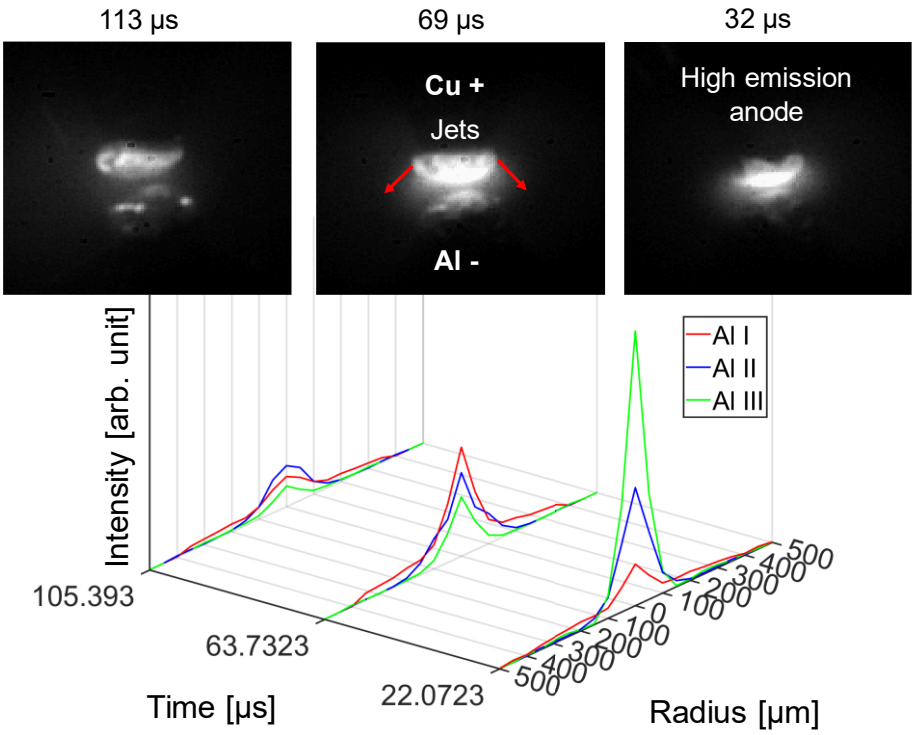

Fig. 7.2: OES resolved in time and space and high-speed imaging of a discharge performed with electric current I = 15 A, copper anode aluminium cathode

Application of two different materials as electrodes allow a proper analysis of the ionisation of species originated from anode and cathode materials. In order to analyse polarity-dependent phenomena of the discharges, the copper lines Cu I 515 nm and Cu II 490 nm are compared to the Al I 394 nm line. Fig. 7.3 shows the two examplary cases of discharges made with current I = 5 A and 15 A applying both polarities.

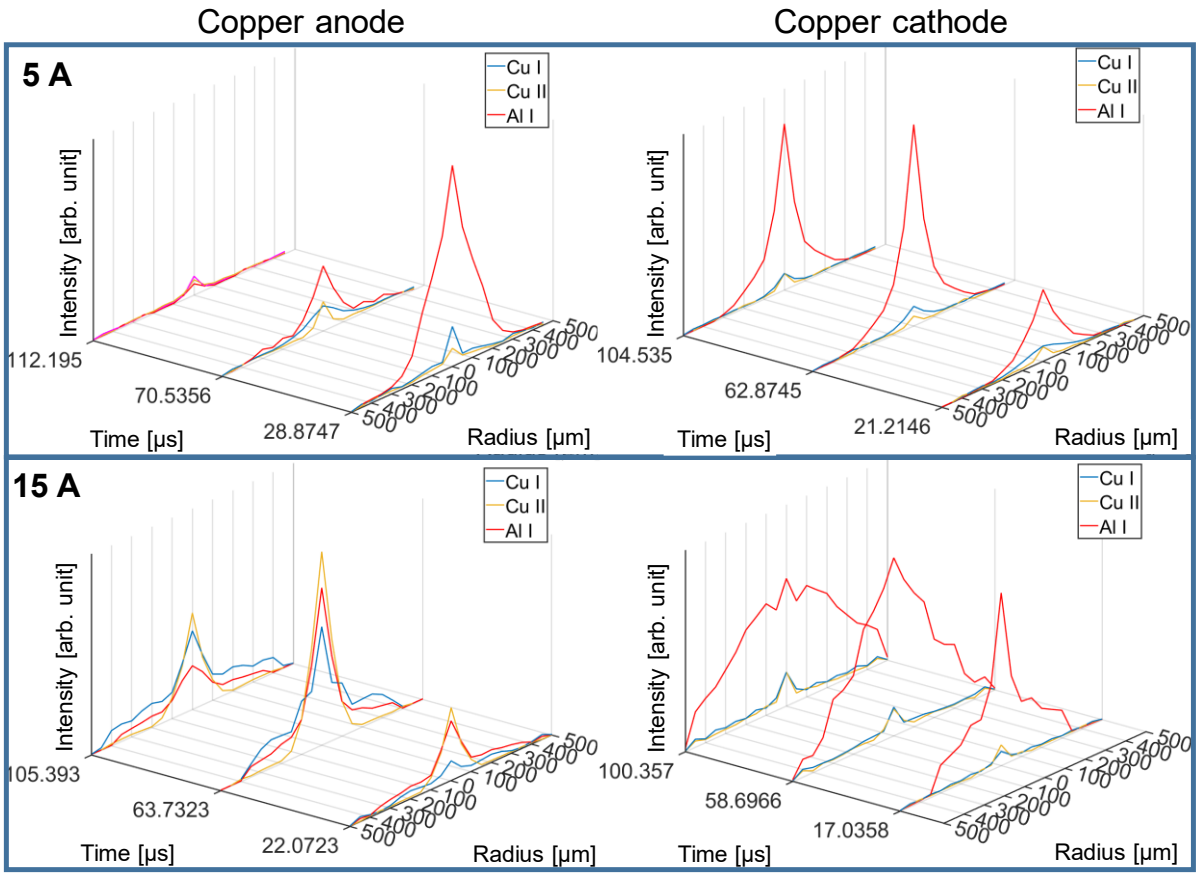

Fig. 7.3: Emission line profiles of copper and aluminium for 5 A and 15 A for both polarities.

Emission of copper lines is very strong when this material is used as anode, whereas the emission is much weaker when this material is used as cathode. This can be clearly observed as shown in Fig. 7.3 for discharges performed with electric current I = 15 A, while for lower energy discharges like those with I = 5 A, the difference is less pronounced and Al I emission is generally dominating.

Those observations can lead to the following conclusions:

- Vaporization of material from both anode and cathode takes place during the discharge
- The metal vapour is dominated by the anode material during the time, mainly visible in line emissions for high current discharges
- Species originated from the anode material are highly ionized as can be seen e.g. for I =15 A in Fig. 7.3 for copper anode and in Fig. 6.5 for aluminium anode
- Aluminium always takes a role in the discharge most likely due to its low melting and vaporization temperature

7.2 High-speed imaging

High-speed imaging allows to observe different phenomena involved near the anode and cathode thanks to a clear view of both electrodes. Therefore, a detailed analysis is reported here using this diagnostic method as shown in Fig. 7.4. the anode material

emits strong light, while its vapour is ejected sideways and towards the cathode. In addition, plasma jets and particle injection are observed coming from both electrodes. The plasma jets leave the electrode sideways, most probably due to the pressure build up in the inter-electrode gap.

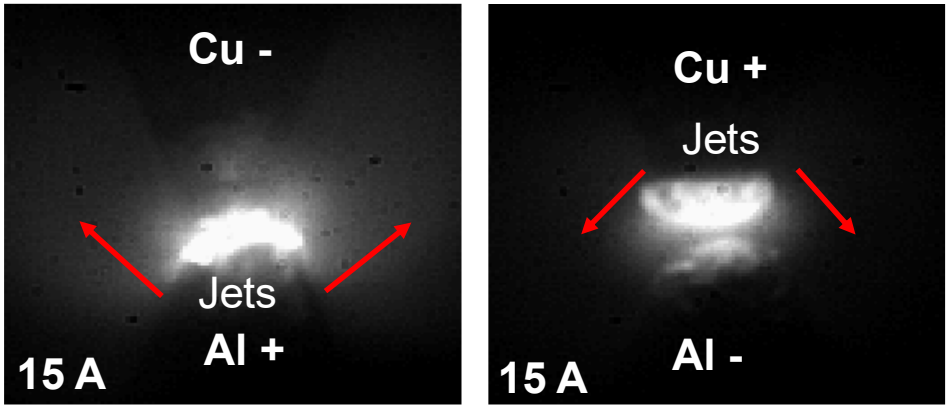

Fig. 7.4: 15 A discharge for both polarities showing a high emissive anode

A detailed view is given in Fig. 7.5 for a discharge performed with I = 5 A. Analysis of the high-speed imaging results indicates that particles are ejected from the electrodes with speeds between 5 and 20 m/s. In literature [8], it has been reported that the cathode can be a source of liquid droplets with sizes varying from 0.1 µm to about 100 µm, which matches with the observations reported here. The plasma jets leave the electrode sideway most likely because of the pressure formed in between the electrodes.

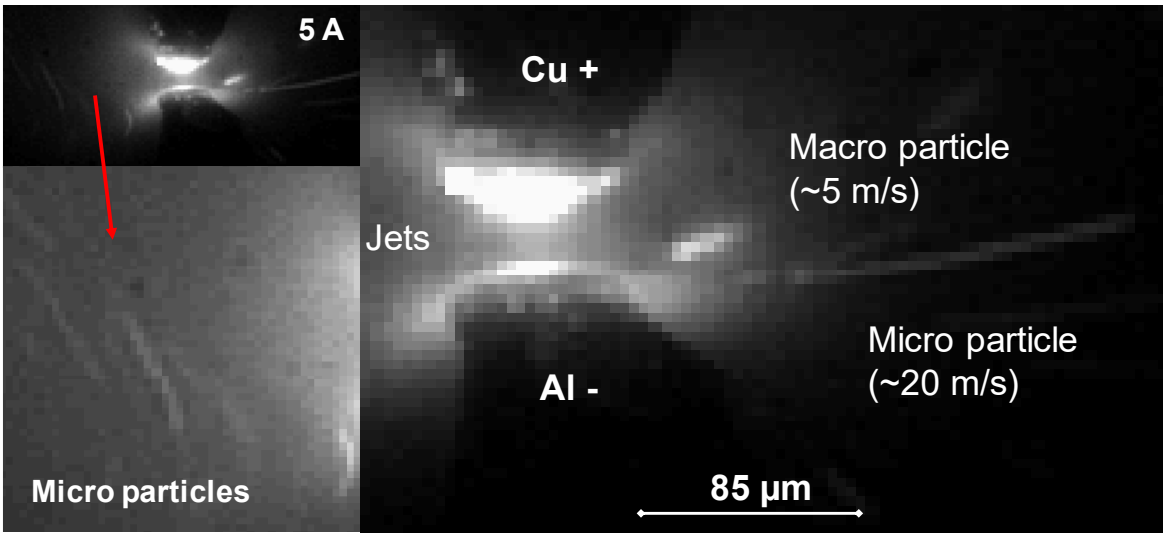

Fig. 7.5: Discharges performed with current I = 5 A with highlights on the fast particles on the left and luminous anode in the right side. In addition, plasma jets can be observed leaving the electrodes sideways.

High-speed imaging of the discharges indicate that discharges have not always the same behaviour and that they change over time. Fig. 7.6 shows its arc root moving on

the aluminium cathode surface. Furthermore, at higher currents, strong erosion on the cathode can be observed, occurring in form of particle removal.

A well-known erosion model that describes explosive particle removal from the electrode is named “thermal runaway”. The electrode surface is supplied with more energy than it can dissipate, which results in extremely high temperatures. This accumulated energy is released by explosions, whereby even solid material can be ionised immediately.

The experiments have shown that aluminium cathode suffers usually a substantially larger particle removal than copper cathode. It probably occurs due to the different thermal properties of these materials, as shown later in Table 7-1. Especially at high current as shown in Fig. 7.6 moving arcs and a strong particle removal can be observed.

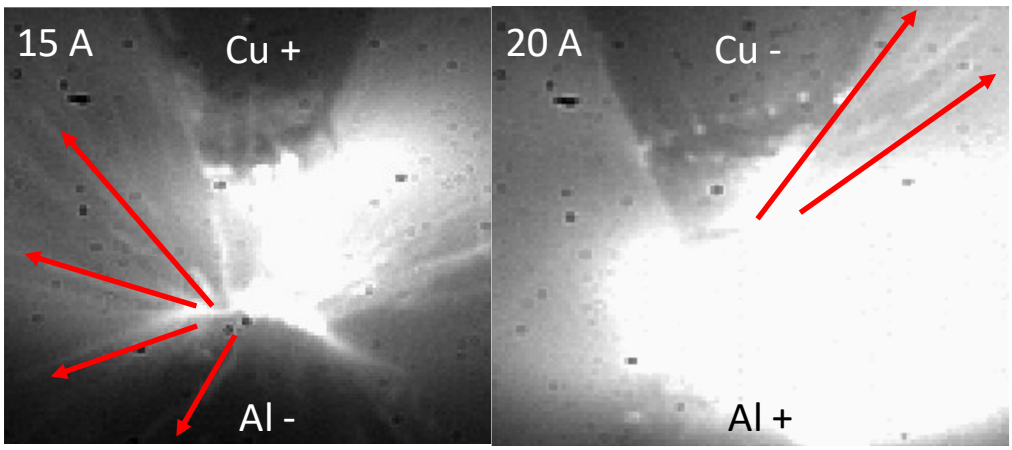

Fig. 7.6: Eruption during a discharge with particle removal

The moving arc could be better observed in discharges between less tipped turned electrodes like shown in Fig. 4.3. Fig. 7.7 shows the arc movement when not restricted to very sharply tipped electrodes. The arc moves in 2 µs from one side to the other and back.

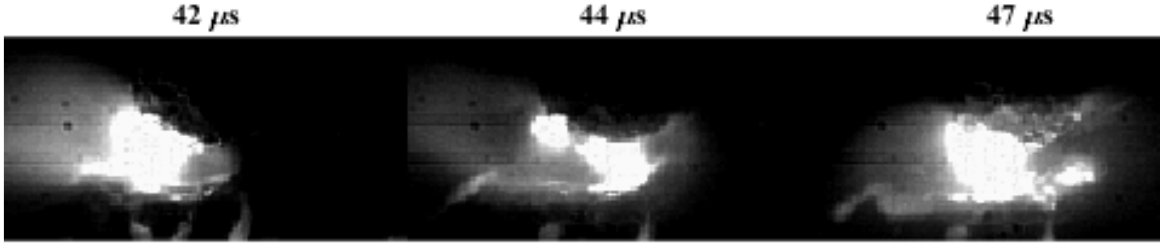

Fig. 7.7: Discharge between electrodes, the copper anode (top) and the aluminium cathode (bottom) with a visible arc root movement, Current I = 20 A

High-speed imaging indicates a constantly moving arc with a speed of around 33 m/s. Very recently, Li and Yang [48] investigated the arc movement by high-speed imaging. Even though their reported working conditions are different than the ones used in the present work, similar values for the arc movement could be observed, ranging from several meters per second to more than 100 m/s.

This observation suggests that a cathode spot is formed. As previously described, the cathode spot can be characterised by a possible arc movement speed between 1-1,000 m/s. In addition, it has been reported that overlapping continuous hot spots can be formed with a non-stationary behaviour. When a crater is visible, the arc root moves along the crater edge on the cathode side, while it melts and removes material. From all the observations, not only from high, one can conclude that EDM discharges are non-stationary, considering a time duration of 100 µs.

7.3 Discussion

From all the observations, high-speed imaging and OES, it can be concluded that EDM discharges are non-stationary looking at a timescale of 100 µs. Optical emission spectroscopy and high-speed imaging clearly show the influence of the polarity by different phenomena on cathode and anode. Furthermore, it can be distinguished between a discharge with and without a visible moving arc root.

Cathode phenomena

Based on high-speed imaging observations, several phenomena can be distinguished at the cathode for EDM, which are described in the following topics.

Spotless cathode (Fig. 7.4 and Fig. 7.6) emits nearly no light, whereas simultaneously provides atoms by evaporation and electrons to the plasma, which can occur by thermionic emission. High temperature of the electrode material surface is necessary to allow this type of emission, which takes place in a relatively large active area. In the case of EDM, which is performed in small gaps, the thermionic emission could occur thanks to the cathode heating that occurs during the process. Once this boundary condition is fulfilled, the discharge with spotless cathode is stable and can achieve stationary state. If the temperature on the cathode surface is not high enough, high-energy electrons leave the cathode via constricted spots. In the case of a spotless cathode, the current is delivered by thermionic emission.

Observing the moving arc in Fig. 7.7. a **cathode spot** can be recognized original at the arc root with a nonstationary behaviour and continuous erosion of the cathode material. Furthermore, material removal by droplets and explosions here identified are as well reported by literature [8].

According to the literature [8], discharges with the above-mentioned properties can develop until an immobile spot is formed. In addition, it normally happens on small electrode surfaces and in a gaseous environment. In this case, the electrode surfaces are easily heated due to the restricted arc movement, low heat dissipation thanks to the electrode shape and gaseous dielectric result in eruptive explosions.

Anode phenomena

In the introduction, active and luminous anode modes were already introduced. Since anode phenomena are not as well researched as cathode phenomena. Therfore analysis and interpretation of OES and high-speed imaging reported in the present work are very challenging.

As recently reported by Macedo et al. [58] EDM discharges performed in air are similar to hot anode vacuum arcs (HAVA). Indeed, many phenomena observed in Fig. 7.4 and Fig. 7.6 fit to the properties of a HAVA. Relatively low current and voltage have been reported for this type of discharge, whereas the cathode is a passive electrode, coated by material originated from the anode erosion. In the present work, the cathode activity is relatively low as well, whereas anode and cathode heat up each other due to the narrow gap. These conditions lead to a steady-state discharge with a spotless cathode. However, some specific properties of the discharges, like Al III emission, reported in the present work do not fit to HAVA in large gaps (>1mm), as it is described in the literature [8].

Ionic Al lines are observed for discharges performed with an aluminium anode at the current of I = 15 A, as shown in Fig. 7.2. These lines are always present in the beginning of the studied discharges. In contrast to HAVA in large gaps, an ionisation near the anode of only around 5% has been reported [8] and no emission of multiple ionic lines are observed. Also, it has been reported that HAVA in large gaps is the final stage of mode transitions, occurring after several microseconds and last for several seconds in steady state. Especially, for the discharges in micrometre gaps, with a strong visible interelectrode plasma and droplets, reported in the present work, the model of HAVA for discharges in large gaps as known from literature fits only partially.

Two additional discharge modes were mentioned in the introduction: the anode spot and the intense arc.

The intense arc mode has properties of strong plasma jets formation, ejected from both electrodes, whereas erosion occurs at both electrodes.

The anode spot mode has been reported to have strong ionization of the anode material, as described by Bacon [2]. Fig. 7.8 shows the observed plasma profiles reported for discharges applying I = 150 A, t = 10 µs and a gap of 3 mm. Both intense arc and anode spot modes have been reported to occur under relatively high power discharges; however, despite the different working conditions, the profiles reported by Bacon [2] match very well to the ones observed in the present work. He indicates that Al III lines emission is strong at the beginning of the discharge, while Al II and Al I lines increase towards its end, similarly to the OES results reported in the present work.

Additionally, Bacon [2] infers that the temperatures calculated by the Boltzmann method are lower than expected. Al II and Al III lines are present in the observed spectra, which led him to the conclusion that the investigated vacuum plasmas were not in LTE.

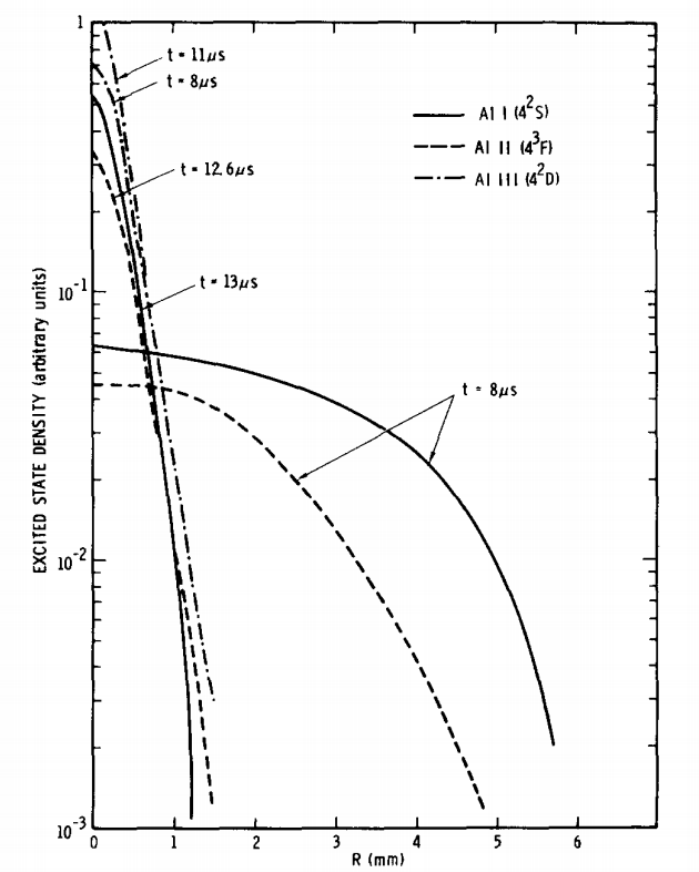

Fig. 7.8: Radial profile with aluminium lines observed by Bacon [2].

The follow-up publication from Bacon and Watts [3] continues the analysis of the phenomena involved in vacuum arc discharges. This research is supported by a CR model and assumes the formation of an electron beam within the centre of the discharge. Ignoring the presence of Al I lines an electron temperature between 10 eV and 30 eV close to the anode was estimated. The calculated beam temperature varies in this case with a different estimation of ion temperature and electron density.

Illustrations and discussion of the situation in EDM

Based on the discussion beforehand presented, the phenomena involved in 100 µs discharges, small gaps (<100 µm), low currents (<20 A) and voltages (<20 V) are now described. Two different situations for the observed discharges in air between tipped electrodes can be distinguished.

The first situation presents a stationary type of discharge with a luminous anode and no visible arc in the intermediate plasma and most likely a spotless cathode such as observed in Fig. 7.5. The physics of a spotless cathode discharge is driven by thermionic emission, in which ions and electrons are emitted from the cathode, as can be visualized in Fig. 7.9. Thermionic emission takes place only at high cathode temperatures which can be realised by bad thermal conductivity to the bulk material and anode jets reaching the cathode. In contrast to the lateral jets, jets facing towards each other in the centre of anode and cathode cannot be differentiated. The collisional

region, where electrons and ions with different directional velocity meet, are close to the anode. The axial position of this region might shift based on the vapour pressure and temperature of the different electrode materials, thereby also the amount of ionized species originated from the electrodes might vary. Electrode erosion is caused mainly by vaporization and secondarily by ejection of debris in case thermal runaway occurs.

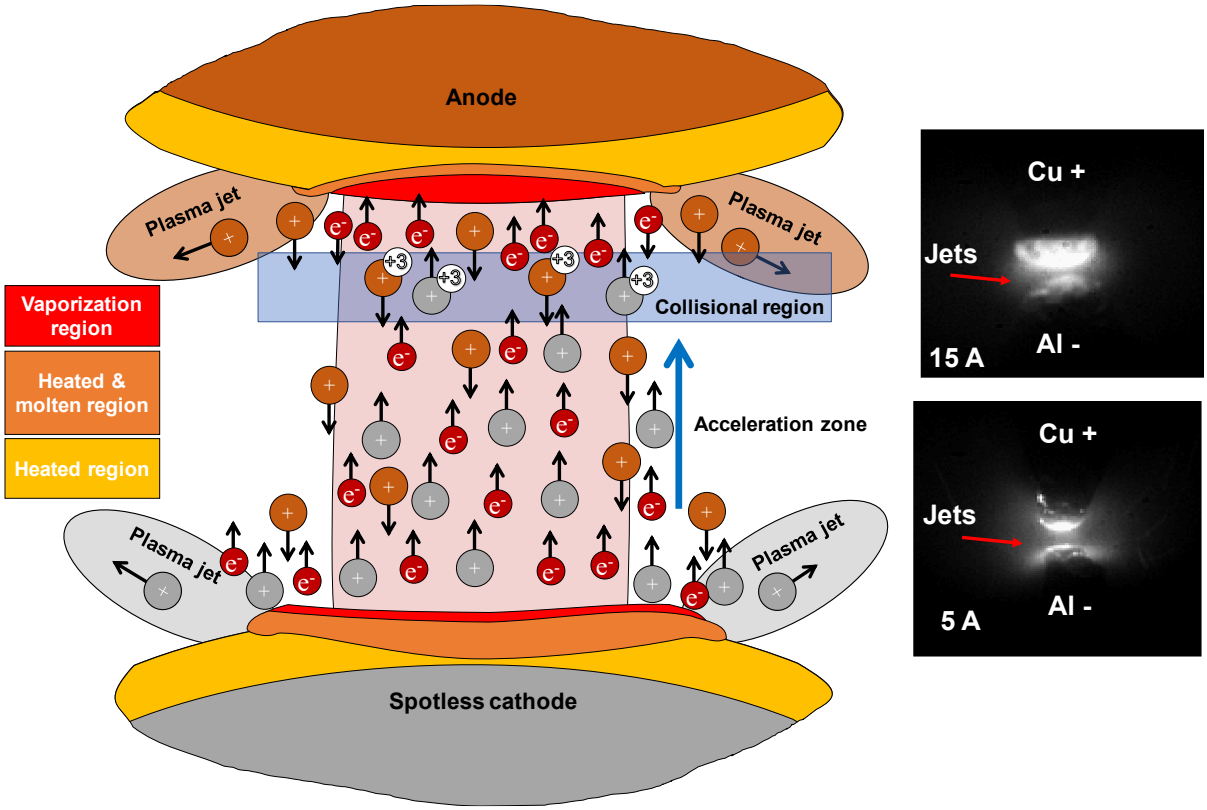

Fig. 7.9: Illustration of a discharge with spotless cathode and a luminous anode spot, this situation takes place if the cathode is widely heated and thermionic emission is dominating

The second situation describes a cathode spot in combination with an anode spot, as schematically presented in Fig. 7.10. The cathode emits electrons by thermionic and field emission from a very constricted and mobile cathode spot. In order to conduct the current in this small area, an electron beam is formed. A collisional region is present and close to the anode spot, such as reported in the first situation. In contrast to the spotless cathode large erosion by thermal runaway occurs due to the moving high energy spot. This results into larger electrode material removal and melting, but also less vaporisation. The interelectrode plasma is very luminous whereas for the spotless cathode type described in the first situation, the luminosity is weaker.

Highly ionized lines and anode spots are visible for both types of discharges described in Fig. 7.9 and Fig. 7.10; however, due to the small gap and limited spatial resolution, hot spot or collisional layers cannot be distinguished by OES in this thesis where vertically no fine resolution of the gap was possible.

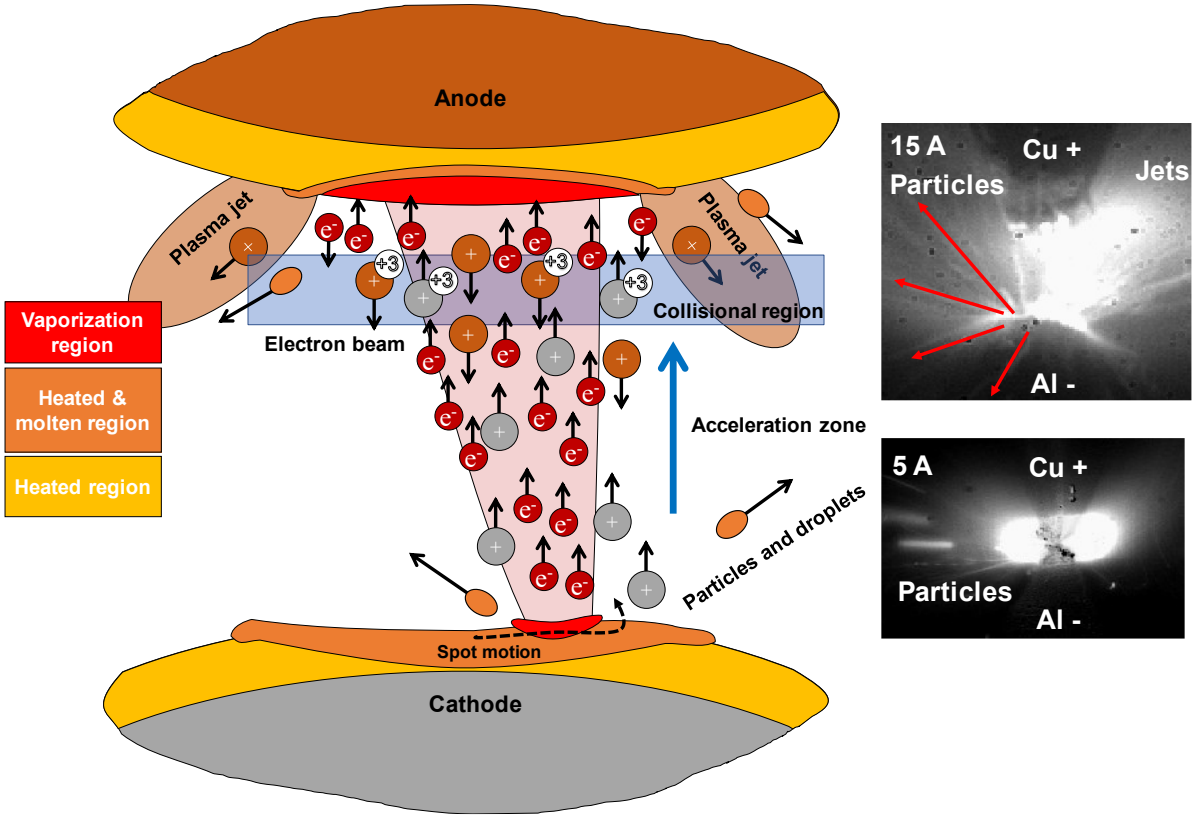

Fig. 7.10: Illustration of a discharge with an anode spot, cathode spot and electron beam; this situation occurs if the cathode is not strongly heated. Thermionic and field emission occur in a very constricted area in the form of a mobile cathode spot.

The discharge presented in Fig. 7.9 has some properties of anode spot arcs, while the one shown in Fig. 7.10 is closer to an intense arc. However, according to the plasma physics literature, anode spot arcs are formed under a significantly higher power than the one used here, while for intense arcs the required energy is even higher than for an anode spot arc.

HAVA is known to occur under low currents and voltages, such as the discharges performed in the present work; nevertheless, other characteristics, such as the Al III lines here observed in the optical emission spectra, do not match the HAVA properties. All the experiments reported in the literature have been performed in large gaps and under high currents, in contrast to the microscale gaps with low currents here presented. The interaction between anode and cathode for this observed type of EDM discharges in the present work is very strong due to the very narrow gap, even at low currents. This can lead to some very specific discharge properties.

However even though the observed electrode phenomena cannot be precisely classified with the physics literature, in the EDM application orientated research this phenomenon is known. Snoeys et al. [87] classified not “normal” EDM discharges as abnormal discharges or “arcing discharges” respectively “arcs”. These abnormal discharges are known to cause surface damage. Therefore, especially in surface finishing several methods exist to detect and filter abnormal discharges. Unfortunately, arcs cannot always be detected by the electric signal. The observed phenomena her

could not be separated by their electrical signal. Discharges which show abnormal current or voltage curves were not investigated. Pillans et al. [77] showed that arcs can be also identified by the total light emission. Arcs show much more emissions than discharges without an arc. In EDM literature focusing on plasma analysis many researches state that they investigate “arc plasma” or “EDM arc plasma“ those papers do not distinguish between visible or not visible arcs. Either they do not see it because of their measurement equipment or because it does not occur in their experimental setup.

Discharges observed in this work could be clearly differentiated with high-speed imaging. OES results evaluated with Abel inversion however show no clear differences. All results analysed showed fast electrons in the plasma centre which is required to transport the high current. The inter electrode gap mechanism to conduction energy by fast electrons must be in both phenomena, arc and no arc root visible, the same. Therefore, the differences between these two situations must be located on the electrodes surface respectively in the plasma sheath. To investigate the close electrode regions a finer resolution is needed.

Alternative to Abel inversion.

Abel inversion is a common tool to investigate EDM plasmas. However, if the erosion plasma shows unstable and asymmetric behaviour, other solutions must be sought.

A different approach to analyse the plasma with spectra simulation is investigated. Instead of inverting the observed profiles a theoretical plasma can be modelled. The emission spectra are simulated for different regions in the plasma and according to the measurements with the fibres integrated as can be seen in Fig. 7.11. In this case the spatially resolved experimental data is directly compared to the simulations.

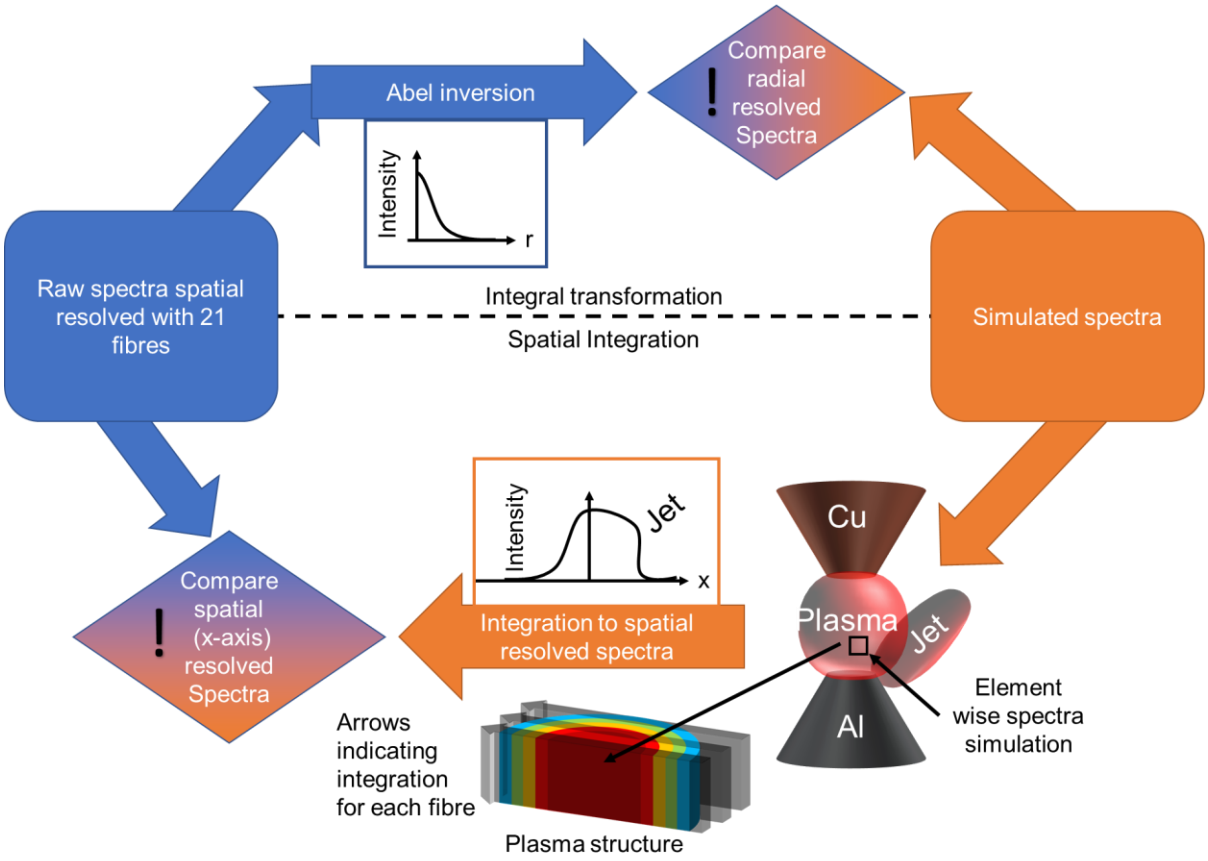

Fig. 7.11: Schematic of two different approaches to analyse emission spectra with emission spectrum simulation. Left to right by Abel inversion. Right to left imitating and estimating the real 3D plasma and integration of it.

The approach of modelling the EDM plasma and integrating the emission spectra has several advantages and disadvantages:

- ✓ Asymmetry of the plasma and special phenomena like plasma jets can be considered.
- ✓ Optical thickness of a plasma can be considered more accurately when the light is passing different plasma layers.
- ✓ Good tool to analyse plasma situations axial along the electrodes theoretically in the gap in a large scope.
- \- Up to now an exact modelling of experimentally observed plasma are unrealistic due to the high degrees of freedom

Exemplarily a typical EDM plasma for a 15 A discharge as described in Chapter 5 is modelled in cylindrical concentric shells, which are discretised in 11 regions, as can be seen in Fig. 7.12 A. Each shell shows a different plasma and the plasma parameters are exemplarily selected based on the values of the observed and analysed spectra with Abel inversion. The plasma composition is given in Fig. 7.12 B.

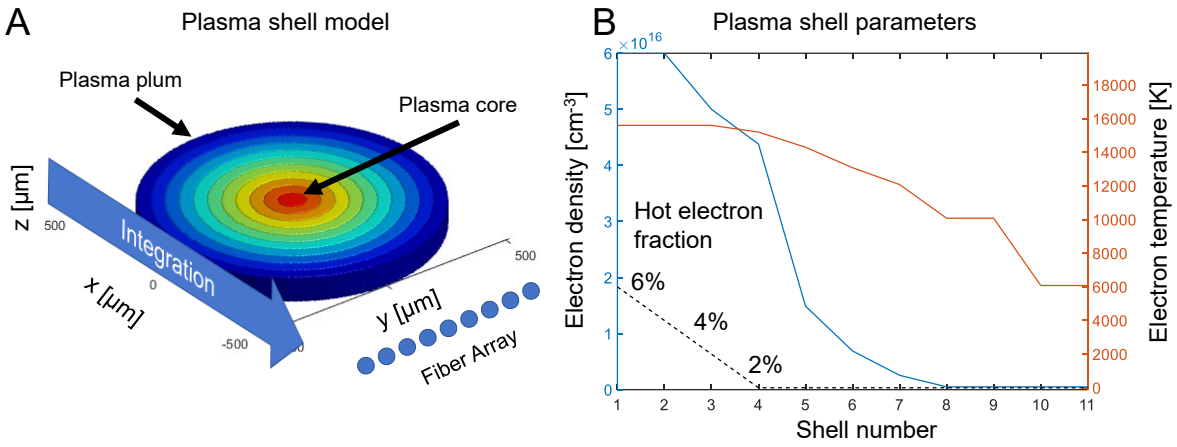

Fig. 7.12: A: Plasma shell model. B: Plasma parameter for each shell, from shell 1 (centre) to 11 (boarder).

The resulting integrated intensity, with each shell in this configuration contributing to the fibres is given in Fig. 7.13. As expected, the centre fibre has contribution from each shell while the board fibres have only emissions from outer shells.

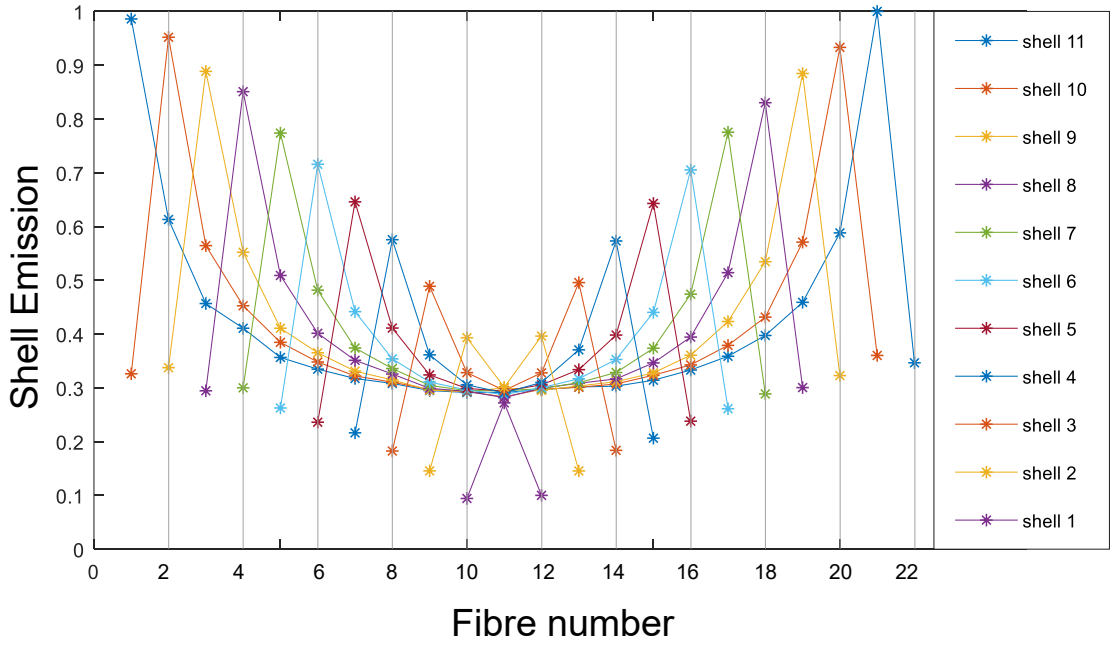

Fig. 7.13: Contribution of emissions from each plasma shell to each fibre. The emission from each disc segment depends on the integration length along the view axis which is different for each fibre position and depends also on the shell radius. Shells which are not on the integration line of a fibre are not contributing to the final emissions for this fibre.

The following model is used to represent different experimental situations and their effect on the spectrum observed by the fibres, results can be seen in Fig. 7.14.

The first two situations, Fig. 7.14 A and B, address a problem of the experimental setup. It cannot be distinguished if a fibre is directed into the plasma centre (A) or if the plasma centre is in between two detection lines of fibres (B). Emission spectra

results of Al I, Al II and Al III lines show that situation A shows a slightly deeper valley in Al I and Al II than situation B. In general, both situations are not much different and the fibre alignment does not seem to be a critical point in this situation.

Situation C shows the influence of the two electrodes, forming a small gap resulting in a far smaller plasma in the centre (limited by the electrodes) than in the border regions (the plasma plume). In this case a gap of 10 µm is modelled. The impact is mainly seen on Al II and Al III emissions. Which are slightly reduced in comparison to situation A. In this case the impact of the electrodes is marginal.

Situations D and E are modelled in order to see how a plasma jet could influence the observed spectra. Since the temperatures of a plasma jet could not be directly measured it was assumed that the jet is represented by an LTE plasma with an electron temperature of 10,000 K and a. electron density of $3 \cdot 10^{16}$ cm^{-3} which are average values in the region in between centre and rim of the plasma.

A jet striking along the fibre axis, situation D, result in a strong increase of Al I emission in the centre fibre. While a jet striking orthogonal to the fibre axis, represented with situation E, broaden the Al I profile in general.

Fig. 7.14 F shows a special situation here the plasma core represented by the three inner shells is shifted in respect to the plasma plum. This model is addressed to the shifts of the plasma like shown in Fig. 4.19, or to a moving cathode spot.

As expected the Al III profile is shifted compared to Al I. A similar result could be also seen in a combination of Situation A and E where a jet would strike only in on direction.

In summary, it can be concluded that the plasma modelling is an additional tool to investigate microplasmas. Especially complex scenarios can be played through theoretically. On experimentally side, situations A B C, the setup shows no huge impact on the gained emission profiles. Which shows that the observed spectra’s characteristic do not come from the arrangement of the fibres but from the plasma itself.

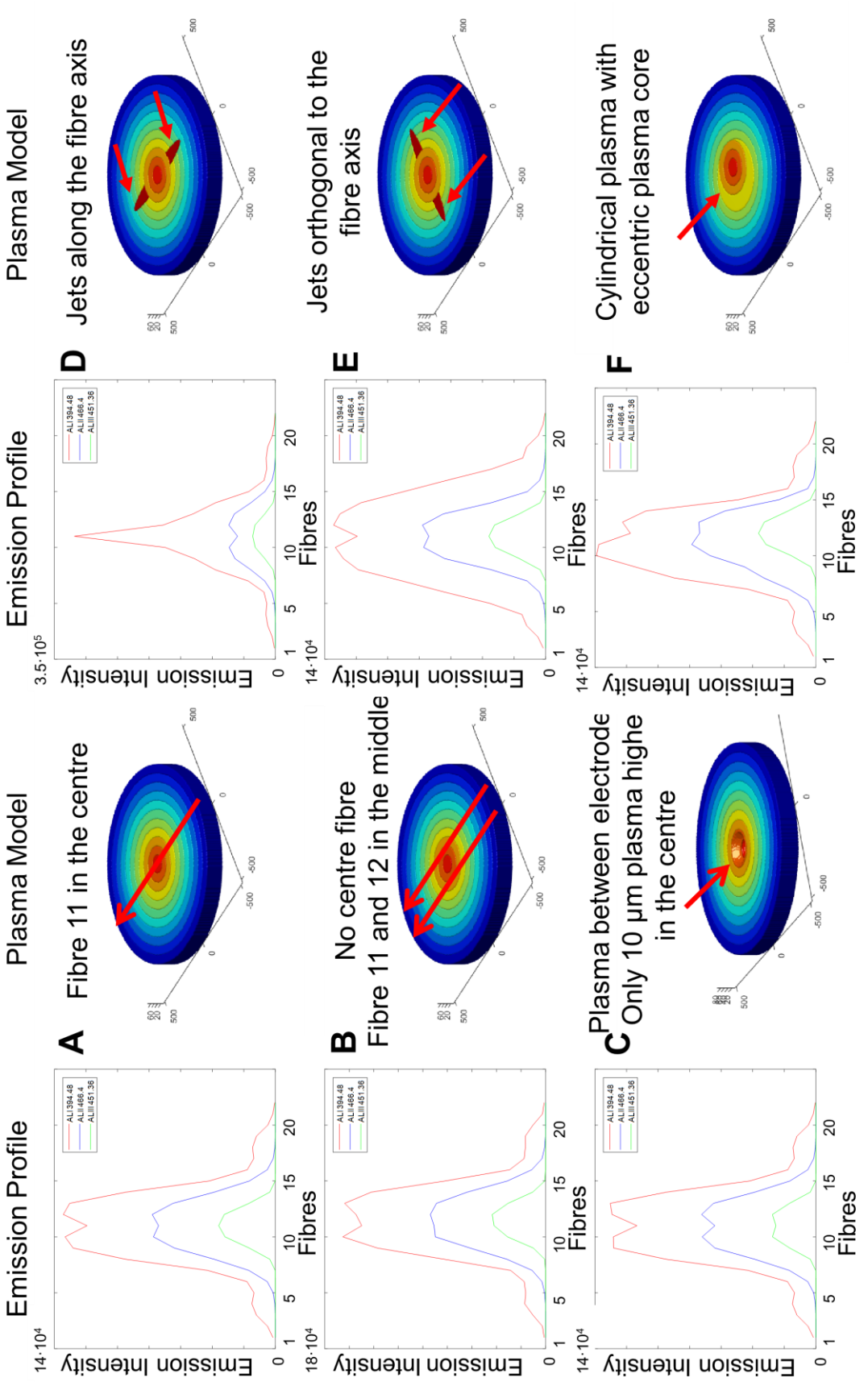

Fig. 7.14: Different model situations and their correspondent emission profile.

Annotations to the electrode geometry

The sharply tipped geometry of the electrodes used in the present analysis leads to a very small area for plasma-material interactions. Although this electrode geometry simplifies the discharge analysis, it also influences the electrical breakdown mechanisms and the plasma properties. Point-type electrodes have a lower heat dissipation than plane-type ones, which promotes the conditions for thermal runaway. Additionally, point-type electrodes are as small as the estimated spot sizes, hampering the possibility to distinguish between hot spots and spotless discharge types.

Annotations to material copper and aluminium

The material properties listed in Table 4-2 show only slight differences between copper and aluminium properties, whereas the discharges and spectroscopic results show clear differences. Besides the boiling point, other important factors for vaporization are the heat of vaporization and heat capacity. The lower the heat capacity and the heat of vaporization, the less energy is required; or with the same energy, a higher temperature can be reached faster. Those values are usually given specific values related to kg or mol respectively. Regarding the fact that the cathode spot has nearly always the same size (although it can split at higher currents), it might be more illustrative to look at the volumetric data, shown in Table 7-1. The impact is especially visible on the heat capacity. From this, it can be deduced that aluminium reaches critical temperatures much faster for the same volume.

Table 7-1 Material properties by volume

Properties	**Copper**	**Aluminium**
Heat of fusion [kJ·mol^{-}]	13	10.6
Heat of fusion [kJ·cm^{-3}]	**1.83**	**1.06**
Heat of vaporization [kJ·mol^{-}]	325.7	303.4
Heat of vaporization [kJ·cm^{-3}]	**45.8**	**30.34**
Heat capacity [J·kg^{-}·K^{-}]	385.43	902.78
Heat capacity [J·cm^{-3}·K^{-}]	**3.438**	**2.4465**

Annotations to the dielectric

EDM is normally performed in liquid dielectric media, such as hydrocarbon oil or deionised water. Therefore, an examination of discharges in liquid dielectric is of high interested. This has been investigated by OES with a setup without spatial analysis of the plasma [94]. The different obstacles to achieve spatial resolution in liquid dielectric are highlighted in the high-speed imaging results presented in Fig. 7.15. Apart from absorption, mirror artefacts cause by the phase boundaries and motion of the formed gas bubble around the discharge make reliable OES results challenging.

Material removal from the workpiece in the form of particles can be observed, such as in air discharges, while the bubble motion can be evaluated to estimate the pressure in the gas bubble, as already done by several researchers [30,34,61].

Inside the bubble there is a gaseous medium, in this case mostly out of carbon and hydrogen, so it could be that discharges in oil are not so different from those in air regarding the electrode phenomena.

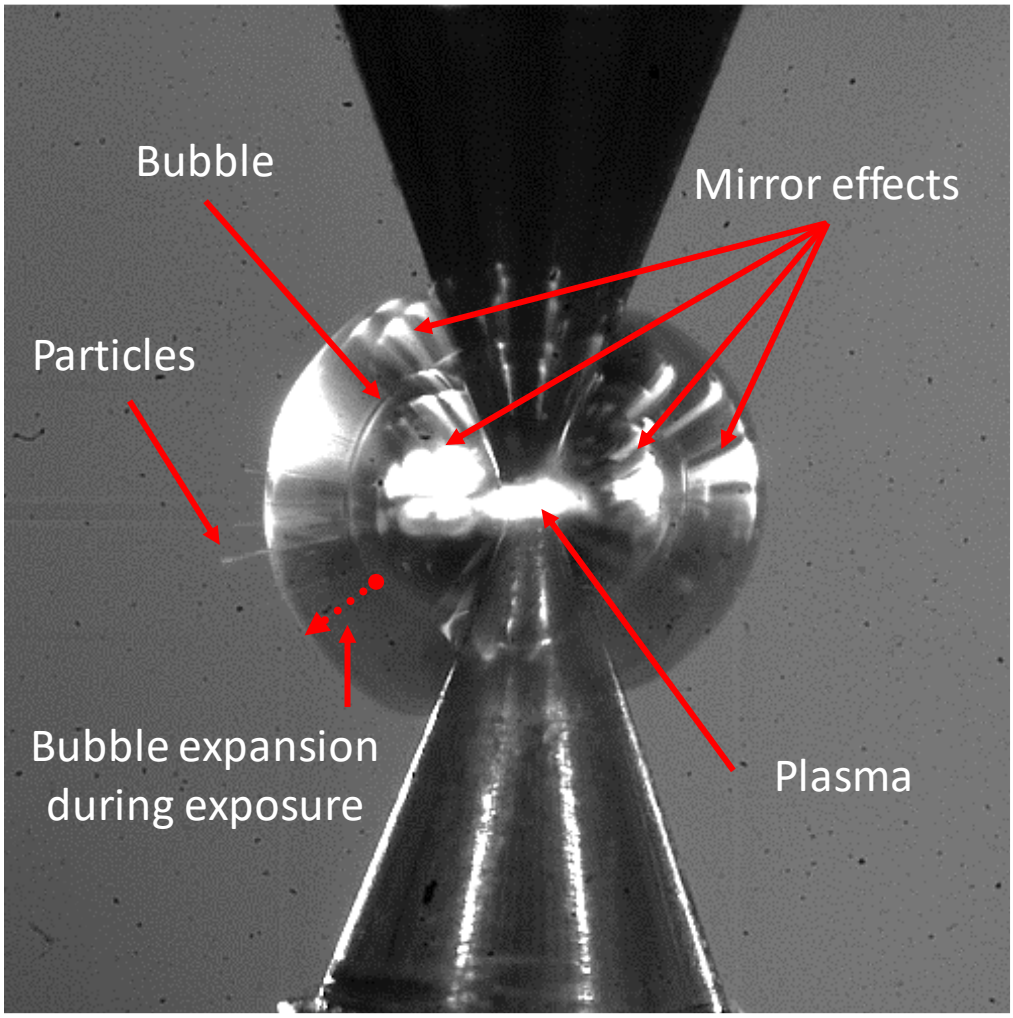

Fig. 7.15: Single discharge in oil between tipped copper and aluminium electrodes.

Another phenomenon that hampers the discharge diagnostics can be observed in in Fig. 7.16, which shows the discharge in oil dielectric. In this type of discharge, spontaneous explosions can occur, caused by fast vaporising dielectric or bubble collapse, which complicates a plasma analysis with spatial resolution.

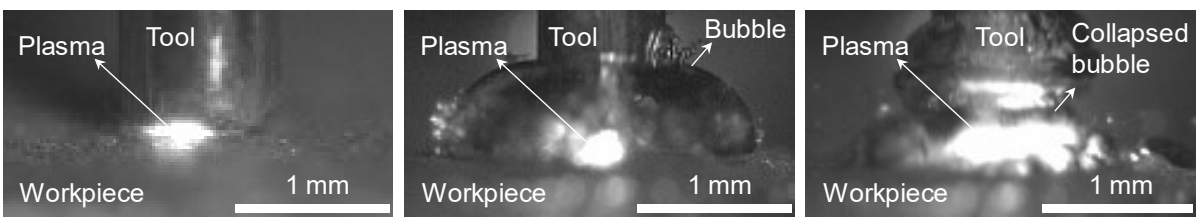

Fig. 7.16: Discharges point to plane in air (left), and oil (middle/right) showing instabilities [94]

8 SUMMARY AND OUTLOOK

The presented work investigates microplasma and introduced improved setups and advanced possibilities for EDM plasma diagnostics.

Using high-speed imaging discharges are observed with an exposure time and framerate of 5 µs at a resolution of 4.25 µm/pixel and frame size of 128*128 pixels. In optical emission spectroscopy the discharges are observed with an exposure time of 8 µs at a framerate of 41 µs realising a spatial resolution of less than 50 µm with more than 21 axial data points.

One discussed question in literature of EDM plasmas is if they are in LTE or non-LTE state, which was also one of the open questions in the predecessor work of FBT Macedo. In the presented work this could now be clarified, experimentally and with plasma physics literature. EDM plasmas must have a fraction of fast electrons transmitting the energy in the plasma centre and are non-LTE plasmas.

This means that the often-used Boltzmann two-line method is only an approximation to the true situation of the plasma temperature. The more suitable way can only be to use CR-models as shown in this thesis. CR models additionally allow to investigate more plasma parameters than the common methods.

Furthermore, the spatial and temporal resolution of the developed test rig allowed to investigate EDM discharges in a process in a more realistic environment without ignition of the discharge by liquids, powders or wires. EDM plasma and their plasma parameters could be observed in radial profiles, revealing a low but effective number of fast electrons peeking the plasma centre. Surrounded by an LTE plasma with dropping electron temperatures and pressures towards the plasma edge. It has been shown that EDM discharges have a complex plasma structure and are affected by both spatial and temporal changes.

Higher current discharges show broader radial emission profiles and higher Al III emission as well as higher values for all investigated plasma parameters such as electron temperature and density.

Time-wise the EDM plasma show dropping values for the hot electron fraction and increasing values for the electron temperature over time, assuming a constant temperature for the hot electrons. An exception can be seen in 5 A discharges which show a different behaviour, the electron temperature stays constant over time. Mostly the current is not high enough to thermalize a large area of the plasma and is very stable.

These differences can be also seen in the material erosion higher currents show far more material removal and result in a larger gap between the electrodes.

Differences can be also observed in different polarities showing an anode dominated discharge. High-speed imaging supports OES also revealing two different EDM discharge behaviours. A situation with no moving arc and another one with an arc explosively removing material. Which are not exactly classified in plasma physics literature but publications suggest that in one situation a cathode spot and and in the other a spotless cathode is observed both with a hot anode.

To fully show the potential of Collisional-Radiative models a geometric plasma model was developed to illustrate various theoretical situations for EDM plasmas. This gives the opportunity to investigate phenomena like moving plasma cores or plasma jets striking from the electrodes surface. In addition, the model demonstrates that the experimental setup is robust to fibre-plasma positioning, provides repeatable results, and accurately represents EDM plasma phenomena.

EDM is known as a very stochastic process, especially for high currents and undefined electrode shapes plasmas are moving strongly. Therefore diagnostics are very challenging and result of plasma properties like temperature and density are less precise. Micro discharges are still underrepresented in scientific literature. The similarities and differences between observed and results reported in literature lead to the conclusion that new definitions for this type of micro-discharges need to be specified. This finding should be used to rethink the heat source designs of simulation models. It should be estimated in which cases the heat source can be simplified.

For longer discharges especially in die sinking a transient heat source design is suggested not only regarding the temperature profile on the surface but furthermore regarding a heat source motion.

With the improved diagnostics for time- and spatially resolved emission spectroscopy, a further step towards the understanding of the phenomena not only for EDM discharges but also for micro discharges in general could be achieved.

Suggestions for experimental investigations

Based on the presented results further steps to tomographic observations or simple 3D observations with three fibre matrixes from different directions are suggested. The limiting factor is currently the efficiency of the high-speed camera with can be either enhanced by a phosphor screen or changing to a silicon photomultiplier matrix. To prove the different interelectrode layers, glass fibres in vertical alignment with much thinner diameter are needed.

To compare emission spectroscopy results and high-speed images two cameras simultaneously recording the same event are needed. This is also helpful to better distinguish between different cathode and anode modes using the same data from both methods.

Suggestions for simulations topics

The EDM plasma can be simulated with PrismSPECT not only in radial direction but also in layers along the electrode rotary axis. Thereby different EDFs can be applied to different regions in the plasma.

Regarding the crater formation the theoretical model introduced in this thesis with a moving cathode spot can be evaluated numerically. Not only with the goal to have a more sophisticated model but also to see where simplifications, like a stationary and Gaussian cylindrical heat source, are justifiable.

Methods like smoothed particle hydrodynamics could help to simulate the different physics involved. The presented plasma model could then be improved and extended to 3D.

Possible research topics in future

To keep EDM a competitive technologies experimental and simulative investigations should help. Always important topics are material removal rate and wear. More recently also new materials and metallurgical modifications on the surfaces become important. In the future, the cooperation together with metallurgists or chemists gets more relevant. Some approaches to involve phase transformation models in thermal based manufacturing processes exits especially in laser and welding applications. They could be developed for EDM as well. The important question of the power deposition to cathode and anode has not yet been resolved. This will still be a major goal in the EDM process and single crater models.

REFERENCES

[1] Ahn, H. J., Kim, K. I., Kim, G., Moon, E., Yang, S. S., Lee, J.-S. (2011) Atmospheric-pressure plasma jet induces apoptosis involving mitochondria via generation of free radicals, PLoS One, 6/11:e28154-e.

[2] Bacon, F. M. (1975) Vacuum arc anode plasma. I. Spectroscopic investigation, Journal of Applied Physics, 46/11:4750-7.

[3] Bacon, F. M., Watts, H. A. (1975) Vacuum arc anode plasma. II. Collisional-radiative model and comparison with experiment, Journal of Applied Physics, 46/11:4758-66.

[4] Beck, C., Cohen, E. G. D. Chapter 6 - Superstatistics: Superposition of Maxwell–Boltzmann Distributions. In: Livadiotis G, editor. Kappa Distributions: Elsevier; 2017. p. 313-28.

[5] Bergs, T., Olivier, M., Gommeringer, A., Kern, F., Klink, A. (2020) Surface Integrity Analysis of Ceramics Machined by Wire EDM Using Different Trim Cut Technologies, Procedia CIRP, 87/:251-6.

[6] Boxman, R. L., Goldsmith, S. (1983) Model of the anode region in a uniform multi-cathode-spot vacuum arc, Journal of applied physics, 54/2:592-602.

[7] Boxman, R. L., Goldsmith, S. (1990) Momentum interchange between cathode-spot plasma jets and background gases and vapors and its implications on vacuum-arc anode-spot development, IEEE transactions on plasma science, 18/2:231-6.

[8] Boxman, R. L., Sanders, D. M., Martin, P. J. (1996) Handbook of Vacuum Arc Science & Technology: Fundamentals and Applications: Elsevier Science.

[9] Chung, H., Lee, R., Chen, M., Ralchenko, Y. (2008) The How To For FLYCHK, URL: https://nltenistgov/FLY/ [2020-03-08].

[10] Colón, C., Hatem, G., Verdugo, E., Ruiz, P., Campos, J. (1993) Measurement of the Stark broadening and shift parameters for several ultraviolet lines of singly ionized aluminum, Journal of Applied Physics, 73/10:4752-8.

[11] Das, S., Klotz, M., Klocke, F. (2003) EDM simulation: finite element-based calculation of deformation, microstructure and residual stresses, Journal of Materials, 142/2:434–51.

[12] Descoeudres, A., 2006, Characterization of electrical discharge machining plasmas: DISS. EPFL No. 3542.

[13] Descoeudres, A., Hollenstein, C., Demellayer, R., Wälder, G. (2004) Optical emission spectroscopy of electrical discharge machining plasma, Journal of Materials Processing Technology, 149/1:184-90.

[14] Descoeudres, A., Hollenstein, C., Demellayer, R., Wälder, G. (2004) Optical emission spectroscopy of electrical discharge machining plasma, Journal of Physics D: Applied Physics, 37/6:875.

[15] Descoeudres, A., Hollenstein, C., Wälder, G., Demellayer, R., Perez, R. (2008) Time- and spatially-resolved characterization of electrical discharge machining plasma, Plasma Sources Science and Technology, 17/2:024008.

[16] Descoeudres, A., Hollenstein, C., Wälder, G., Perez, R. (2005) Time-resolved imaging and spatially-resolved spectroscopy of electrical discharge machining plasma, Journal of Physics D: Applied Physics, 38/22:4066.

[17] DiBitonto, D. D., Eubank, P. T., Patel, M. R., Barrufet, M. A. (1989) Theoretical models of the electrical discharge machining process. I. A simple cathode erosion model, Journal of Applied Physics, 66/9:4095-103.
[18] Ecker, G., Paulus, I. (1988) The short vacuum arc. II. Model and theoretical aspects, IEEE Transactions on Plasma Science, 16/3:348-51.
[19] Farrall, G. A., Boxman, R. L., Sanders, D. M., Martin, P. J. (1996) Handbook of Vacuum Arc Science & Technology: 2 - Arc Ignition: Elsevier Science.
[20] Foest, R., Schmidt, M., Becker, K. (2006) Microplasmas, an emerging field of low-temperature plasma science and technology, International Journal of Mass Spectrometry, 248/3:87-102.
[21] Franzke, J., Kunze, K., Miclea, M., Niemax, K. (2003) Microplasmas for analytical spectrometry, Journal of Analytical Atomic Spectrometry, 18/7:802-7.
[22] GFMS (Juni 2016) 3DS – der neue Standard für erodierte Oberflächen im Spritzguss GF Maschining Solutions, Schorndorf.
[23] Gigosos, M. A., Cardeñoso, V. (1996) New plasma diagnosis tables of hydrogen Stark broadening including ion dynamics, Journal of Physics B: Atomic, Molecular and Optical Physics, 29/20:4795.
[24] Go, D. B., Pohlman, D. A. (2010) A mathematical model of the modified Paschen's curve for breakdown in microscale gaps, Journal of Applied Physics, 107/10:103303.
[25] Griem, H. R. (2005) Principles of plasma spectroscopy: Cambridge University Press.
[26] Gu, L., Zhang, F., Zhao, W., Rajurkar, K. P., Malshe, A. P. (2016) Investigation of hydrodynamic arc breaking mechanism in blasting erosion arc machining, CIRP Annals, 65/1:233-6.
[27] Holsten, M., Koshy, P., Klink, A., Schwedt, A. (2018) Anomalous influence of polarity in sink EDM of titanium alloys, CIRP Annals, 67/1:221-4.
[28] Iza, F., Kim, G. J., Lee, S. M., Lee, J. K., Walsh, J. L., Zhang, Y. T., et al. (2008) Microplasmas: Sources, Particle Kinetics, and Biomedical Applications, Plasma Processes and Polymers, 5/4:322-44.
[29] Jüttner, B., Puchkarev, V. F., Hantzsche, E., Beilis, I., Boxman, R. L., Sanders, D. M., et al. (1996) Handbook of Vacuum Arc Science & Technology: 3 - Cathode Spots: Elsevier Science.
[30] Kanemaru, M., Sorimachi, S., Ibuka, S., Ishii, S. (2011) Single bubble generated by a pulsed discharge in liquids as a plasma microreactor, Plasma Sources Science and Technology, 20/3:034007.
[31] Karanassios, V. (2004) Microplasmas for chemical analysis: analytical tools or research toys?, Spectrochimica Acta Part B: Atomic Spectroscopy, 59/7:909-28.
[32] Kitamura, T., Kunieda, M. (2014) Clarification of EDM gap phenomena using transparent electrodes, CIRP Annals, 63/1:213-6.
[33] Kitamura, T., Kunieda, M., Abe, K. (2013) High-Speed Imaging of EDM Gap Phenomena using Transparent Electrodes, Procedia CIRP, 6/:314-9.
[34] Kitamura, T., Kunieda, M., Abe, K. (2015) Observation of relationship between bubbles and discharge locations in EDM using transparent electrodes, Precision Engineering, 40/:26-32.
[35] Kliuev, M., 2019, EDM Drilling and Milling of Aerospace Materials: DISS. ETH Zürich No. 25826.

[36] Kliuev, M., Florio, K., Akbari, M., Wegener, K. (2019) Influence of energy fraction in EDM drilling of Inconel 718 by statistical analysis and finite element crater-modelling, Journal of Manufacturing Processes, 40/:93.
[37] Kliuev, M., Maradia, U., Wegener, K. (2018) EDM Drilling of Non-Conducting Materials in Deionised Water, Procedia CIRP, 68/:11-6.
[38] Klocke, F. (2007) Fertigungsverfahren 3: Springer Berlin Heidelberg.
[39] Kojima, A., Natsu, W., Kunieda, M. (2008) Spectroscopic measurement of arc plasma diameter in EDM, CIRP Annals, 57/1:203-7.
[40] Kramida, A., Ralchenko, Yu., Reader, J. and NIST ASD Team (2019) NIST Atomic Spectra Database (version 5.7.1), [Online]. Available: https://physics.nist.gov/asd [Sun Aug 09 2020]. National Institute of Standards and Technology, Gaithersburg, MD. DOI: https://doi.org/10.18434/T4W30F.
[41] Kunieda, M., Kitamura, T. (2018) Observation of Difference of EDM Gap Phenomena in Water and Oil Using Transparent Electrode, Procedia CIRP, 68/:342-6.
[42] Kunieda, M., Kobayashi, T. (2004) Clarifying mechanism of determining tool electrode wear ratio in EDM using spectroscopic measurement of vapor density, Journal of Materials Processing Technology, 149/1:284-8.
[43] Kunieda, M., Overmeyer, L., Klink, A. (2019) Visualization of electro-physical and chemical machining processes, CIRP Annals, 68/2:751-74.
[44] Kunieda, M., Yoshida, M., Taniguchi, N. (1997) Electrical Discharge Machining in Gas, CIRP Annals, 46/1:143-6.
[45] Kunze, H.-J. (2009) Introduction to Plasma Spectroscopy: Berlin, Heidelberg : Springer.
[46] Kunze, H. J. (2009) Introduction to Plasma Spectroscopy: Springer Berlin Heidelberg.
[47] Lazarenko, B. R., Krasyuk, B. A. (1964) Electrospark machining of metals: New York : Consultants Bureau.
[48] Li, Q., Yang, X. (2020) Study on arc plasma movement and its effect on crater morphology during single-pulse discharge in EDM, The International Journal of Advanced Manufacturing Technology, 106/11:5033-47.
[49] Li, Y., Tirumala, R., Rumbach, P., Go, D. B. (2013) The Coupling of Ion-Enhanced Field Emission and the Discharge During Microscale Breakdown at Moderately High Pressures, IEEE Transactions on Plasma Science, 41/1:24-35.
[50] Lieberman, M. A., Lichtenberg, A. J. (2005) Principles of plasma discharges and materials processing. 2nd ed. ed: Hoboken : Wiley.
[51] Livadiotis, G. Chapter 1 - Statistical Background of Kappa Distributions: Connection With Nonextensive Statistical Mechanics. In: Livadiotis G, editor. Kappa Distributions: Elsevier; 2017. p. 3-63.
[52] Livadiotis, G. Chapter 5 - Basic Plasma Parameters Described by Kappa Distributions. In: Livadiotis G, editor. Kappa Distributions: Elsevier; 2017. p. 249-312.
[53] Loveless, A. M., Garner, A. L. (2017) A universal theory for gas breakdown from microscale to the classical Paschen law, Physics of Plasmas, 24/11:113522.
[54] Macedo, F. T. B., 2018, Fundamental Investigation of Dry EDM Plasmas: DISS. ETH Zürich No. 25415.
[55] Macedo, F. T. B., Wiessner, M., Bernardelli, G. C., Kuster, F., Wegener, K. (2018) Fundamental Investigation of EDM Plasmas, Part II: Parametric

Analysis of Electric Discharges in Gaseous Dielectric Medium, Procedia CIRP, 68/:336-41.
[56] Macedo, F. T. B., Wiessner, M., Hollenstein, C., Esteves, P. M. B., Wegener, K. (2017) Fundamental investigation of dry electrical discharge machining (DEDM) by optical emission spectroscopy and its numerical interpretation, The International Journal of Advanced Manufacturing Technology, 90/9:3697-709.
[57] Macedo, F. T. B., Wiessner, M., Hollenstein, C., Kuster, F., Wegener, K. (2016) Dependence of Crater Formation in Dry EDM on Electrical Breakdown Mechanism, Procedia CIRP, 42/:161-6.
[58] Macedo, F. T. B., Wiessner, M., Hollenstein, C., Kuster, F., Wegener, K. (2016) Investigation of the Fundamentals of Tool Electrode Wear in Dry EDM, Procedia CIRP, 46/:55-8.
[59] Macedo, F. T. B., Wiessner, M., Hollenstein, C., Martendal, C. P., Kuster, F., Wegener, K. (2019) Anode Power Deposition in Dry EDM, International Journal of Precision Engineering and Manufacturing-Green Technology, 6/2:197-210.
[60] MacFarlane, J., Golovkin, I., Wang, P., Woodruff, P., Pereyra, N. (2007) SPECT3D–A multi-dimensional collisional-radiative code for generating diagnostic signatures based on hydrodynamics and PIC simulation output, High energy density physics, 3/1:181-90.
[61] Maradia, U., 2014, Meso - Micro EDM: DISS. ETH Zürich No. 22024.
[62] Maradia, U., Filisetti, E., Boccadoro, M., Roten, M., Dutoit, J. M., Hengsberger, S. (2018) Increasing the Injection Moulding Productivity through EDM Surface Modulation, Procedia CIRP, 68/:58-63.
[63] Maradia, U., Kliuev, M., Baumgart, C. (2018) Efficient machining of complex-shaped seal slots for turbomachinery, CIRP Annals, 67/1:209-12.
[64] Maradia, U., Scuderi, M., Knaak, R., Boccadoro, M., Beltrami, I., Stirnimann, J., et al. (2013) Super-finished surfaces using meso-micro EDM, Proc Cirp, 6/:157-62.
[65] Mariotti, D., Sankaran, R. M. (2010) Microplasmas for nanomaterials synthesis, Journal of Physics D: Applied Physics, 43/32:323001.
[66] Miller, H. C. (1996) Handbook of Vacuum Arc Science & Technology: 5 - Anode Phenomena: Elsevier Science.
[67] Morimoto, K., Kunieda, M. (2009) Sinking EDM simulation by determining discharge locations based on discharge delay time, CIRP Annals, 58/1:221-4.
[68] Mujumdar, S. S., Curreli, D., Kapoor, S. G. (2018) Effect of Dielectric Conductivity on Micro-Electrical Discharge Machining Plasma Characteristics Using Optical Emission Spectroscopy, Journal of Micro and Nano-Manufacturing, 6/3.
[69] Mujumdar, S. S., Curreli, D., Kapoor, S. G., Ruzic, D. (2014) A Model of Micro Electro-Discharge Machining Plasma Discharge in Deionized Water, Journal of Manufacturing Science and Engineering, 136/3:031011-.
[70] Mujumdar, S. S., Curreli, D., Kapoor, S. G., Ruzic, D. (2015) Modeling of melt-pool formation and material removal in micro-electrodischarge machining, Journal of Manufacturing Science and Engineering, 137/3:031007.
[71] Nagahanumaiah, Ramkumar, J., Glumac, N., Kapoor, S. G., DeVor, R. E. (2009) Characterization of plasma in micro-EDM discharge using optical spectroscopy, Journal of Manufacturing Processes, 11/2:82-7.
[72] Natsu, W., Ojima, S., Kobayashi, T., Kunieda, M. (2004) Temperature Distribution Measurement in EDM Arc Plasma Using Spectroscopy, JSME

International Journal Series C Mechanical Systems, Machine Elements and Manufacturing, 47/1:384-90.
[73] Natsu, W., Shimoyamada, M., Kunieda, M. (2006) Study on Expansion Process of EDM Arc Plasma, JSME International Journal Series C Mechanical Systems, Machine Elements and Manufacturing, 49/2:600-5.
[74] Nestor, O., Olsen, H. (1960) Numerical methods for reducing line and surface probe data, SIAM review, 2/3:200-7.
[75] Ochkin, V. N. (2009) Spectroscopy of low temperature plasma: Weinheim : Wiley-VCH.
[76] Patel, M. R., Barrufet, M. A., Eubank, P. T., DiBitonto, D. D. (1989) Theoretical models of the electrical discharge machining process. II. The anode erosion model, Journal of Applied Physics, 66/9:4104-11.
[77] Pillans, B. W., Evensen, M. H., Taylor, H. F., Eubank, P. T., Ma, L. (2002) Fiber optic diagnostic techniques applied to electrical discharge machining sparks, Journal of Applied Physics, 91/4:1780-6.
[78] Pretzler, G. (1991) A new method for numerical Abel-inversion, Zeitschrift für Naturforschung A, 46/7:639-41.
[79] Radmilović-Radjenović, M., Radjenović, B. (2008) Theoretical study of the electron field emission phenomena in the generation of a micrometer scale discharge, Plasma Sources Science and Technology, 17/2:024005.
[80] Raizer, Y. P. (1991) Gas discharge physics: Berlin [etc.] : Springer.
[81] Rakhovsky, V. I. (1984) Current Density Per Cathode Spot in Vacuum Arcs, IEEE Transactions on Plasma Science, 12/3:199-203.
[82] Reinhard, N. (2012) Laser-Induced Breakdown Spectroscopy : Fundamentals and Applications: Berlin, Heidelberg : Springer.
[83] Roth, R. A., 2015, Trockene Funkenerosion. DISS. ETH Zürich No. 22025: VDI Verlag.
[84] Rupf, S., Lehmann, A., Hannig, M., Schäfer, B., Schubert, A., Feldmann, U., et al. (2010) Killing of adherent oral microbes by a non-thermal atmospheric plasma jet, Journal of Medical Microbiology, 59/2:206-12.
[85] Samsonov, G. V. (2012) Handbook of the Physicochemical Properties of the Elements: Springer Science & Business Media.
[86] Schumacher, B. M. (2004) After 60 years of EDM the discharge process remains still disputed, Journal of Materials Processing Technology, 149/1:376-81.
[87] Snoeys, R., Dauw, D. F., Kruth, J. P. (1983) Survey of adaptive control in electro discharge machining, Journal of Manufacturing Systems, 2/2:147-64.
[88] Stroth (2018) Plasmaphysik: Springer Berlin Heidelberg.
[89] Tao, J. J., Ni, J., Shih, J. A. (2012) Modeling of the anode crater formation in electrical discharge machining, Journal of Manufacturing Science and Engineering, 134/1:11002.
[90] Uhlmann, E., Schimmelpfennig, T.-M., Perfilov, I., Streckenbach, J., Schweitzer, L. (2016) Comparative Analysis of Dry-EDM and Conventional EDM for the Manufacturing of Micro Holes in Si3N4-TiN, Procedia CIRP, 42/:173-8.
[91] Van Dijck, F. A. S., R. (1971) Investigation of electro discharge machining operations by means of thermo-mathematical model (secondary source), CIRP Annals - Manufacturing Technology, 20/:35–7.
[92] Wang, P. (1991) Computation and Application of Atomic Data for Inertial Confinement Fusion Plasmas, PhDT.

[93] Weingaertner, E., Kuster, F., Wegener, K. (2012) Modeling and simulation of electrical discharge machining, Procedia CIRP, 2/:74-8.
[94] Wiessner, M., Macedo, F. T. B., Martendal, C. P., Kuster, F., Wegener, K. (2018) Fundamental Investigation of EDM Plasmas, Part I: A Comparison between Electric Discharges in Gaseous and Liquid Dielectric Media, Procedia CIRP, 68/:330-5.
[95] Wiessner, M., Martendal, C. P., Esteves, P. M. B., Kunze, K., Wegener, K. (2019) Analysis Of Eroded Ti-6al-4v Single Craters And Surfaces In Oil By Electron Microscopy And Optical Emission Spectroscopy, 25th ABCM International Congress of Mechanical Engineering.
[96] Yeo, S. H., Kurnia, W., Tan, P. C. (2007) Electro-thermal modelling of anode and cathode in micro-EDM, Journal of Physics D: Applied Physics, 40/8:2513–21.
[97] Zhang, M., Zhang, Q., Dou, L., Liu, Q., Dong, C. (2016) Comparisons of single pulse discharge crater geometries in EDM and EAM, Journal of Manufacturing Processes, 22/:74-81.
[98] Zhao, W., Gu, L., Xu, H., Li, L., Xiang, X. (2013) A Novel High Efficiency Electrical Erosion Process – Blasting Erosion Arc Machining, Procedia CIRP, 6/:621-5.

LIST OF PUBLICATIONS

M. Wiessner (2019) Funkenerosives Bohren, Herausforderungen und Chancen für die Luft- und Raumfahrtindustrie, 12. Fachtagung Funkenerosion WZL der RWTH Aachen

M. Wiessner (2017) Herstellung von selbstreinigenden Oberflächen durch funkenerosive Bearbeitung, 11. Fachtagung Funkenerosion WZL der RWTH Aachen

M. Wiessner, C. Martendal, P. Esteves, K. Karsten, K. Wegener (2019) Analysis of Eroded Ti-6al-4v Single Craters and Surfaces in Oil By Electron Microscopy and Optical Emisson Spectroscopy, COBEM 2019, 25th International Congress of Mechanical Engineering, Uberlandia, Brazil Keynote

H. Büttner, G. Vieira, M. Wiessner, K. Wegener (2019) Burr Free Micro Milling for Electrodes in Die-Sinking EDM, COBEM 2019, 25th International Congress of Mechanical Engineering, Uberlandia, Brazil

M. Wiessner, FBT Macedo, C. Martendal, F. Kuster, K. Wegener (2018) Fundamental Investigation of EDM Plasmas, Part I: A Comparison between Electric Discharges in Gaseous and Liquid Dielectric Media, 19th CIRP Conference on Electro Physical and Chemical Machining, Bilbao, Spain

FBT Macedo, M. Wiessner, G. Bernardelli, F. Kuster, K. Wegener (2018) Fundamental Investigation of EDM Plasmas, Part II: Parametric Analysis of Electric Discharges in Gaseous Dielectric Medium, 19th CIRP Conference on Electro Physical and Chemical Machining Bilbao, Spain

M. Wiessner, P. Blaser, S. Böhl, J. Mayr, K. Wegener (2018) Evaluation of thermal errors of 5-axis machine tools by on-machine measurements of a thermal test piece, Conference on Thermal Issues in Machine Tools, Dresden

P. Blaser, P. Hernández Becerro, J. Mayr, M. Wiessner, K. Wegener (2017) Thermal errors of a large 5-axis machine tool due to cutting fluid influences – evaluation with thermal test piece, American Society for Precision Engineering, Charlotte, USA

FBT Macedo, M. Wiessner, C. Hollenstein, F. Kuster, K. Wegener (2016) Investigation of the Fundamentals of Tool Electrode Wear in Dry EDM, 7th HPC 2016 – CIRP Conference on High Performance Cutting, Chemnitz, Germany

FBT Macedo, M. Wiessner, C. Hollenstein, F. Kuster, K. Wegener (2016) Dependence of Crater Formation in Dry EDM on Electrical Breakdown Mechanism, 18th CIRP Conference on Electro Physical and Chemical Machining, Tokyo, Japan

M. Wiessner, M. Gebhardt, W. Knapp, K. Wegener (2014) Test piece for visualization of thermally induced deviations on five-axis machine tools, euspen – Special Interest Group Meeting: Thermal Issues, Zürich, Switzerland

FBT Macedo, M. Wiessner, C. Hollenstein, C. Martendal, F. Kuster, K. Wegener (2019) Anode Power Deposition in Dry EDM, International Journal of Precision Engineering and Manufacturing-Green Technology

M. Wiessner, P. Blaser, S. Böhl, J. Mayr, W. Knapp, K. Wegener (2018) Thermal test piece for 5-axis machine tools, Precision Engineering

FBT Macedo, M. Wiessner, C. Hollenstein, P. Esteves, K. Wegener (2016) Fundamental investigation of dry electrical discharge machining (DEDM) by optical emission spectroscopy and its numerical interpretation, The International Journal of Advanced Manufacturing Technology